USE OF THE FAST FOURIER TRANSFORM FOR TRANSIENT MAGNETIC FIELDS

T J E Miller BSc AFIMA Mem IEEE
Professor P J Lawrenson DSc AFIMA Fel IEEE FIEE CEng

1. INTRODUCTION

In many engineering problems it is important to know how transient electromagnetic fields diffuse through conducting or permeable bodies. Such problems include the design of protective shields (for superconductors or instruments), and of many components in machines, transformers and magnets. Of interest usually are the transient distribution of force and heat associated with eddy currents, variations of impedances, and the transient distributions of magnetic flux and current.

Several methods of analysis have been applied to the transient diffusion problem, ranging from 'classical' analysis to purely numerical methods of relatively recent origin. The numerical methods are generally more powerful, but have not been developed to the stage where their use can be regarded as routine or even efficient. This paper develops the solution of transient field problems by Fourier transform techniques, and by means of the digitally calculated fast Fourier transform it enables solutions to be obtained very efficiently and flexibly.

The method has the important advantage of evaluating at an intermediate stage the frequency-response function of the field quantity of interest. This function is itself of considerable value in understanding and estimating the penetration of the diffusing field, and may be obtained by any conventional method: analytical, numerical or experimental. The frequency response function entirely characterises the field quantity of interest in a way which makes the calculation of the time response a routine and efficient matter using the fast Fourier transform. The response to almost any transient excitation function can be computed rapidly and easily.

The paper begins with a review of methods available for solving this class of problem and discusses the relative advantages of the integral transform method. The analytical methods for obtaining the frequency response function of interest involve the solution of the complex Poisson equation, for which powerful methods are already available and are still developing.

The application of the general method is then explained in relation to the particular problem of screening a superconducting winding from an externally applied, transient magnetic field. The example is taken from the design of a superconducting a.c. generator. It is essential to limit the magnitude and the rate of change of magnetic field in the region of the superconductor, and this is done by interposing a cylindrical screen (or screens) between the superconducting winding (with which it rotates) and the machine's armature (transient currents in which would be responsible for the most troublesome changes in magnetic field). It is necessary to be able to calculate reliably the way in which flux inside the screen changes following a sudden change in armature current. The shielding property of the screen is characterised by the screening ratio frequency response function S(f), which is the complex ratio between the magnetic field at a point at frequency f and at zero frequency. The transient response is then evaluated using the F.F.T. and S(f) for the illustrative case of a step change of armature current. A brief discussion of screening properties is given for single and double screens. It has been found that interactions between concentric screens, and between screens and field winding, can have a degrading influence on the shielding effectiveness, and this is discussed briefly.

2. METHODS AVAILABLE FOR TRANSIENT DIFFUSION

The general linear diffusion process is described by the equation

$$\text{curl curl } H = -\frac{\mu}{\rho}\frac{\partial H}{\partial t} \qquad (1)$$

in which H is the magnetic field strength vector. Three main methods for solving this equation are: direct analytical solution; direct numerical solution; and solution by integral transform. The analytical method[6] is restricted to the simplest geometries with a small number of field components, and produces solutions in the form of an infinite sum of exponential terms e^{-t/τ_n}, which may be slow to converge. The method is best used with step or impulse excitation functions; more general excitation functions require Duhamel's integral, which is cumbersome; the approach is comparatively inflexible, limited and inefficient. Direct

numerical methods (e.g. Crank & Nicolson[7], Dufort & Frankel[9], Alternating Direction Implicit method[8]) are much more powerful, in that a larger number of field components can be dealt with, extending the application to more complicated geometries. (They are also the only methods capable at present of dealing with nonlinearities.) However, it is often necessary to solve large numbers of simultaneous equations at every time step, and convergence problems in both space and time domains are possible. The entire solution must be repeated for every new excitation function to which the response is required, and this involves the computation of the field quantities at all points in the problem even when only localised values are needed.

The transform method escapes from most of the limitations of these two methods: by dividing the problem into a 'space-dependent' part and a 'time-dependent' part, which in linear problems can be solved independently, it makes possible a 'once for all' space solution which can subsequently be used in the calculation of the transient response to any excitation function. The space solution is in the form of a frequency response function for each point in the field of interest, and this function is itself often of physical significance and of considerable value in understanding and characterising the diffusion properties of the device in question. The set of frequency response functions for all points in the field are the solution to the complex Poisson equation, for which powerful analytical and numerical methods are available. The frequency response functions can also be obtained experimentally. Because the same functions are used to characterise the spatial variation of the field in the calculation of transient response for all excitation functions, experimental or analytical work is greatly reduced. A further reduction in computational effort is possible when the field is of interest at only a few points, since the transient response at each of these points can be obtained by the transform from the appropriate local frequency response functions independently of all other field points.

Although the integral transform approach is by no means new, its advantages can be realised only if a reliable and efficient method of computing inverse transforms is available. In recent years the fast Fourier transform[2,3,4] calculated by the method of Cooley and Tukey has greatly advanced the efficiency of the Fourier transform approach, and whereas this development has been fully exploited in communications and circuit theory there appear to be few applications to electromagnetic field transients.

3. BASIS AND FORMULATION OF THE TRANSFORM METHOD

The Fourier transformation of equation 1 replaces the operator $\partial/\partial t$ by $j\omega$ to produce the complex Poisson equation:

$$\text{curl curl } H(j\omega) = - j\omega \frac{\mu}{\rho} H(j\omega) \qquad (2)$$

which is solved for a range of values of ω ($=2\pi f$). If the phasor solution is written

$$H(f) = S(f)\, H_0 e^{j2\pi ft} \qquad (3)$$

where $H_0 e^{j2\pi ft}$ is the excitation function phasor at frequency f, then $S(f)$ is a frequency-response function which characterises the magnetic field at each point. The physical interpretation of $S(f)$ is usually important, and examples of this will be seen below, but its main usefulness here is in the determination of transient response. For any excitation function $H_0(t)$ whose Fourier transform is $H_0(f)$, the transient response of the field is given immediately by

$$H(t) = \mathcal{F}^{-1}\left\{S(f)H_0(f)\right\} \qquad (4)$$

The inverse transformation is computed efficiently by means of the F.F.T. algorithm. At this stage the flexibility of the method is clear. The same function $S(f)$ can be used for all excitation functions $H_0(f)$. Of course the transient response of the entire field can only be obtained by repeated application of equation (4) for each field point in turn, but since $S(f)$ is known at all points from the solution of equation (2), this is a straightforward and routine calculation which, because of the F.F.T., is also economical.

The flexibility of the method is further enhanced by the ease with which, if necessary, the excitation transform $H_0(f)$ can be calculated from $H_0(t)$ using the F.F.T. This important advantage extends the method to excitation functions of virtually any waveshape. The essential characteristics of the field are implicit in $S(f)$ and not locked up in a particular transient response to a particular excitation function, as would be the case with an analytical or direct numerical method. At the

same time, the responses to particular excitation functions can be easily and quickly obtained.

There remains the difficulty of solving the complex Poisson equation. Although this is complex, it at least has one independent variable fewer than equation (1). Powerful methods are available for its solution, particularly in problems of only one or two space dimensions, and considerable effort is at present directed towards methods for three-dimensional solutions. Even where direct physical measurement is the only available means of analysis, frequency response functions like S(f) are the most economical and generally useful quantities to measure.

The F.F.T. algorithm calculates the discrete Fourier transform (D.F.T.) and/or its inverse, which are given by

$$g_d(k\Delta t) = \frac{1}{T}\sum_{\ell=0}^{N-1} G_d(\ell\Delta f)e^{j2\pi k\ell/N} \quad , k=0,1,2,\ldots N-1$$

$$G_d(\ell\Delta f) = \sum_{k=0}^{N-1} g_d(k\Delta t)e^{-j2\pi k\ell/N} \quad , \ell=0,1,2,\ldots N-1 \qquad (5)$$

This relation may be regarded as the digital equivalent of the continuous Fourier Transform. Several standard papers[2,3,4] describe the formation of the sampled and truncated functions $g_d(k)$ and $G_d(\ell)$ from the corresponding continuous functions g(t) and G(f), and only the briefest outline is given here. First, the periodic 'aliased' functions

$$g_a(t) = \sum_{m=-\infty}^{\infty} g(t + mT)$$

$$G_a(f) = \sum_{m=-\infty}^{\infty} G(f + mF) \qquad (6)$$

are formed by the juxtaposition at intervals of T (or F) of the central or most significant part of g(t) or G(f), as in Fig 1. Then one period of each of the aliased functions is sampled at N equally spaced points:

$$g_d(k) = g_a(k\Delta t), \quad k=0,1,2,\ldots N-1$$

$$G_d(\ell) = G_a(\ell\Delta f), \quad \ell=0,1,2,\ldots N-1 \qquad (7)$$

This procedure is illustrated for an example G(f) in Fig 1. F and T are related by FT = N, so that $\Delta f = F/N = 1/T$ and $\Delta t = T/N = 1/F$. The inverse D.F.T. of $G_d(\ell)$ is $g_d(k)$ which approximates g(t) for $t < T/2$ just as $G_d(\ell)$ approximates G(f) for $f < F/2$.

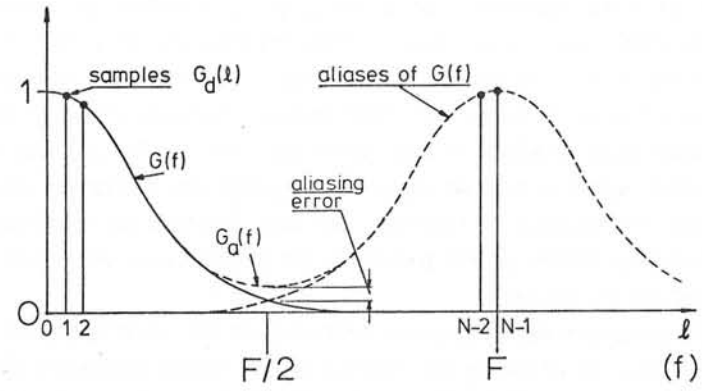

Fig 1 Aliasing and sampling

Two possible sources of error need to be mentioned. First, the 'truncation' of the aliased function, which arises because only a finite number N of samples are taken, is equivalent to multiplying G(f) by a rectangular 'data window' so that the resulting transform g(t) is convolved with a (sin t)/t function. This appears as a ripple on g(t) around t = 0 (Gibbs' phenomenon), and may be avoided by multiplying G(f) by a smoother data window, such as the Hanning or the Dolph-Chebyshev[4]. Secondly, the Nyquist frequency F/2 must be chosen to be higher than the highest frequency component present in G(f), so as to avoid aliasing errors.

4. TRANSIENT MAGNETIC FIELDS IN CYLINDRICAL SCREENS

4.1 Application of the Transform Method

The transform method has been applied to the transient screening problem in the superconducting a.c. generator. Fig 2 is a schematic diagram showing the positions of the principal components in a 2-dimensional model of this. A rotating field configuration has been assumed. The superconducting winding, of radius r_f, must be protected from magnetic field transients caused by changes in armature current. For this purpose a cylindrical screen (or a double screen) is fixed to the rotor, and it is here assumed to rotate synchronously with the field winding. It is

necessary to calculate the way in which the magnetic field inside the screen changes following changes in armature current, and to determine the way in which the properties of the screen affect these changes. This study is later extended to include the effect of a short-circuited field winding.

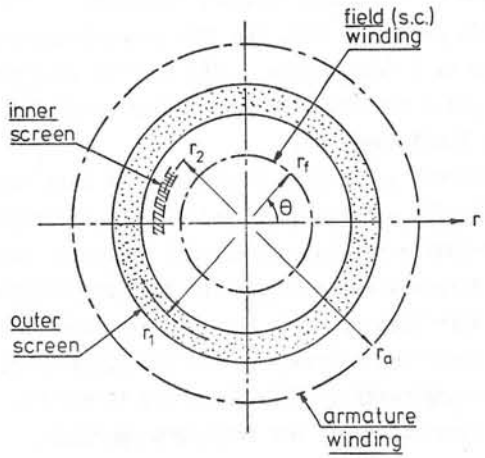

Fig 2 Basic superconducting machine configuration

Frequency response

The first step is to determine the field under harmonic excitation. With only an axial component of current (and thereafter also of vector potential) this can be obtained from the solution of equation (2). Assuming a sinusoidal distribution of armature current, equation (2) reduces to

$$\frac{d^2H}{dr^2} + \frac{1}{r}\frac{dH}{dr} - \left[\frac{p^2}{r^2} + j\omega\frac{\mu}{\rho}\right]H = 0 \qquad (8)$$

The solution of this equation is described in detail in Ref 1 and can be written

$$H_\theta = -\frac{K}{2}\left(\frac{r}{r_a}\right)^{p-1} S(f)e^{j2\pi ft}\sin p\theta \qquad (9)$$

for the tangential component inside the screen. S(f), the screening ratio frequency response function, is the ratio between the phasor value of H_θ at frequency f and at zero frequency. It is a complex expression involving Bessel functions (see Ref 1). In simple cases it can be evaluated algebraically, but when the number of concentric components exceeds three the algebra becomes cumbersome and the transfer-matrix method described by Freeman[10] is useful. Where the full three-dimensional variation of the field is necessary numerical methods may be necessary to find S(f).

In the simple case of a single screen with a field winding (which may be short circuited), at low frequencies it is possible to obtain an appropriate expression for S(f) by using asymptotic expressions for the Bessel functions when these have small arguments. This formula is

$$S(f) = 1/\left[1 + j2\pi f\, T_D\,(1-\lambda)\right] \qquad (10)$$

where $\lambda = (r_f/r_1)^2$. In this form it applies to the case with the short-circuited field winding, the armature current being symmetrically disposed about the direct axis. When the field winding is open, or when the armature current is symmetrical about the quadrature axis, $\lambda = 0$. The time constant T_D is given approximately by $T_D = \mu_0 r_1 h/2\rho$. It can be seen that the effect of a short-circuited field winding is to shorten the effective time constant of the screen, which weakens the screening effectiveness; this effect is discussed in Section 4.2.

Transient response

The transient response to any excitation function can now be obtained directly from equation (4). The particular excitation function to be considered here is a step of armature current from 0 to K (see Appendix). This type of change is one of the most severe in the machine and corresponds closely to the effective d.c. transient following a sudden terminal short circuit. The excitation function in terms of H_θ is

$$H_{\theta 0} = -\frac{K}{2}\left(\frac{r}{r_a}\right)^{p-1}\sin p\theta\; u(t) = H_{\theta 0}u(t) \qquad (11)$$

where u(t) is the unit step function. The necessary Fourier transform of this can be obtained analytically as

$$H_{\theta 0}(f) = -\frac{K}{2}\left(\frac{r}{r_a}\right)^{p-1}\sin p\theta\;\left[\pi\delta(f) + \frac{1}{j2\pi f}\right] \qquad (12)$$

and equation (4) gives the transient response as

$$H_\theta(t) = -\frac{K}{2}\left(\frac{r}{r_a}\right)^{p-1}\sin p\theta\;\mathcal{F}^{-1}\left\{\left[\pi\delta(f) + \frac{1}{j2\pi f}\right]S(f)\right\} = h_\theta(t)H_{\theta 0} \qquad (13)$$

$h_\theta(t)$, the normalised transient response, is evaluated by means of the F.F.T. and is used in presenting results. S(f) is first sampled at equally spaced frequencies $\ell\Delta f$, ℓ=0,1,2...N-1; then the function $S(\ell\Delta f)/j2\pi\ell\Delta f$ is formed sample by sample, and the step response is given in discrete form by

$$h_\theta(k\ t) = \frac{1}{2}S(0) + \mathcal{F}^{-1}\left\{ S(\ell\Delta f)/j2\pi\ell\Delta f \right\},\ k=0,1,2...N-1 \qquad (14)$$

In the Appendix, it is shown that the discrete transform is to be evaluated in the form

$$\mathcal{F}^{-1}\left\{\frac{S(\ell\Delta f)}{j2\pi\ell\Delta f}\right\} = \frac{4}{T}\left\{\frac{1}{2}R(0) + \sum_{\ell=1}^{N/2-1} R(\ell)\cos\frac{2\pi k\ell}{N} + \frac{1}{2}R\left(\frac{N}{2}\right)\cos\pi k\right\} + \frac{1}{2}$$

$$k=0,1,2...N-1 \qquad (15)$$

where $R(\ell) = \mathrm{Re}\left[S(\ell\Delta f)/j2\pi\ell\Delta f\right]$, ℓ=0,1,2...N-1. Δt and Δf are, of course, related by $\Delta t = 1/N\Delta f$. The principle of causality is needed to obtain equation (15) (see Appendix). The real and imaginary parts of $S(f)/j2\pi f$ may not always both have a limit as $f \to 0$. In screening problems it will usually be possible to formulate S(f) so that as $f \to 0$, $S(f)/j2\pi f$ tends to a purely real or purely imaginary number; for example, in the formulation used here for the single screen, as $f \to 0$, S(f) tends to the value given by equation 10, and

$$R(\ell) = \mathrm{Re}\left[S(\ell\Delta f)/j2\pi\ell\Delta f\right] \to -T_D \quad \text{as } \ell \to 0 \qquad (16)$$

In cases more complicated than the one with a single screen, the first sample R(0) was formed by backward extrapolation to $\ell = 0$ ($f = 0$). The imaginary part $\mathrm{Im}\left[S(\ell\Delta f)/j2\pi\ell\Delta f\right]$ does not have a limit as $\ell = 0$, which is why the cosine transform was used rather than the sine transform.

An alternative way of avoiding the problem of the limit at f = 0 in this problem would have been to operate with 1 - S(f) and the sine transform, since $\mathrm{Im}\left[\{1 - S(\ell\Delta f)\}/j2\pi\ell\Delta f\right]$ has a limit as $\ell \to 0$. Physically this implies operating purely on the magnetic 'reaction' field of the screen currents, as contrasted with S(f) which implies operating on the total magnetic field (reaction + applied).

The use of the cosine transform halves the computer storage and time requirements as compared with the full exponential transform. This saving is valuable if accurate results are required, particularly when the transient is oscillatory or varies especially rapidly through time. In such cases the errors, and particularly the d.c. error, are reduced by taking a larger number N/2 of samples, so that the fine structure of both the frequency response and the time response can be adequately represented (i.e. Δf, Δt small). The time taken to compute the time response is proportional to N $\log_2$ N and is otherwise independent of the complexity of the excitation or frequency response functions. For all the results presented in this paper N = 512, and this proved adequate for 1% accuracy without recourse to a data window. The Fortran programme used to compute the transforms was a standard library routine requiring 4 sec execution time (on an ICL 1906A computer).

It is of interest to compare this time with that required to compute S(f). Typically for a 'double screen' problem a Fortran programme based on the transfer-matrix method computed 256 frequency samples of S(f) in 20 sec. In a three-dimensional problem the computation of S(f) would certainly take much longer, while the time required to evaluate the transient response would not increase at all (except as a result of any increase in the complexity of S(f) requiring larger N). This comparison emphasises the flexibility of the transform approach.

4.2 Results

General The results presented below* describe the screening behaviour of cylindrical screening systems in terms of both the screening ratio frequency response function S(f) (Figs 3 and 5) and the transient response to the step of armature current (Figs 4 and 6) computed by F.F.T. In all cases the screening system has the nature of a low-pass filter, as can be seen from the shape of the curves in Figs 3 and 5. Correspondingly the step responses have, broadly, the characteristic 'overdamped' shape of Figs 4 and 6. So far as S(f) is concerned, the frequencies 2 Hz (near the natural oscillation frequency of the rotor), 50 Hz (the system frequency) and 100 Hz (effective negative sequence frequency) are important, whereas the important feature of the transient responses is the maximum rate of change of field. It is difficult to specify precisely what would be acceptable levels for S(f) and dB/dt at the field winding, but values of the order of 0.1 at 2 Hz are 0.001 at 50 Hz for S(f), and a maximum of 1 T/sec for dB/dt, are desirable.

The first pair of graphs (Figs 3 and 4) show the characteristics of a

* All results are for the case p = 1 only

single screen with the field winding open-circuited. The second pair (Figs 5 and 6) show, first, the screening characteristics of a double screening system; and secondly, the effect of short-circuiting the field winding.

Single screens (Figs 3 & 4)

The materials, diameters and thicknesses of the screens are typical of those receiving attention. The solid lines denote stainless steel, and the dotted lines aluminium alloy screens, with the screen thickness marked (in mm) on each curve. As would be expected, S(f) decreases with rising frequency. The transient rise of field strength is shown in terms of the normalised circumferential component h_θ because when the field winding is short-circuited (see below) this is the only component which exists. The screens with the lower S(f) curves produce the slowest rate of rise in H_θ. Screening is improved by increasing both the conductivity and the thickness of the screen. The straight line on Fig 4 shows the constant rate of rise in h_θ corresponding to 1 T/sec, and illustrates that in this particular example, aluminium alloy would be preferable from screening considerations alone.

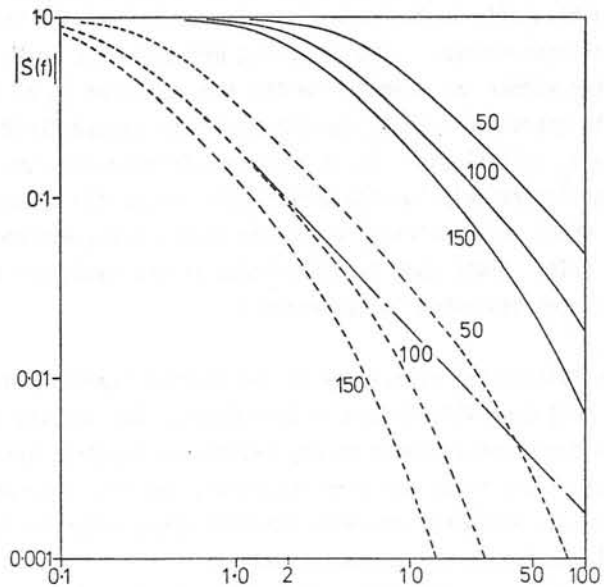

Fig 3 S(f) - single screens

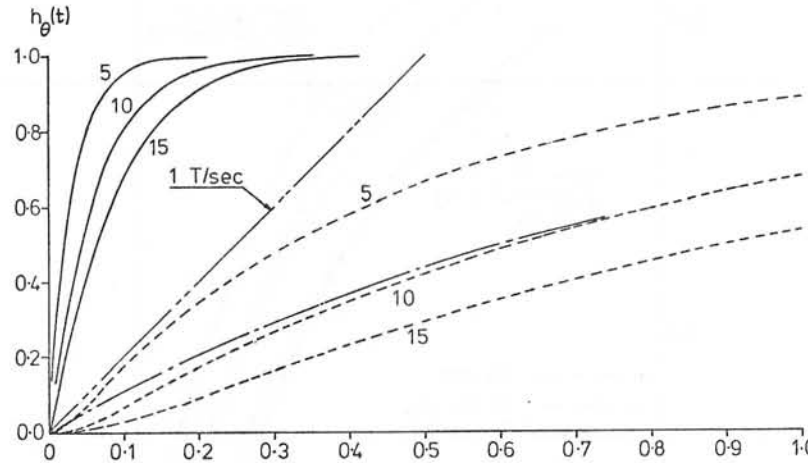

Fig 4 Transient response $h_\theta(t)$ - single screens

In the single screen case an approximate formula is possible (equation 16) and results obtained using this and its inverse transform $1 - e^{-t/T_D}$ are also plotted in Figs 3 and 4. In this simple case the agreement in S(f) is good up to about 5Hz, and the transient response is quite adequate, making it possible to characterise the screening conveniently in terms of the parameter $T_D = \mu r_1 h/2\rho$. The diameter of the screen has little extra effect except through T_D (and $1 - \lambda$, see Section 4.1 and below. $\lambda(r_f/r_1)^2$

Double screens, with field-winding open-circuited

The double screen arrangement has been proposed for its mechanical and thermodynamic advantages[5]. Figs 5 and 6 show some of the properties of a double screen in which the inner has a long time constant (T_{D2} = 1 sec) for good screening, while the outer is designed for maximum mechanical strength and has a shorter time constant T_{D1} = 0.1 sec). Figs 5 and 6 are plotted for three separations between the screens, altered by changing the radius of the inner, and it can be seen from the lower S(f) curves in Fig 5 that when the field winding is open circuited, the separation between the screens has little effect. The lower of the two straight lines on Fig 6 corresponds to 1 T/sec when the field winding is open-circuited and shows that this screening system meets the broad

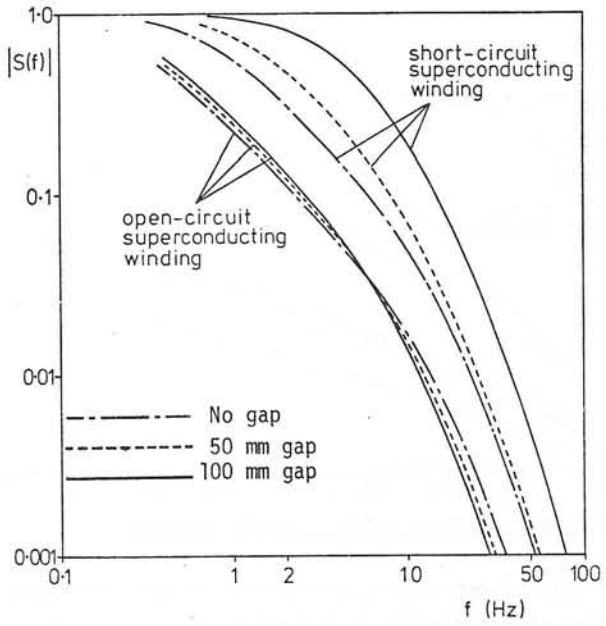

Fig 5 S(f) - double screens

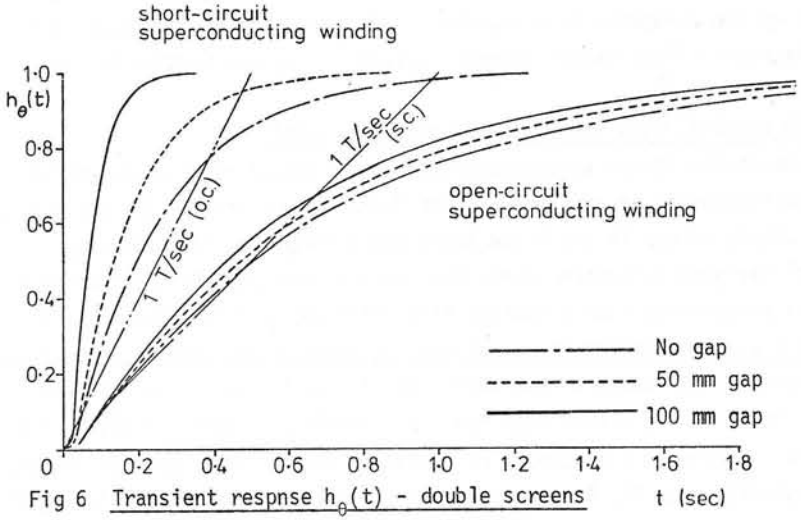

Fig 6 Transient respnse $h_\theta(t)$ - double screens

requirement mentioned earlier in terms of dB/dt.

Double screen with field winding short-circuited

The superconducting winding short circuited at its terminals, or closed through a low* resistance, has a long time constant and behaves effectively in the direct axis as a diamagnetic cylinder or radius r_f. The associated change in the form of the magnetic field inside the screens influences their screening properties, and this can be seen in Figs 5 and 6. Under these conditions the normal field H_r(or B_r) is zero at r_f, while H_θ is increased by a maximum factor of 2. Fig 5 shows that the effect of short-circuiting the field winding is to force S(f) to higher values and, correspondingly, to increase the rate of change of field inside the screen. The effectiveness of the screen is diminished by an amount which depends mainly on the separation between the inner screen and the field winding. In Figs 5 and 6 as the gap between screens widens the approach of the inner screen to the field winding worsens the degradation of screening. In the particular example shown here, Fig 6 shows that the degradation of screening by the field winding causes the maximum rate of rise of field to considerably exceed the prescribed 1 T/sec, particularly in the case with minimum gap between the field winding and the inner screen. The screening effectiveness could be recovered by increasing either the diameter or the time constant T_D of the inner screen. In approximate terms the effect of the closed field winding is to increase T_D to $T_D(1-\lambda)$. It is important to note that the degradation of screening occurs only 'on the direct axis' (i.e. for armature current excitation which is symmetrical about the direct axis) and not on the quadrature axis. This fact is significant in the design of the 'heteropervious' screen described in Reference 1.

CONCLUSION

The flexibility and efficiency of the Fourier Transform method using the F.F.T. have been illustrated in this paper. The ability of the method to find the transient response to any excitation function arises from the independence of the space and time solutions, and this also gives rise to the intermediate frequency response function whose value in physical terms is well illustrated in the screening problem.

The screening characteristics of single cylindrical screens have been briefly described. The double screen has been examined and it has been

* i.e. one which makes the field-winding L/R time constant >> T_D

shown that the separation between screens of fixed time constants has little effect on screening when the field winding is open-circuited. When the field winding is closed through a low resistance, it can have a degrading influence on the screening properties. This influence is worse when the screen is close to the field winding.

REFERENCES

1. Miller T J E and Lawrenson P J: 'Penetration of transient magnetic fields through conducting cylindrical structures', Proc IEE to be published (1976)
2. Cooley J W, et al: 'Application of the FFT to computation of Fourier integrals, Fourier series, and convolution integrals', IEEE Trans, vol AU-15, pp 79-84 (1967)
3. Cooley J W, et al: 'The Finite Fourier Transform', IEEE Trans, vol AU-17, pp 77-85 (1969)
4. Bergland G D: 'A guided tour of the FFT', IEEE Spectrum, vol 6, pp 41-52 (1969)
5. Luck D L and Thullen P: 'Double Shielded Superconducting Field Winding', US Patent No 3 764 835 (October 1973)
6. Smythe W S: 'Static and Dynamic Electricity' (McGraw-Hill, New York, 2nd Edn 1950)
7. Crank J and Nicolson P: Proc Cambridge Phil Soc, Vol 43, pp 50-67 (1947)
8. Smith G D: 'Numerical Soluction of Partial Differential Equations' (O.U.P., 1974)
9. Lim K K and Hammond P: 'Numerical Method for determining the electromagnetic field in saturated steel plates', Proc IEE, vol 119, No 11, pp 1667-1674 (1972)
10. Freeman E M: 'Equivalent circuits from electromagnetic theory: low frequency induction devices', Proc IEE, 121 (10), pp 1117-1121 (1974)

APPENDIX

Since h_θ is real, from equation (14)

$$h_\theta(k\Delta t) = \frac{1}{T}\sum_{\ell=0}^{N-1}\left\{R(\ell)\cos\frac{2\pi k\ell}{N} - X(\ell)\sin\frac{2\pi k\ell}{N}\right\} + \frac{1}{2}$$

with $R(\ell)$ even and $X(\ell)$ odd in ℓ. Splitting h_θ into odd and even parts, $h_\theta = h_{Od} + h_{E\nu} + 1/2$, with $h_{Od} \leftrightarrow X$ and $h_{E\nu} \leftrightarrow R$. If the system is causal, i.e., $h_\theta(-k) = 0$, then it can be shown that $h_\theta(k) = 2h_{E\nu}(k) + 1$.

$h_E(k)$ is evaluated by F.F.T. as

$$h_{E\nu}(k) = \frac{1}{T}\sum_{\ell=0}^{N-1} R(\ell)\cos\frac{2\pi k\ell}{N} \qquad k = 0,1,2\ldots N-1$$

from which equation (15) follows since $R(\ell)$ is even in ℓ.

Evaluation of $H_{\theta 0}$ with K = 1 (step change K of armature current)

If the per-unit synchronous reactance x_d is 0.5 pu and the rated flux-density at the armature winding B_{so} is 1.0 Tesla (these may be regarded as typical values), then 1 per-unit armature current flowing in all three phase windings will produce a flux-density $x_d B_{so}$ everywhere inside the armature winding; thus $B_{\theta 0} = x_d B_{so} i_a$ and $H_{\theta 0} = B_{\theta 0}/\mu_o$.

Discussions following paper:

(Trowbridge) Will you please comment on the way you solve for space part of the problem in your program.

(Miller) See comment by Prof Laurenson (co-author)

(Freeman) I should like to congratulate the authors on the elegant technique they describe in their paper. I would like to comment on the calculation of the frequency response using the transfer matrix method. It is now possible to greatly reduce the time required to calculate the elements of the matrices. Principally, Bessel functions can be completely avoided. Finally, could the authors comment on the calculation of the upper end of the frequency spectrum? How high a frequency is required, and is it possible to use an approximation for the screening ratio?

(Miller) The use of the transfer matrix method is only a particular example of a way of calculating the frequency response in a particular illustrative problem. In a more complicated problem, particularly in three dimensions, the transfer matrix method would not be appropriate with or without Bessel functions. There is no particular difficulty calculating the kind of Bessel functions described in the paper (see also Ref 1).

In the case of cylindrical screens it is possible to use an approximation for the screening ratio of the form $1/(1+j\omega T)$, or even one with more than one pole, provided appropriate values of T can be estimated. In complicated or 3-D problems this often is not possible. It is not necessary to have information at the high frequency end of the spectrum because this only affects the early part of the transient. Roughly speaking, a spectrum truncated at 1KHz will give a corrupt transient response for t< 1 msec only. The degree of corruption is small in this example because S is very small at 1KHz.

(Lawrenson) The space-variable part of the problem is reduced effectively to the solution of the complex Poisson equations and all the well known and efficient methods can be applied to their solution. Accordingly the boundary shapes, conditions etc use no more limited than they are in the static (time-transient) case . The FFT then provides an extremely efficient means of converting their space-variable solution over a range of frequencies (frequency response) into whatever time response is required.

(Steel, CERL) Do the authors anticipate any difficulties in using their fourier transform method if they apply it to system studies which include the power system, the turbine and steam generator? The latter two items have significant non-linearities notably those related to the governor system and therefore the fourier transform must be used with great caution.

(Miller) We do not use the FFT itself to solve the 'system equations' of the governed turbine generator, but only to solve transient magnetic field problems. We are also working on the'system' problem which includes electric circuit equations and non linear differential equations describing the turbine and a.v.r. controls; for this we use a specially formulated method of the 'state space' type which takes into account not only non-linearities but also the frequency dependence of the machine parameters. Incidentally the FFT can be useful here in obtaining frequency-response characteristics from measured time responses on a model machine. Used in this 'identification' problem, the FFT is being used for quite a different application from that discribed in the paper, namely the computation of transient magnetic fields.

(Umstatter, CERN) You mentioned computing times of 20 sec for evaluating the spectrum and 4 sec for the transform. I confirm this experience that the time for transformation of the spectrum is often negligibly short compared to the time required for obtaining it. Could you comment on the speed referred to other, faster computers? I remember computing times of 30 ms for transformation compared to 1 sec for evaluation of the spectrum on a CDC7600.

(Miller) The time taken for the transformation depends on the speed of the computer and the number of samples in the frequency response (or time response). We used a 256-point transform (N=512) on an ICL 1906A

computer, taking 4 sec. I think there are computers capable of doing this much faster but I am not exactly sure what is the fastest possible speed. When the transform takes 4 sec compared with a much longer time for S(f), one is not generally too worried to reduce this time.

(Yeh, Oak Ridge National Lab) How many frequencies are needed to get a good representation for the time-dependent pulse or step funtion?

(Miller) In the particular examples I have used to illustrate the method, we have smooth frequency response functions and smooth time responses, and reasonable results can be obtained with as few as 64 or even 32 points. In general one trades the number of points against accuracy, even with smooth functions, and I have used 256 points (N=512) in all the examples. With a complicated frequency or time functions of course the number of samples must be large enough to reproduce the fine structure.

THE CALCULATION OF MAGNETIC FIELDS IN AIR CORED ELECTRIC MACHINES

Turner D.R., Prior D.L., and Rahim Y.H.A.
Department of Electrical Engineering and Electronics, The University of Liverpool, Liverpool, L69 3BX.

1. Introduction

The work which gave rise to the magnetic field calculations described in this paper, is concerned with the transient terminal performance of air cored alternators, particularly the proposed designs of superconducting a.c. generators.[1] The prediction of transient performance is obtained by a step by step solution of the electric circuit equations,[2] and thus the role of the field analysis was the determination of inductances, both self and mutual. This meant that the methods used in the field analysis did not have to produce accurate values of flux density at all points in space, rather the requirement was for the integral of the flux over a surface (bounded by winding) to be reasonably accurate. There was also the practical requirement that as part of a larger programme the field analysis had to be economical of time.

These two considerations led to the development of a hybrid analytical numerical technique described in the paper and which has proved very successful for the model tested.

2. Description of the Laboratory Model

Plate 1 shows the laboratory model which has been used in the work. It is seen that it has the salient features of the earlier proposals[1] for a.c. superconducting generators, an iron-less magnetic circuit and an outer eddy current environmental screen. Because of the linearity of the problem considered low flux densities are acceptable, and hence room temperature windings are used and these are supported by wooden structures. One feature not shown on the plate is the rotor screen, which is required in the full sized machine to protect the superconducting winding from time changing fields experienced during faults etc. This screen is a thin walled aluminium cylinder which is a sliding fit onto the rotor structure. The latter is connected to a shunt D.C. machine and is balanced to allow operation at 3000 r.p.m.

3. Calculation of the magnetic field including the environmental screen.

a) Numerical solution

The field due to the stator (or rotor) saddle type windings in air is calculated using the Biot-Savart equation[3]

$$\underline{dB} = \frac{\mu J}{4\pi r^2} \underline{dl} \times \underline{r}$$

where $\underline{dl}$ is the vector current element and $\underline{r}$ is a unit vector from the element to the point under consideration. The calculation is organized in such a way that the components of flux density at a point due to the straight portion and the end winding are available separately.

b) Analytical Solution

Because the environment screen, and subsequently the rotor screen, is expected to play a significant role in modifying the field, a solution which includes its effects is necessary. An exact numerical solution would be difficult so a two dimensional analytical solution is obtained and the results modified as explained in subsequent sections.

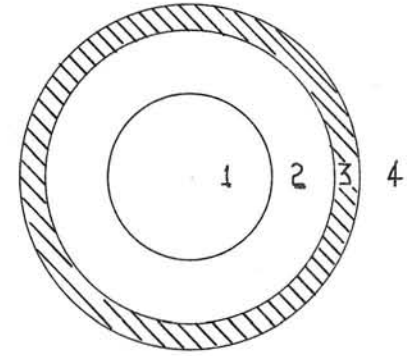

Fig. 1.

Region 1 Winding interior
2 Air
3 Screen
4 Exterior (Air)

Neglecting displacement currents and assuming div A = 0 then Maxwells equations reduce to

$$\frac{\delta^2 A}{\delta r^2} + \frac{1}{r}\frac{\delta A}{\delta r} + \frac{1}{r^2}\frac{\delta^2 A}{\delta \theta^2} = 0 \text{ regions 1 2 and 4}$$

and

$$\frac{\delta^2 A}{\delta r^2} + \frac{1}{r}\frac{\delta A}{\delta r} + \frac{1}{r^2}\frac{\delta^2 A}{\delta \theta^2} = \frac{\mu}{\sigma}\frac{\delta A}{\delta t} \text{ region 3}$$

for the infinitely long system whose cross-section is shown in figure 1. The current in the rotor winding between regions 1 and 2 (considered to be the exciting winding) is represented by a Fourier series

$$k_z = Rc \sum_{n=1}^{\infty} \hat{k}_{zn} e^{-jn\theta} e^{j\omega t}$$

where k_z is line current density.

Application of the appropriate boundary conditions yields the values of the constants in the solutions of the differential equations and hence the radial and tangential flux densities are found using

$$B_r = \frac{1}{r} \frac{\delta A}{\delta \theta} \text{ and } B_\theta = - \frac{\delta A}{\delta r}$$

c) Modification for finite length

Consider a portion AB of a straight wire. (fig. 2). The flux density at P due to a current in this wire is given by

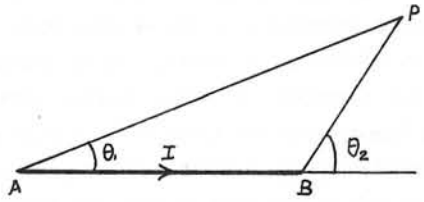

Fig. 2.

$$B_p = B_\infty \frac{\cos\theta_1 - \cos\theta_2}{2.}$$

where B_∞ field due to infinitely long straight wire. Now the model used for the analytical solution may be assumed to have an exciting winding consisting of an infinite number of such current elements, each of which is thus modified by a factor $\frac{\cos \alpha' - \cos\beta'}{2}$, which varies around the machine. Hence the modified, finite length, value of flux density is given by

$$B_{ss} = B_\infty \frac{\cos \alpha - \cos \beta}{2}$$

where B_{ss} is the modified flux density (either radial or tangential) due to the straight length of the exciting winding in the presence of the outer screen,

B_∞ is the solution of the analytical method

and $(\cos \alpha - \cos \beta)$ is the average value of the individual element terms $(\cos \alpha' - \cos \beta')$

The evaluation of this average value showed that it could be obtained by a rapidly convergent series. This modification of the analytical solution yields information about the components of flux density due to the straight portion of the exciting winding, but ignores the end windings which in an ironless machine are important.

d) Derivation of the effect of the endwindings in the presence of the environmental screen

Let B_{sa} be the component of flux density (either radial or tangential) due to the straight portion of the exciting winding, with no screen

B_{ss} as above but with the environmental screen.

B_{ea} the component of flux density due to the end winding, with no screen.

and B_{es} the component of flux density due to the endwinding with screen.

The values of B_{sa} and B_{ea} are derived from the Biot-Savart calculations and B_{ss} by the method described in 3 c). It is assumed that under the steady state operation considered the eddy current screen has a demagnetising effect given by

$$\frac{B_{ss}}{B_{sa}}$$

and hence the value of flux density due to the endwinding with the screen present is given by

$$B_{es} = B_{ea} \frac{B_{ss}}{B_{sa}}$$

and then the total flux density at a point is

$$B_{ss} = B_{ss} + B_{es}$$

This calculation is performed on the spatial components. B_r, B_θ, B_z in turn.

From the solution of the field problem the inductances - stator and rotor self and stator to rotor mutual - are derived by an integration of the radial component of flux density over appropriate surfaces bounded by the windings.

4. Comparison of Predicted and Experimental results

Measurements of flux density at various points in the model were made by search coil techniques under steady state conditions. Some of the results are presented in graphs 1 and 2 which show the measured and predicted flux densities in the axial centre of the machine and at stator and screen radii respectively. In graph 2 the predicted and measured radial flux density were both sensibly zero when the screen was in position.

It is seen that the agreement between predicted and measured values is good, and good correlation of the tangential component at the screen radius (graph 2) is particularly encouraging.

Further evidence of the accuracy of the technique is afforded by a comparison of measured and predicted inductances shown in table 1.

TABLE 1

Parameter	Predicted Value	Measured Value
L_a stator self ind	240 mH	242 mH
L_F field self ind	94 mH	93 mH
M_F field to mutual ind	51 mH	49 mH

The agreement between predicted and measured values of flux density is less accurate near the ends of the screen at radii similar to the screen radius. This is because the technique ignores the circumferential currents in the screen. The effect is however localised and acceptable for the problem considered.

5. Determination of the effect of the rotor screen

Unlike the environmental screen where the steady state performance is the more important, the rotor screen is primarily concerned with transient conditions such as faults. For "thin" screens which could be represented by circuits with constant parameters, it was thought that the steady state parameters would be suitable for the prediction of transient behaviour. Additionally the calculation of the steady state field distribution for the different positions of the screen and exciting winding would be a useful check of the validity of the technique. Some of these field values are given in graph 3, which shows the measured radial flux density at two radii between the rotor and the stator, and the distribution calculated by the analytical/numerical technique. It is seen that the agreement is good.

In the prediction of the transient terminal performance of the machine, the rotor screen is represented by short circuited windings, whose inductance parameters are determined from the field solution.

To evaluate the resistance as a lumped parameter either the technique of Laithwaite [4] could be used, or the power loss of the screen can be evaluated and then it be assumed that the screen is replaced by a specific winding whose resistance is such as to given the appropriate loss. Using the second technique the power loss in a conducting plate of thickness 2b in a magnetic field is such as to give an effective resistance per unit surface area of

$$R = \frac{1}{2\sigma\delta}\,\frac{\sinh(2b/\delta) + \sin(2b/\delta)}{\cosh(2b/\delta) - \cos(2b/\delta)}$$

In this instance it was assumed that the winding which replaces the screen is the same as the rotor winding at the screen radius, whence (6)

$$R = \frac{3\rho}{4\delta}\,\frac{l_t N^2}{\pi r}\,\frac{\sinh(2b/\delta) + \sin(2b/\delta)}{\cosh(2b/\delta) - \cos(2b/\delta)}$$

where ρ = resistivity
δ = skin depth
l_t = length of mean turn
N = number of turns
r = mean radius

In addition to calculating the magnetic field by the previously described technique, the idea of the replacement winding was employed. Once the inductance and resistance parameters of the winding have been determined it is a simple matter to determine the current in the screen by circuit analysis (for steady state operation in this instance), and hence the field distribution can be found using the Biot-Savart equation. The results of this are also presented on graph 3 (broken line) and whilst it is seen that the technique is not as accurate as the analytical numerical technique the results are encouraging.

6) Prediction of Transient Performance

Using the step by step technique of Reddy and Jones [2] and the values of circuit parameters derived from the field analysis, the short circuit performance of the machine can be predicted. Graph 4 shows the experimental and predicted results for a line-line short circuit on the model machine, the agreement between the measured and the predicted values is seen to be good. The broken peaks on the graph of field current show its value when the rotor screen is removed, illustrating the small but definite screening effect of the thin aluminium cylinder.

References

(1) Appleton, A.D. and Anderson, A.F. "A Review of the Critical Aspects of Superconducting A.C. Generators". Proc. of the 1972 Applied Superconductivity Conference, IEEE Pub. No. 72 CH0682-5-TABSC, p 136

(2) Reddy, I.C.T. and Jones C.V. "Line-Line Short Circuit of Synchronous Machines: Illustration of Computer Aided Machine Analysis" Proc. IEE Vol 118, Jan 1971, p 161.

(3) Lawrenson P.J. "The Magnetic Fields of End-Winding of Turbo-Generators" Proc IEE, Vol 108, March 1961, p 538

(4) Laithwaite, E.R. "Induction Machines for Special Purposes" Newnes, London 1966.

(5) Hammond P. "Applied Electromagnetism" Pergamon Press, London 1971

(6) Rahim Y.H.A. Ph.D Thesis "Predictions of the Transient Parameters of an Air Cored Alternator" Liverpool University (1975)

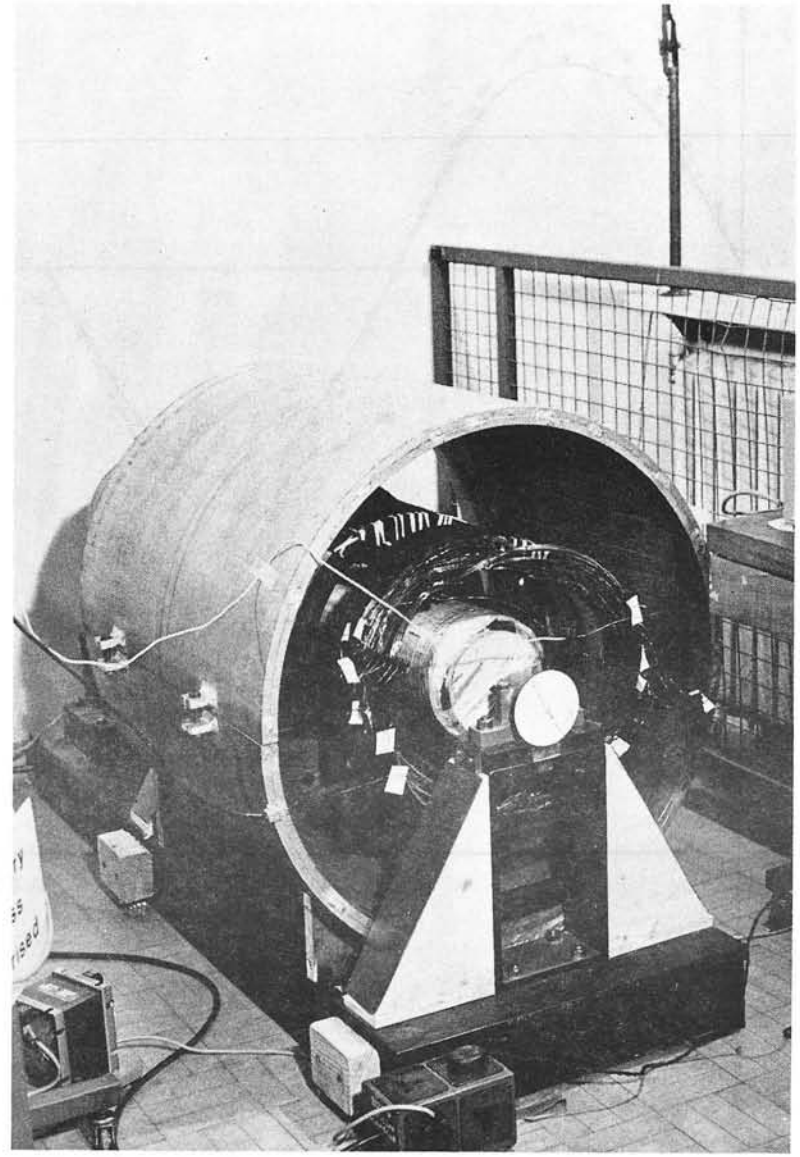

Plate 1 - The laboratory model

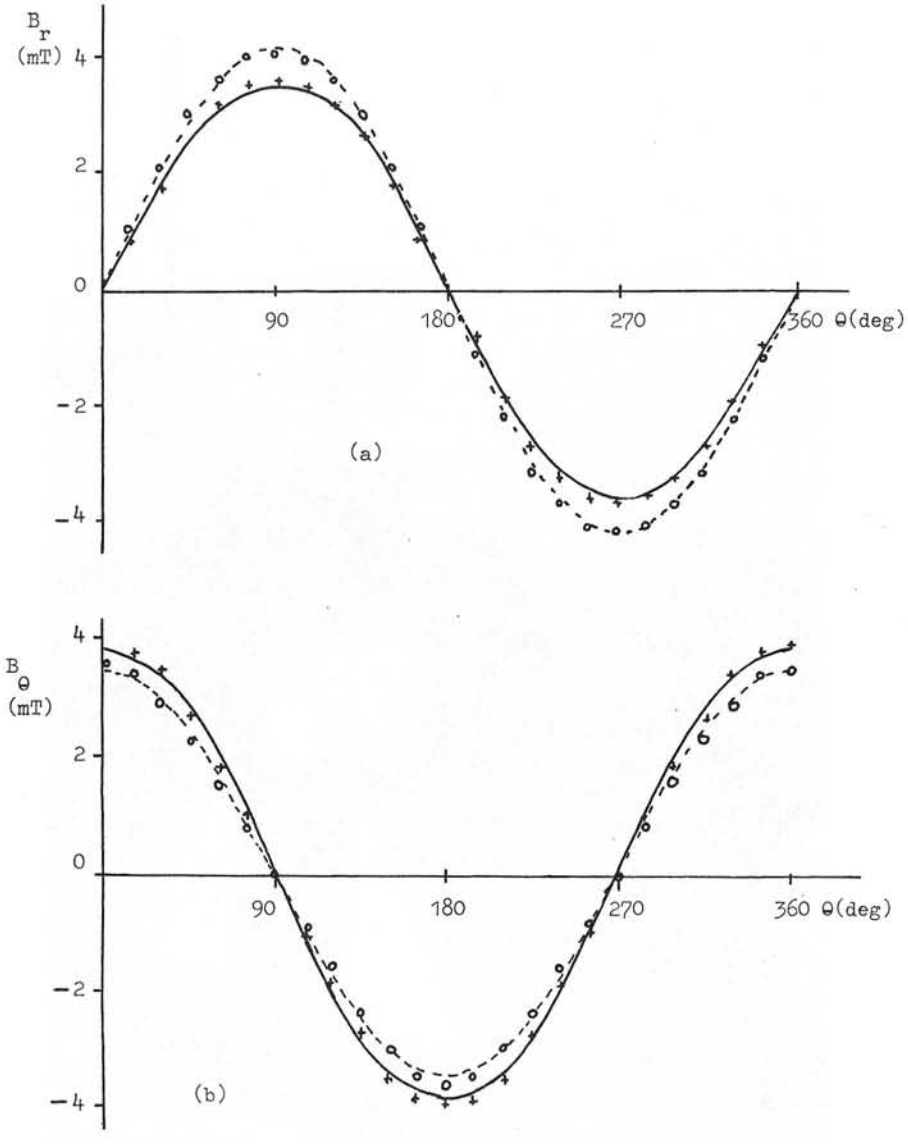

Graph 1 - Flux density at the centre of the stator
a - radial, b - tangential
——— predicted in presence of the sceen
+ + + measured " " " " "
- - - - predicted in air
. . . . measured " "

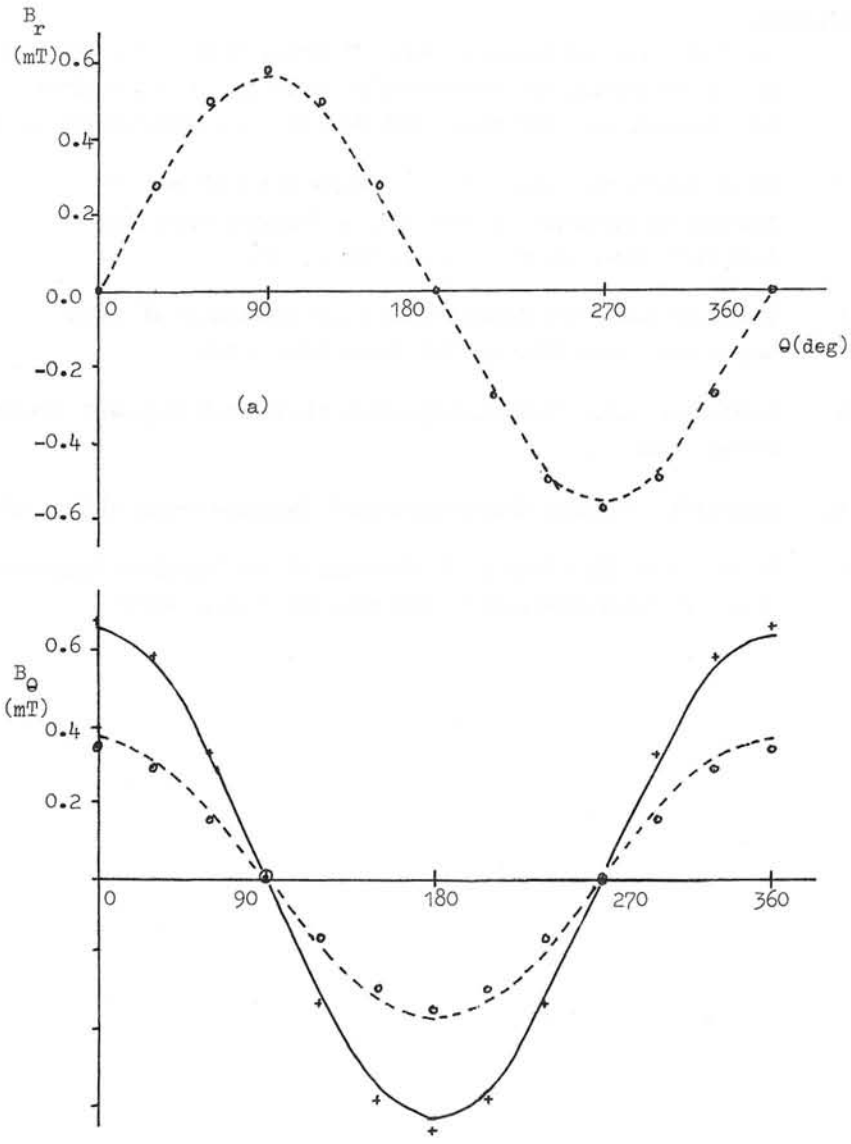

Graph 2 - Flux density at the centre of the screen,
a - radial, b - tangential
——— predicted in presence of screen,
- - - - predicted in air
+ + + + measured in presence of screen,
. . . . measured in air

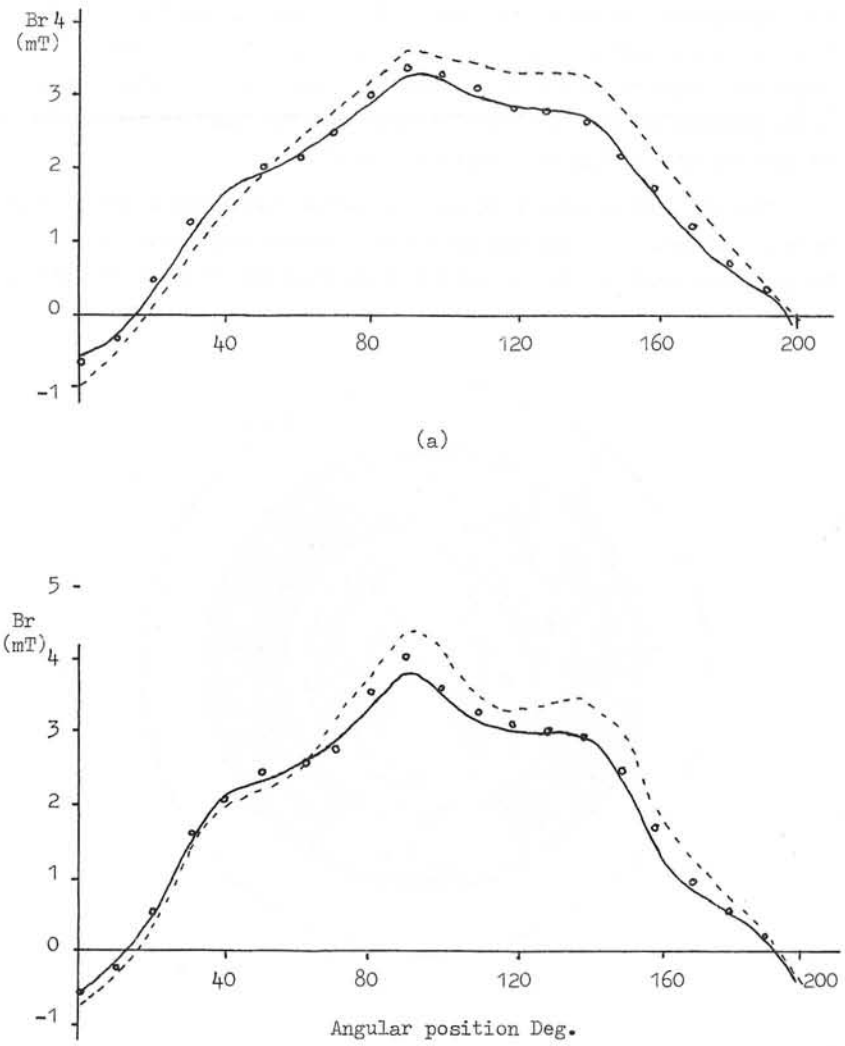

Graph 3 - Variation of radial flux density with angular position at t = 0, and a - r = 13.5 & b - r = 15 cm, using the thin screen.

——— analytical numerical method

- - - - numerical method using winding replacement

. . . . measured

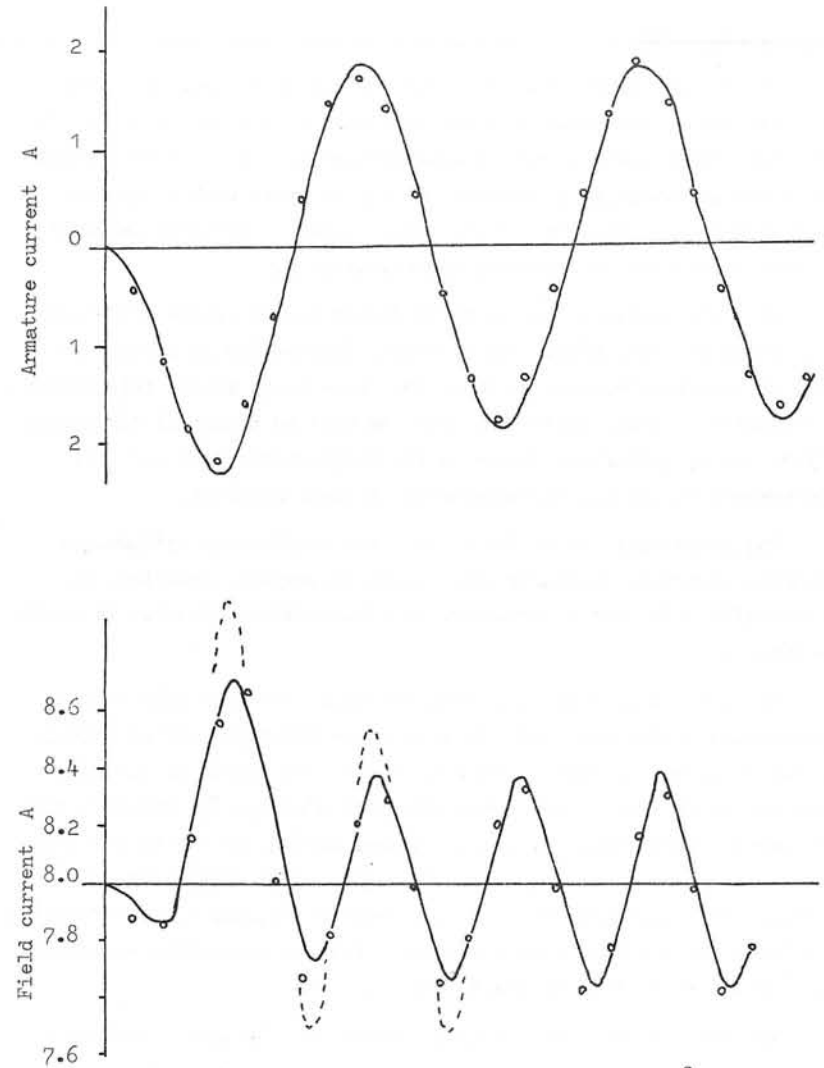

Graph 4 - Line-line short-circuit at = 90°

V_F = 90 V I_F = 8 A

——— predicted

. . . . measured

P. DEL VECCHIO(°); G. SACERDOTI(o) and G.M. VECA(°)

Electromagnetic Behaviour of a Rotating Screen for a Superconducting Inductor of a Synchronous Machine.

1. - INTRODUCTION

The present tendency to increase the specific power of a single unit has led to the study of generators with a power higher than 1000 MVA. For such a power it was thought convenient (1) , both economically and technically, to propose the use of units with a superconducting inductor, in spite of the large number of problems involved in their operation at cryogenic temperatures.

In these machines, the magnetic fields in the stator are higher than those of conventional units, with a dissipation in excitation that is practically equal to zero. The power being equal, this allows a reduction in size, weight and cost, as well as potential advantages (4)(6) during operation, thanks to the comparatively low per-unit synchronous reactance, characteristic of these machines.

The morphology (1)(4)(5)(6) of the synchronous cylindrical symmetry machines, presently under study in various countries, is practically only one; a section of an illustrative character is shown in fig. 1.

The s.c. field winding externally shows, integral with it a cylindrical conducting screen to which many functions are entrusted; in the first place, that of magnetic shield for fields at any rate variable in respect of the superconductive winding; secondarily, that of damper of the rotor swing oscillations during the little and great perturbations. Furthermore, with its high thermal diffusivity, it protects the superconductor from the dangers deriving from overheating. The last, but not the least function is that of preventing vibrations and overstresses in a non stationary state (4).

All these numberless functions cannot be effectively performed by one single conducting cylinder, as proposed in the early works on s.c. generators, as some functions call for characteristics in conflict with one another. It thus became apparent (5) that at least two concentric shields are required: the outer, at room temperature, performing the function of damper, and the inner at the liquid He temperature, acting as a magnetic shield.

For the sake of concreteness, the Authors have considered in this work the screen of a 1300 MVA alternator, with a morphology similar to that indicated in fig. 1, presently in progress of study at ANSALDO

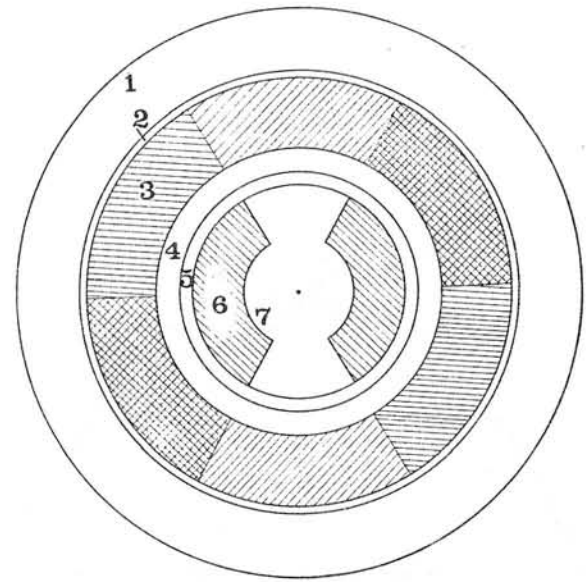

Fig. 1 - Cross sectional view (not in scale) of a synchronous machine with a supercontucting inductor. 1) - Iron magnetic screen 2) - Air gap 3) - Stator windings 4) - Air gap and dewar's place 5) - Electromagnetic screen 6) Superconducting winding 7) - Rotor

(o) of the National Laboratories of CNEN in Frascati.
(°) of the the Electrotechnics Institute of the University of Roma.

of Genoa, and have studied, using the potential vectors analytical method (2)(3)(7), its behaviour at the stationary state proviging numerical results for a special case.

The method , however, has a more general validity and is used also in non stationary cases, as summarily described hereunder.

2. Method for the Determination of the Current Induced in the Screen, and equivalent alternator circuit.

It was pointed out (2)(3)(7), that inside a machine with a morphology similar to that shown in fig. 1, the principle of the superimposition of the effects is valid with an optimal approximation, even if the presence of iron is found outside the stator, on the condition that its saturation is still distant ; with regard to the magnetic field computation within the screen, the additive property was thus applied to the potential vectors determined each time as shown hereunder.

Once a reference system in cylindrical coordinates, fig. 2a) and 2b), is chosen, which is integral with the stator; and if we neglect the edge effect(°), the Poisson -like equation, developed in Fouruer's series for the partial harmonics due to the J current density distribution, will be, as it is well-known, as follows (2)(3):

$$\nabla^2 A_z = -\Sigma \mu J_n \cos n \theta \qquad (1)$$

where

$$J_n = \frac{4}{\pi n} J \operatorname{sen} n \theta_o \qquad (n = 1, 3, 5, \ldots)$$

with "n" being the harmonic order, θ_o the geometric angle with the indicative meaning in fig. 2, and J the current density generating the field, constant along r.

(°) that is, in the assumption of a very long machine in respect of the diameter.

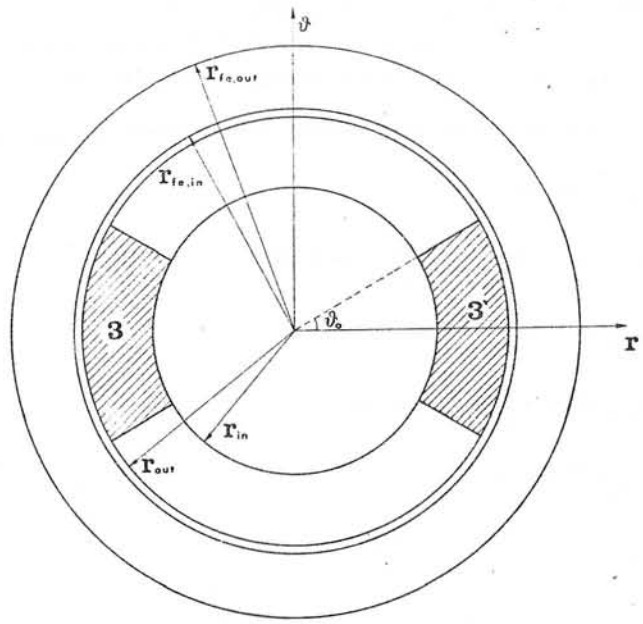

Fig. 2a)
Cross sectional view of stator in which are indicated the geometrical parameters used in the formulas.

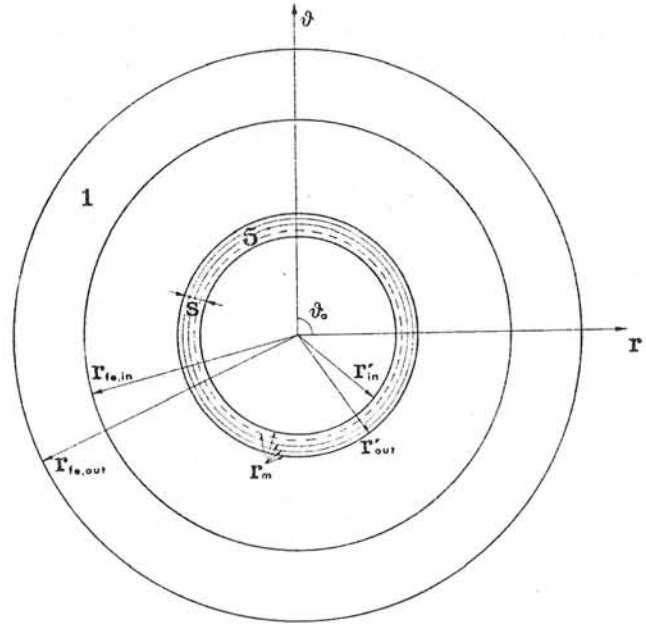

Fig. 2b)
Corss sectional view of electromagnetic screen in which are indicated the geometrical parameters as well as some shells.

From (1), taking into account the fact that physically the magnetic field has a finite value for r = 0 and 0 for r tending to the infinite, the potential vectors relative to the general harmonic "n" in the various regions of the machine are given by the following expressions derived from Coupland[2]:

$$A_{I,n} = J_n A_{i,n} r^n \cos n\theta$$

$$A_{II,n} = J_n (K_r^2 + a_{2,n} r^n + a_{3,n} r^{-n}) \cos n\theta$$

$$A_{III,n} = J_n (a_{4,n} r^n + a_{5n} r^{-n}) \cos n\theta$$

$$A_{IV,n} = J_n (a_{6,n} r^n + a_{7,n} r^{-n}) \cos n\theta$$

$$A_{V,n} = J_n a_{7,n} r^{-n} \cos n\theta$$

where

$$K = - \frac{\mu_o}{4-n^2}$$

and the indices I, II, III, IV, V indicate the following regions of the machine, respectively:

(I): $r < r_{in}$; (II): $r_{out} < r < r_{in}$; (III) $r_{fe,in} < r < r_{out}$

(IV): $r_{fe,out} < r < r_{fe,in}$; (V): $r > r_{fe,out}$

where by r_{in} and r_{out} there were indicated, respectively, the internal and external radius of the cylindrical symmetry winding involved by the current generating field, and the other radiuses have the meaning indicated in fig. 2.

The coefficients a_{1n}, a_{2n},...a_{8n} are derived from relations 2 bearing in mind that in correspondence of the separation surfaces of the various regions, components $B_{rin} = \frac{1}{r} \frac{\partial A_{in}}{\partial \theta}$ and $H_{\theta in} = \frac{1}{\mu} \frac{\partial A_{in}}{\partial r}$, for i = I,II,III,IV, V, are continuous. These coefficients are a function of the geometric parameters alone, and are practically independent from the relative permeability of the iron of stator's outer screen, on condition that $m_{rf} > 20$ (2) (3); they are of the following type:

$$a_{1,n} = - K \frac{n+2}{2n} (r_{out}^{2-n} - r_{in}^{2-n}) + K \frac{n-2}{2n} (r_{out}^{n+2} - r_{in}^{n+2}) \cdot$$

$$\frac{(r_{rf}^2-1)(r_{fe,out}^{2n} - r_{fe,in}^{2n})}{r_{fe,in}^{2n} \left[(\mu_{,f}+1)^2 r_{fe,out} - (\mu_{rf}-1)^2 r_{fe,in}^{2n}\right]}$$

The relations mentioned above and obtained for a case of current density distribution constant over a period of time, can be generalised, for application to the case of rotating machines with a geometry similar to that indicated in fig. 1, taking into account the fact that the J_n density of current will be expressible by means of an analytical law of the following type:

$$J_n (t,\theta) = J_n e^{i(n\theta - \omega_{nt})}$$

characteristic of the rotating magnetic field, consequent to the presence of three windings, of the type shown in fig. 2a), suitably placed in the space, through which there circulate sinusoidal currents dephased in time. In the case in which the three currents form a balanced system, they give birth to a field synchronous with the rotor, without interacting, therefore, with the screen. If we consider instead the presence of the space and time harmonics of an order higher than the first one, and the presence of a dissymmetry in the values of the currents circulating in the three phases owing to a dissymmetrical load, are generated which fields of pulsations $\omega_n = - \frac{n-1}{n} \omega$ not synchronous with the rotor. Therefore, in these assumptions, the magnetic fields that will interact with the screen, will be derived from potential vectors of the type:

$$A_n (t,\theta) = A_n J_n \ell^{i(n - \omega_{nt})}$$

If the screen is divided into "M" shells, as shown in fig. 2b),

the potential vectors due to the stator, calculated in the mid point of the m-nth shell and having a relative movement in respect to it, are given by:

$$A^{o}_{n,m} = a_{1,n}\, r^{*n}_{m}\, J_{o,n}\, e^{j(n\,\theta - \omega_n t)} \quad (m = 1,2...M)$$

where r^{*}_{m} is the mean radius of the m-nth shell and 'o' is the index used for denominating the stator.

Since the screen is divided into M shells, of any Δm thickness (the smaller Δm the better the approximation made by assuming density $J_{m,n}$ as being constant along r), the potential vector of m-nth shell will be given by the sum of the following M+1 terms:

$$A^{o}_{n,m} = F_{o,n}(r^{*}_{m})\, J_{o,n}\, e^{j(n\,\theta - \omega_n t)}$$

$$A^{1}_{n,m} = F_{1,n}(r^{*}_{m})\, J_{1,n}\, e^{j(n\,\theta - \omega_n t + \alpha_{1,n})}$$

$$A^{2}_{n,m} = F_{2,n}(r^{*}_{m})\, J_{2,n}\, e^{j(n\,\theta - \omega_n t + \alpha_{2,n})}$$

$$\cdots\cdots\cdots\cdots\cdots\cdots\cdots\cdots\cdots\cdots$$

$$A^{M}_{n,m} = F_{M,n}(r^{*}_{m})\, J_{M,n}\, e^{j(n\,\theta - \omega_n t + \alpha_{M,n})}$$

where, by $F_{1,n}(r^{*}_{m})$ we intended to indicate the analytical expression of the geometrical parameters relative to the i-nth shell, that contributes in the formation of the field, an expression calculated for $r = r^{*}_{m}$, the medium radius of the shell in which the field is considered.

For example, for the first shell

$$F_{o,n}(r^{*}_{1}) = a_{1,n}\, r^{*n}_{1}$$

$$F_{1,n}(r^{*}_{1}) = k\, r_1^{\,2} + a_{2,n}\, r^{*n}_{1} + a_{3,n}\, r^{*-n}_{1}$$

$$\cdots\cdots\cdots\cdots\cdots\cdots\cdots\cdots\cdots\cdots$$

$$F_{M,n}(r^{*}_{1}) = a_{4,n}\, r^{*n}_{1} + a_{5,n}\, r^{*-n}_{1}$$

where $a_{1,n}$, $a_{2,n}$, $a_{3,n}$, $a_{4,n}$, $a_{5,n}$ are calculated as previously indicated.

From the expression $\bar{E} = -\frac{\partial \bar{A}}{\partial t}$, written in cylindrical coordinates, taking into account the situation under examination and recalling that $\bar{E}_n = \rho \bar{J}_n$, we obtain:

$$\rho_m\, J_{m,n} e^{j(n\,\theta - \omega_n t + \alpha_{m,n})} = \sum_{i=0}^{M} - \frac{\partial A^{i}_{n,m}}{\partial t} \quad (m = 1,2...M) \qquad (3)$$

where by ρ_m we indicated the resistivity of the m-nth shell(°). If we neglect in (3) the dependence on time and angle, we obtain:

$$(4)\quad \rho_m\, J_{m,n} e^{j\alpha_{m,n}} = \sum_{i=0}^{M} - j\omega_n\, F_{i,n}(r^{*}_{m})\, J_{i,n} e^{j\alpha_{i,n}} \quad (m=1,2...M)$$

it being a system of equations in the unknowns $J_{m,n}\, e^{j\alpha_{m,n}}$ with known terms equal to $j\omega_n F_{o,n}(r^{*}_{m})\, J_{o,n}$, that admits univocal solutions, and the greater the fractioning of the screen, the more accurate such solutions will be.

Being thus made known for each shell the $J_{m,n}\, e^{j\alpha_{m,n}}$ distribution of the current density, the determination of the magnetic field within all the points of the machine is immediate, because, the additive property being valid, we will have:

$$(5)\quad \begin{aligned} \bar{B}_{r,n}(r,t,\theta) &= \sum_{i=0}^{M} B^{i}_{r,n} = \sum_{i\neq 0}^{M} \frac{1}{r}\, \frac{\partial A^{i}_{n}(r,t,\theta)}{\partial \theta} \\ \bar{B}_{\theta,n}(r,t,\theta) &= \sum_{i=0}^{M} B^{i}_{\theta,n} = \sum_{i=0}^{M} - \frac{\partial A^{i}_{n}(r,t,\theta)}{\partial r} \end{aligned}$$

where the analytical expression of each A^{i}_{n} is known, and where all its numeric coefficients are also known.

The effectiveness the screen is thus determined by means of the attenuation coefficient as defined by the following ratio:

(°) This resistivity may change with the index "m" as a result of the disuniform distribution of temperature in the screen, and also and chiefly if we consider a multi-shield configuration of the screen, such shields being made of different materials.

$$G_n = \frac{| \bar{B}_{r,n}(r'_{in},t,\theta) |}{| \bar{B}_{r,n}(r'_{out},t,\theta) |}$$

where r'_{in} and r'_{out} are the inner and outer radiuses of the screen, respectively.

It is further possible to determine the Joule power dissipated in the screen as a result of the induced currents, through the following expression:

$$P_n = \sum_{m=1}^{M} P_m = \frac{1}{2} \sum_{m=1}^{M} \rho_m |\bar{J}_m|^2 (r^2_{m,out} - r^2_{m,in})$$

where $r_{m,out}$ and $r_{m,in}$ are the outer and inner radius of the m-nth shell, respectively.

Again, it is also possible to determine the equivalent impedance of a phase of the stator, when the alternator works in a steady condition.

If we indicate by r^*_o the value of the radius which identifies the mean circumference of the stator, the potential vector $A^*_{n,o}(t)$ calculated in r^*_o is given by the sum of its own field plus the summatory of the fields due to the M shells plus the potential due to the field winding:

$$A^*_{n,o}(t) = A^o_{n,o}(t) + \sum_{i=1}^{M} A^i_{n,o}(t) + A^{field}_{n,o}$$

Therefore, the electric field in r^*_o will be due to the field of the currents circulating in the stator plus that due to the derivative made in respect of the time of the total potential vector:

$$\bar{E}_n = \rho_{stator} \bar{J}_{o,n} + \frac{\partial A^*_{n,o}}{\partial t} = (\rho_{stator} + \rho')\bar{J}_{o,n} + j\omega_n L' \bar{J}_{o,n}$$

where by ρ' we indicated an equivalent fictitious resistivity to be summed up to that of stator, which does not represent anything but the sum of the all the contributions in phase with $\bar{J}_{o,n}$ of the summatory $\frac{\partial A^*_{n,o}}{\partial t}$, while L' is the imaginary part.

The equivalent impedance of a stator phase results, therefore, from the following expression:

$$Z_{eq,n} = \frac{(\rho_{stator} + \rho') + j\omega_n L'}{\rho_{stator}} R_o$$

where R_o is the resistance of the winding of a stator phase.
As it is obvious, to calculate Zeq,n with a higher degree of approximation, one should not confine oneself to the calculation of the potential vector $A^*_{n,o}(t)$ on the mean radius r^*_o, but it would be necessary to calculate both the potential vector and the electric field, turn by turn, with reference to the actual winding distribution.

Finally, if we want to consider the more general case of currents at any rate variable throughout time and with no relation between the phases and the amplitudes flowing through the three stator wingings, for the determination of the field generated by the stator, the three distinct contributions of the single windings will have to be considered in order to determine both the current distribution in the M shells of the screen and the mutual couplings of the three phases. Therefore, the total field in any point of the machine shall be calculated by an expression of the following type:

$$(6) \quad A(t) = A_{s,1}(t) + A_{s,2}(t) + A_{s,3}(t) + A_{s,f}(t) + \sum_{m=1}^{M} A_m$$

where $A_{s,1}$, $A_{s,2}$ and $A_{s,3}$ are the potential vectors due to the three stator phases, $A_{s,f}$ is the potential due to the field winding, and the summatory indicates the contributions offered by the M shells.

Assuming to be able to express, by first approximation, for each stator winding, the distribution of the turns with the following formulae:

$$N_{s,1} = N_1 \cos\theta + N_2 \cos(2\theta + \beta_2) + N_3 \cos(3\theta + \beta_3) + .. N_k \cos(k\theta + \beta_k)$$

$$N_{s,2} = N_1 \cos(\theta + \frac{2}{3}\pi) + \ldots\ldots$$

$$N_{s,3} = N_1 \cos(\theta + \frac{4}{3}\pi) + \ldots\ldots$$

where β_k is the angle which takes into account the pitch of the winding, the current density for each phase and for a given harmonic will be given by:

$$J_{n,s,k} = \frac{I_k(t)}{r_o \Delta r \, d\theta} N_{sk} \qquad (k = 1,2,3)$$

where r_o^* is the value of the radius which identifies the mean circumference of the stator whose thickness is Δr.

On the other hand, the voltage induced, by length unit, on each stator winding will be given by:

$$E_k = - \int_0^{2\pi} \frac{\partial A}{\partial t}(t) N_{sk} \, d\theta \qquad k = 1,2,3$$

where the potential vector A(t) will be expressible with relation (6).

Using the above mentioned expressions it will be thus possible to solve all the problems considered for the case in a steady state and also for the unsteady state, even though in the latter instance computations will be more laborious.

Conclusive considerations

For the sake of brevity, the Authors have shown a diagram giving the Joule power dissipated in the screen in the case of one single shield and considering one single amplitude shell proportional to the penetration depth of the frequency field (fig. 3).

The metod may attain an accuracy at any rate high, by reducing the thickness of the shells into which the screen and the stator are divided. This clearly occurs with a marked proliferation of the equations required for the determination of the necessary quantities; the basic value of the method is its intuitiveness and simplicity if a fair compromise is maintained with the desired accuracy. This method also allows to identify a mathematical model, very close to the actual one, that simulates its dynamic behaviour.

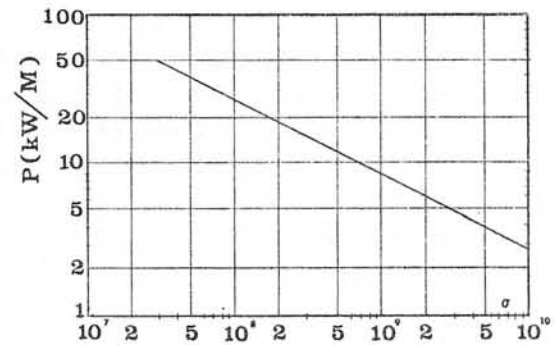

Fig. 3 - Diagram giving the Joule power dissipated in the screen in the case of one single shield and considering one single amplitude shell proportional to the penetration depth of the frequency field. $r_{fe,out}$=1.550 M, $r_{fe,in}$=0.950 M, r_{out}=0.900 M, r_{in}=0.575 M, r'_{out}=0.510 M, r'_{in}=0.500 M
0.169 A/mm^2 backward density current due to an unsymmetrical load.

BIBLIOGRAPHY

(1) - M.J.Jefferies et al., Prospects for superconductive generators in the electric utility industry, IEEE Transactions paper n.T 73.252-4 (1973)

(2) J.H.Coupland, Equations and folmulae for magnets with air cored windings of "saddle coil" tipe, Rutherford High Energy Laboratory Report RHEL/R 203 (1970)

(3) G.Veca et al., Determinazione della distribuzione di corrente negli induttori di turboalternatori con avvolgimenti superconduttivi, Atti e Memorie dell'Accademia Patavina di Scienze, Lettere ed Arti, vol.LXXXVI, (1973-1974), Parte II

(4) T.A.Keim et al., Electromechanically driven and tuned vibrations in superconduting alternators, IEEE PES Winter-Meeting N.Y. January 25-30 1976

(5) D.Luck et al., Double shielded superconducting field winding, U.S.Patent n°3,764,835, Oct.9, 1973

(6) T.H.Einstein -System performance characteristics of superconducting alternators for electric utility power generation, IEEE Trans. PAS-94, n°2, March/April 1975

(7) P.Del Vecchio et al. Comportamento elettromagnetico dello schermo rotorico di un turboalternatore con induttore superconduttore, LNF-75/51(R)

COMPUTER AIDED STEADY-STATE AND TRANSIENT SOLUTIONS OF QUASI-ONE DIMENSIONAL FIELD PROBLEMS IN INDUCTION DEVICES

by Dr. E.M. Freeman
Department of Electrical Engineering, Imperial College, London.

1.1 Introduction

Many induction devices can be represented, in cross-section, by multi-region models, as depicted in Figs. 1 and 2. The excitation is provided by an infinitesimally thin current sheet, which can be sinusoidally distributed in space. The problem is to solve the field equations for the various field components so that the complex power flow and the forces, if any, can be determined. The object of the paper is to show how, by suitable formulation of the problem, a computer may be used to advantage. Initially, the method of solution was purely algebraic and the coming of computers simply saved calculation time. Over the years, computers have been employed at earlier and earlier stages in the solution. Now the point has been reached where very little preliminary algebra is required before the computer can take over both the steady state and transient solutions of the problem.

This is done using two methods based on transmission line analogues. In the first, the transmission line model is represented by strings of micro-T-circuits, each one of which models a short section of line. Then by using a circuit analysis package, such as ECAP or SPICE, the steady state and transient behaviour may be determined. In the second, a scalar Riccati equation is derived for the wave impedance of the model. This method is suitable for sinusoidal steady state problems only.

To illustrate the historical development, reference will be made to two problems. The first is the planar problem with a travelling wave of excitation, Fig. 1, and the second is that of a rotating magnetic field, as in a rotary induction motor, Fig. 2.

The term "quasi-one dimensional" is used in the title. This is because cisoidal variations of the field in one direction can be included in the analysis. Under certain conditions devices with cisoidal variation in two directions can be modelled, but great care is required.

1.2 Historical development

Purely algebraic approaches to the planar and cylindrical problems can be found frequently in the literature, e.g. references 1, 2 and 3. Separation of variable theory was used to produce a solution in each region. Enclosed regions required two arbitrary constants and unbounded regions, one constant. Using the appropriate boundary conditions, algebraic expressions were derived and hence, algebraic expressions obtained for the field variables. Lengthy algebra was often required to obtain closed expressions for power and forces. The advent of computers initially made little difference. The computer was used simply to calculate numerical values from the algebraically derived expressions. The number of regions was limited by the vast amount of algebraic manipulation required. As a first step in introducing the computer to the problem, as other than a calculator, some authors solved numerically for the arbitrary constants, e.g. ref. 4. For an N-region problem, there are $(2N - 2)$ arbitrary constants. It was thus necessary to invert a $(2N-2) \times (2N-2)$ matrix with complex coefficients. This is time consuming and could require a large computer.

It was possibly Pipes[5], who first showed, in a machines context, that a transfer matrix could be used to simplify the problem, by linking a pair of unknown quantities on either side of a region. The technique was used later for the travelling and rotating wave problems[6,7]. The transfer matrix can be derived algebraically, or numerically, with the aid of a computer. The use of a transfer matrix completely removes the limitation on the number of regions.

The transfer matrix form of solution suggests a transmission line. Indeed, a search of the literature showed that Cullen and Barton[8] had already appreciated this point in a 1958 paper. They took the problem one step further, making use of the concept of "wave impedance" in a machine. This idea was extended in ref. 9 to develop an equivalent circuit, as seen from the terminals, using circuital rather than field quantities. The equivalent T-circuit for a single enclosed region can

be called a macro-T-Circuit. This is to distinguish it from a micro-T-circuit[10], which can represent a very thin or elemental region. The advantages of a macro-T equivalent circuit are obvious, but there are also advantages in sub-dividing conducting regions down into a large number of micro-T-circuits. If this is done, then the device can be represented by a long string of such circuits, in cascade. On most computers some form of circuit analysis package is available. Thus the behaviour of the equivalent circuit can be studied, under both steady state and transient conditions. The transient solution for a multi-region model might otherwise be extremely difficult to obtain[11-13]. The use of higher transcendental functions can be avoided completely, for both transient and steady state operation.

An alternative method has also been developed based on the scalar Riccati equation. This is suitable for sinusoidal steady state solutions only. The custom, in the past, has been to obtain values for the field variables in a device. If, instead one thinks in terms of wave impedance, then the Riccati form of equation may be employed. In its generalised form, it links the wave impedance to the rate of change of wave impedance, with respect to the direction of interest. It was found that the Riccati method was much faster, easier to program and easier to understand, than many of the other methods. Higher transcendental functions are completely avoided, one only needs Maxwell's equations and a suitable integration sub-routine.

In the following sections the two new methods are described in detail.

2.1 Theory of the transmission line for the planar model

The excitation is of the form $K_x = \mathrm{Re}\ K \exp(j(\omega t - ky))$. Hence only E_x, H_y and H_z exist; E_y, E_z and H_x are all zero. Furthermore, there is no variation of the field in the x-direction. It follows that E_x and H_y are linked by the equations[8]:

$$\frac{\partial E_x}{\partial z} = -j\omega\mu H_y \quad \text{and} \quad \frac{\partial H_y}{\partial z} = -E_x(\sigma + k^2/j\omega\mu) \qquad (1)$$

where μ is the permeability of the region under consideration
σ is the conductivity

$k = 2\pi/\lambda$, λ = wavelength

The "transmission line" equations are:

$$\frac{\partial V}{\partial z} = -ZI \quad \text{and} \quad \frac{\partial I}{\partial z} = -YV \qquad (2)$$

where Z and Y are the impedance and admittance per unit length of line.

Hence, comparing coefficients:

$$Z = j\omega\mu \quad \text{and} \quad Y = \sigma + k^2/j\omega\mu \qquad (3)$$

Thus a short section of line, of length g, can be modelled by the circuit shown in Fig. 3.

By joining a number of these micro-T-circuits in cascade, a complete circuit can be assembled, which represents a multi-layer model. The steady state sinusoidal behaviour can then easily be established. The transient behaviour, for any applied E or H waveform, can be found by using a circuit analysis package. At present the author is using ECAP and SPICE. It should not be overlooked that it is unnecessary to feed the details of the circuit into the computer directly. It is usually possible to feed the basic model parameters into the computer, and let the program generate the circuit parameters for the circuit analysis package.

As a check on the method, a simple problem was tried. This was the problem of a conducting semi-infinite half space with a step E or H waveform applied at the surface. This problem is discussed in many text-books, either in the field form, or as an infinite length transmission line.

To model it, as described above, the wavelength is set to zero, and the circuit parameters calculated using equations (3). The transient E and H waveforms were everywhere found to agree very closely with the exact analytical results. Of course, it is necessary to do a certain amount of experimenting in order to find the optimum thickness of a sub-region and the number of such regions. Much depends on the shape of the applied transient and the degree of accuracy required.

2.2 Theory of the transmission line for the cylindrical model

The excitation takes the form $K_z = \mathrm{Re}\ K \exp(j(\omega t - \alpha\theta))$. Hence, only E_z, H_θ and H_r exist. It follows that E_z and H_θ are linked by the relationships:

$$\frac{\partial E_z}{\partial r} = j(\omega\mu/r)(rH_\theta) \quad \text{and} \quad \frac{\partial(rH_\theta)}{\partial r} = E_z(\sigma r + \alpha^2/jr\omega\mu) \qquad (4)$$

Hence $Z = j\omega\mu/r$ and $Y = \sigma r + \alpha^2/jr\omega\mu$ (5)

Thus a short section of line, of length g, can be modelled by the circuit shown in Fig. 4. Note the change of variable from H_θ to rH_θ. Students of Kron's work[14] will appreciate that such transformations are necessary, once one gets away from the cartesian coordinate system.

The range of devices which can be modelled using this technique is wide[7]. It includes not only rotary induction devices, but also the transverse screening problem (where $\alpha = 1$) and the plated conductor problem (where $\alpha = 0$).

The transmission line impedances are a function of radius. The line is thus a non-uniform transmission line[15], closely related to the Heaviside-Bessel line[16].

3.1 The Riccati method

The book by Watson[17] provides a most useful introduction to the Riccati equation. It was named after Count Riccati, who was one of several people interested in a certain form of linear differential equation in the early part of the eighteenth century. In ref. 18 can be found a list of basic references, which the present author has found extremely useful in studying the Riccati equation.

The general form of the scalar Riccati equation[17] is:

$$\frac{dZ}{dr} = P + QZ + RZ^2 \qquad (6)$$

where P, Q and R are given functions of r.

In a transmission line context, this equation relates the rate of change of wave impedance (or admittance) to the wave impedance (or admittance)[18]. Normally, the solution to a transmission line problem implies that the voltage and current distributions along the line are to be established. However, very often distributions are of no use at all, one simply requires to know the input impedance to the line. The object is then to derive an equation of the form shown above. Then, instead of seeking an analytical solution, which could involve higher transcendental functions, the equation is solved by numerical integration.

3.2 The planar model Riccati equation

Looking in the positive z direction, the wave impedance is : $Z = E_x/H_y$. Substituting this in equations (1), and solving for Z, results in the following:

$$\frac{dZ}{dz} = -j\omega\mu + Z^2(\sigma - jk^2/\omega\mu) \qquad (7)$$

To solve numerically, start at $z \gg z_7$ and with Z set to almost any arbitrary value, integrate towards $z = z_4$. Simply remember to change the material parameters at region boundaries and avoid large changes in Z, if necessary by reducing the step length.

This method was tried successfully against the analytical solution for a wide range of planar models. The exercise can be repeated looking downwards, and hence the input wave impedance can be determined at the current sheet, together with the power and forces. Some experimenting is required to get the optimum integration step length. It is usually fairly safe to start with a step length less than 5% of the skin depth of a region.

The method can be extended to determine the macro-equivalent circuit model. This involves three integrations across each region, two in one direction and one in the other direction.

3.3 The cylindrical model Riccati equation

Repeating the exercise for the cylindrical model, looking outwards, one obtains:

$$\frac{dZ}{dr} = -j\omega\mu + Z^2(\sigma - j\alpha^2/\omega\mu r^2) + Z/r \qquad (8)$$

Note the extra term Z/r, but otherwise the equation is of the same basic form.

The advantages of using the Riccati equation are greater here than for the planar model. No Bessel functions are required, and in the case of anisotropic regions, one is spared the problem of dealing with Bessels of non-integer argument[18].

Again the numerical solution was checked against the analytical solution for a wide range of models, very close agreement was obtained.

3.4 General comments

A Riccati type equation can also be obtained for cylindrical induction devices having axially travelling waves[17]. The extension to include simple anisotropy is straightforward and is described in ref. 18.

It is worth noting the following fact. The wave impedance at a point, is purely inductive if, up to that point, no conducting material has been encountered in the integration. The wave 'inductance' can thus be obtained, so saving time, if another frequency is to be considered.

4. Conclusions

Two methods for solving field problems in multi-region induction devices have been described. In the first, it was shown that an equivalent circuit, consisting of micro-T-circuits, could be obtained, which could then be analysed using a circuit analysis package. The method is only limited by the number of nodes that can be accommodated by the package. Any E or H waveform can be applied, and one avoids completely the mathematical difficulties inherent in some of the alternative methods.

In the second method, suitable only for the steady state problem, it has been shown that a Riccati type equation could be easily derived, thus avoiding the use of higher transcendental functions.

Both methods require only the basic field equations and some elementary knowledge of field theory. They are also within, or almost within, the capacity of existing programmable calculators. Bearing the various advantages in mind, it would appear that these techniques could be taught at a much lower level in undergraduate courses than is possible using conventional analytical techniques.

5. References

1 LAWRENSON, P.J., REECE, P. and RALPH, M.C.: "Tooth-ripple losses in solid poles", Proc. IEE, 1966, 113, (4), pp.657-662.

2 PARTS, I.R.: "Electromagnetic field distribution in liquid metal acyclic converters", Magnitnya Gidrodinamika, 1965, VI, 3, pp.127-138.

3 HAGUE, B.: "Electromagnetic problems in electrical engineering", O.U.P., 1929.

4 WILSON, J.C., ERDELYI, E.A. and HOPKINS, R.E.: "Aerospace composite-rotor induction motors", IEEE Trans., 1965, AES-3, Suppl., pp.18-23.

5 PIPES, L.A.: "Matrix theory of skin effect in laminations", J. Franklin Inst., 1965, 262, pp.127-138.

6 GREIG, J. and FREEMAN, E.M.: "Travelling-wave problem in electrical machines", Proc. IEE, 1967, 114, (11), pp.1681-1683.

7 FREEMAN, E.M.: "Equivalent circuits from electromagnetic theory: low-frequency induction devices", ibid, 1974, 121, (10), pp.1117-1121.

8 CULLEN, A.L. and BARTON, T.H.: "A simplified electromagnetic theory of the induction motor, using the concept of wave impedance", ibid, 1958, 105C, pp.331-336.

9 FREEMAN, E.M.: "Travelling waves in induction machines: input impedance and equivalent circuits", ibid, 1968, 115, pp.1772-1776.

10 CARPENTER, C.J.: "Three-dimensional numerical solution of eddy currents in thin plates", ibid, 122, 1975, (6), pp.681-688.

11 SMYTHE, W.R.: "Static and dynamic electricity", McGraw Hill, 1950.

12 CARSLAW, H.S. and JAEGER, J.C.: "Operational methods in applied mathematics", O.U.P., 1948, 2nd ed, Chapters 9 and 10.

13 BRATOLJIC, T.: "Electromagnetic transients in superconducting turbogenerators", City University Electrical Machines Conference, 1974.

14 KRON, G.: "Equivalent circuit of the field equations of Maxwell - I", Proc. IRE, 1944, pp.289-299.

15 KAZANSKY, B.G.: "Outline of a theory of non-uniform transmission lines", Proc. IEE, 1958, 105C, (7), pp.126-138.

16 McLACHLAN, N.W.: "Bessel functions for engineers", O.U.P., 1961, Chapter 6.

17 WATSON, G.N.: "A treatise on the theory of Bessel functions", C.U.P., 1966.

18 FREEMAN, E.M.: "Wave impedance of induction devices using the scalar Riccati equation", Proc. IEE, 1976, 123, (2), pp.145-148.

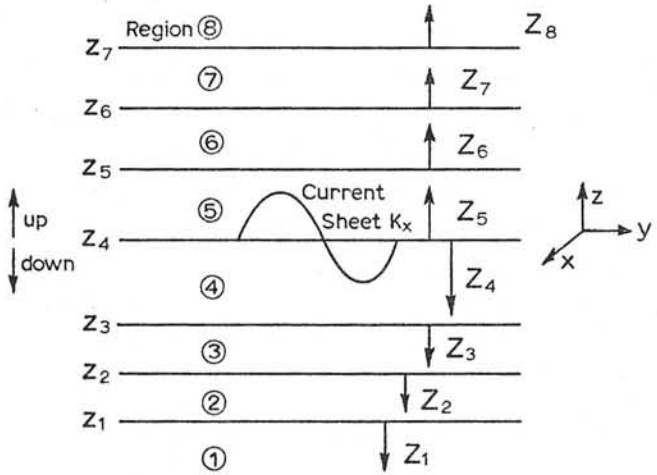

Fig. 1 Multi-region planar model.

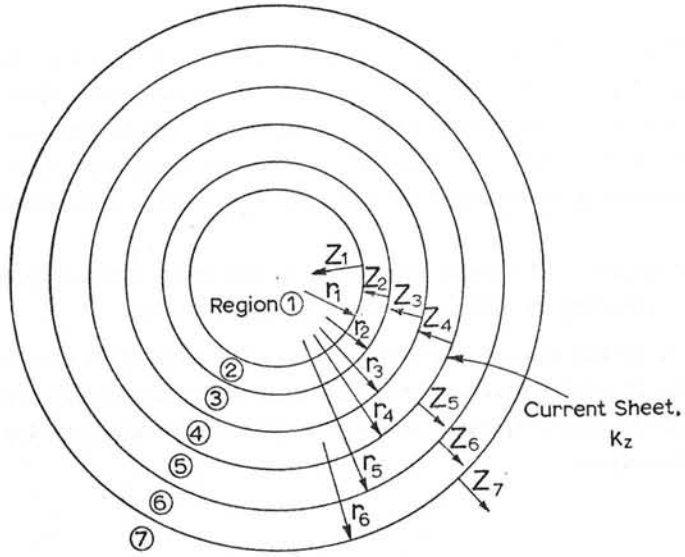

Fig. 2 Multi-region cylindrical model.

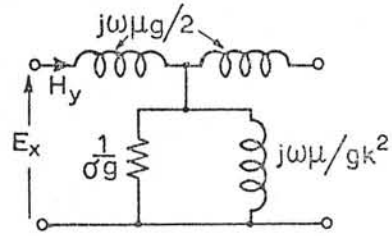

Fig. 3 Planar model micro-T-circuit.

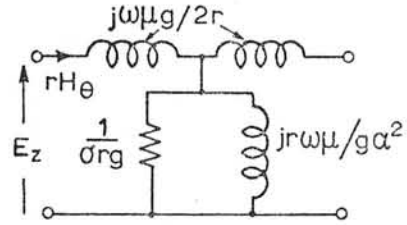

Fig. 4 Cylindrical model micro-T-circuit.

Discussions following paper:

(Miller) I would like to know how the field values at more general field points than at the interfaces can be extracted when using this method. I would also like to know if Dr Freeman can see any way in which the principle of splitting up solid conductors into multiple layers can be extended to deal with fully three dimensional problems?

(Freeman) The field quantities at any point may easily be obtained by introducing an artificial boundary at that point.

The method can only accommodate material variations in one direction. The so called three dimensional multi-layer treatments are really only one-dimensional, with sinusoidal variation of the exciting field in two dimensions.

THE INTEGRAL EQUATION METHOD APPLIED TO EDDY CURRENTS

C S Biddlecombe, C J Collie, J Simkin, C W Trowbridge
Rutherford Laboratory, Chilton, Didcot, Oxon. OX11 0QX

ABSTRACT

An algorithm for the numerical solution of eddy current problems is described, based on the direct solution of the integral equation for the potentials. In this method only the conducting and iron regions need to be divided into elements, and there are no boundary conditions.

Results from two computer programs using this method for iron free problems for various two-dimensional geometries are presented and compared with analytic solutions.

1. INTRODUCTION

In this paper the general eddy current problem is formulated as an integral equation for the potentials and an algorithm for its solution is presented. Results from two programs dealing with two-dimensional limits to the iron free problem are described. The method is an extension of the technique used in the GFUN[1] magnetostatics program.

Formulations of the eddy current problems have been classified by Carpenter[2], who points out that in the integral formulation the scalar potential ϕ has to be included somehow to ensure that the current cannot flow normal to the surface of the conductor. The formulation in A developed here seems the simplest for the general problem, though a formulation in H is also possible for linear problems. A direct solution in terms of J was also considered but in that case the direct imposition of a boundary condition seemed unavoidable, thus nullifying the main advantage of the integral equation method.

2. FORMULATION FOR IRON FREE REGIONS

2.1 The integral equation for the potentials. The basic field equations for eddy currents are[3] in SI units.

$$\nabla \times E = -\partial B/\partial t \quad (2.1.1) \qquad \nabla \times H = J \quad (2.1.2)$$

$$\nabla \cdot B = 0 \quad (2.1.3) \qquad \nabla \cdot J = 0 \quad (2.1.4)$$

$$J = \sigma E \quad (2.1.5) \qquad B = \mu H \quad (2.1.6)$$

that is, displacement currents are neglected, free charges are only present on surfaces, and Ohms Law applies. Also the vector potential A, whose existence follows from (2.1.3), is defined in the Coulomb gauge, so:

$$B = \nabla \times A \quad (2.1.7) \qquad \nabla \cdot A = 0 \quad (2.1.8)$$

The integral equation is to be set up for the potentials so first eliminate B between (2.1.1) and (2.1.7):

$$\nabla \times (E + \partial A/\partial t) = 0 \quad (2.1.9)$$

There is therefore a scalar potential ϕ satisfying from (2.1.5) and (2.1.9):

$$J = \sigma E = -\sigma(\partial A/\partial t + \nabla \phi) \quad (2.1.10)$$

For a region of constant conductivity (2.1.4) implies that ϕ is harmonic within the region ($\nabla^2 \phi = 0$).

The eddy currents are to be calculated in some (multiply connected) conducting region under the influence of a known driving field. That is:

$$A(\underline{r}) = A_o(\underline{r}) + \frac{\mu_o}{4\pi} \int \frac{J(\underline{r}')}{|\underline{r}-\underline{r}'|} dV \quad (2.1.11)$$

in which $A_o(\underline{r})$ represents the driving field and the 2nd term is the vector potential at $\underline{r}$ due to the eddy currents in terms of the current produced at the source point $\underline{r}'$. The integration is over the conducting regions of interest. It is only in the Coulomb gauge that (2.1.11) gives the solution of (2.1.2) for the vector potential due to a current. So in the

integral equation formulation nothing is gained by eliminating ϕ from (2.1.10) by using a different gauge as can be done for differential formulations[2], since ϕ would have to be reintroduced into (2.1.11) to give the equation the right divergence.

Substituting (2.1.10) into (2.1.11) yields the integral equation for $\partial A/\partial t$:

$$\underline{A}(\underline{r}) = \underline{A}_o(\underline{r}) - \frac{\mu_o}{4\pi} \int \frac{\sigma(\underline{r}')}{|\underline{r}-\underline{r}'|} \left(\frac{\partial \underline{A}(\underline{r}')}{\partial t} + \nabla\phi(\underline{r}')\right) dV \qquad (2.1.12)$$

The equation for ϕ is obtained by taking the divergence of (2.1.12) and applying (2.1.8) and Gauss's theorem:

$$-4\pi\sigma(\underline{r})\phi(\underline{r}) = \int \left\{ \frac{\sigma(\underline{s}')}{|\underline{r}-\underline{s}'|} \frac{\partial \underline{A}(\underline{s}')}{\partial t} + \sigma(\underline{s}')\phi(\underline{s}')\nabla \left(\frac{1}{|\underline{r}-\underline{s}'|}\right)\right\} . d\underline{S}$$

$$- \int \left\{ \nabla\sigma(\underline{r}') . \left(\frac{1}{|\underline{r}-\underline{r}'|} \frac{\partial \underline{A}(\underline{r}')}{\partial t} + \phi(\underline{r}')\nabla\left(\frac{1}{|\underline{r}-\underline{r}'|}\right)\right\} dV \qquad (2.1.13)$$

Where $\underline{s}'$ is a point on the surface of the conductor and the 1st integral is over the surface S of the conductor. Physically this expresses the condition that no charge can leave the conductor surface, as can be seen immediately in the constant conductivity, harmonic ϕ situation by taking Green's theorem[4] for a harmonic function and inserting the condition $(\partial A/\partial t + \nabla\phi) . d\underline{S} = 0$, which by (2.1.10) stipulates that no current leaves the conductor. (2.1.13) shows the condition to be imposed at the internal boundary if the conductor contains more than one material, but most commonly the 2nd term in (2.1.13) is zero, which is assumed in what follows. The treatment of the scalar potential is then similar to the integral boundary method formulation for magnetostatics used in[5].

2.2 Discretisation. To solve (2.1.12) and (2.1.13) for $\partial A/\partial t$ and ϕ the conductor is divided into N elementary volumes: L facets of these elements form the surface of the conductor (see Figure 2.2.1). To evaluate the integrals some functional form for the variation of $\partial A/\partial t$ and $\nabla\phi$ within each element must be assumed. For the existing programs,

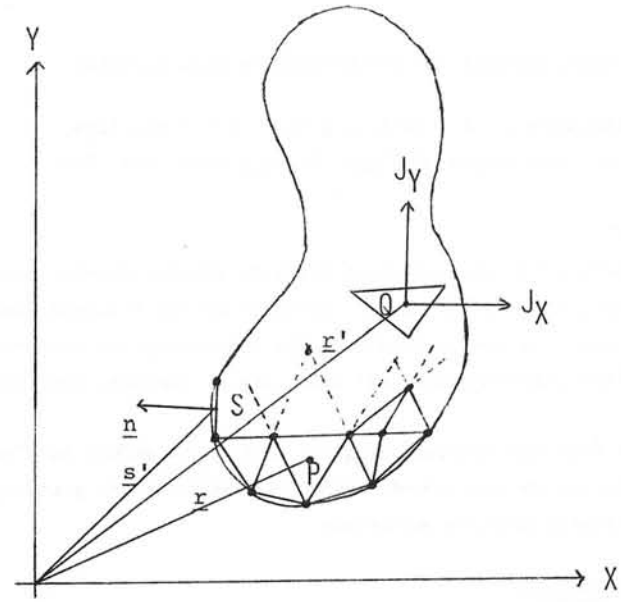

FIGURE 2.2.1 - MESH IMPOSED ON THE CONDUCTING REGION

results from which are described in Section 3, the simplest scheme of constant values for each component of $\partial A/\partial t$ and for ϕ was adopted. Thus (2.1.12) (2.1.13) are approximated by:

$$\underline{A}(\underline{r}) = \underline{A}_o(\underline{r}) + \sum_{N \text{ elements}_j} \left\{ R_j \left(\frac{\partial \underline{A}}{\partial t}\right)_j + R_j (\nabla\phi)_j \right\} \qquad (2.2.1)$$

$$\phi(\underline{r}) = \sum_{L \text{ facets}_k} \left\{ T_k (\phi)_k + U_k \left(\frac{\partial \underline{A}}{\partial t} . \underline{n}\right)_k \right\} \qquad (2.2.2)$$

$$\nabla\phi(r) = \sum_{L \text{ facets}_k} \left\{ V_k (\phi)_k - T_k \left(\frac{\partial \underline{A}}{\partial t} . \underline{n}\right)_k \right\} \qquad (2.2.3)$$

where $\underline{n}$ is the unit vector normal to surface facet k, and (2.2.3) is obtained by differentiating (2.1.13) wrt the coordinates of the field point $\underline{r}$.

The coupling coefficients (R, T, U, V) are simple integrals over the volume or surface of the elements, for example:

$$R_j = -\frac{\mu_o \sigma}{4\pi} \int_{\text{elements}_j} \frac{dV}{|\underline{r}-\underline{r}'|}$$

Expressions for these integrals are given in [6].

By setting the field point $\underline{r}$ to the centre of each element in turn a matrix is constructed acting on 3N components of $\partial A/\partial t$ and L surface values of ϕ:

$$\left[\begin{array}{c|c} G_A & G_B \\ \hline G_C & G_D \end{array}\right] \left[\begin{array}{c} \frac{\partial A}{\partial t} \\ \hline \phi \end{array}\right] = \left[\begin{array}{c} A - A_o \\ \hline 0 \end{array}\right] \qquad (2.2.4)$$

Note that the equations for the components of $\partial A/\partial t$ are coupled through the scalar potential ϕ. This formulation in terms of a constant value for $\partial A/\partial t$ and ϕ within each element accepts a certain mismatch between the facet centre value in (2.2.3) and the element centre values needed when the coupled equations are formed by substituting the $\nabla\phi$ values from (2.2.3) into (2.2.1). This disadvantage would not apply to a higher order variation based on nodal values as the parameters.

Note also that the formulation can be readily adapted to employing a driving electric field ϕ_o instead of the magnetic field A_o.

2.3 Computational procedure. Direct solution of (2.2.4):

$$\left[\begin{array}{c} \partial A/\partial t \\ \hline \phi \end{array}\right] = G^{-1} \left[\begin{array}{c} A-A_o \\ \hline 0 \end{array}\right] \qquad (2.3.7)$$

yields $\partial A/\partial t$ values in terms of the unknown values of A. To complete the solution this set of 3N first order differential equations has to be solved in terms of the initial conditions. Less expensively, the steady state solution for sinusoidal drive fields can be solved by replacing $\partial A/\partial t$ in (2.3.1) by $j\omega$ and obtaining the amplitude and phase lag at each element from the real and imaginary parts of the solution. For the general transient case the numerical solution can be obtained with the following procedure:

(a) Divide the conductor into elements.

(b) Construct G matrix

(c) Set the initial conditions, that is $A = A_o$ at $t = 0$.

(d) Solve for $\partial A/\partial t$ and ϕ.

(e) Advance the solution of 3N differential equations through some time increment.

(f) Update $A_o = A_o(t)$.

(g) Iterate steps (d) - (f) until the required time interval is covered.

Currents, fields and forces may then be obtained at any space time point by using $J = -\sigma(\partial A/\partial t + \nabla\phi)$ and $B = \nabla \times A$, with $\nabla\phi$ from (2.2.3) and $\nabla \times A$ obtained analagously to (2.2.3) by differentiating (2.1.12) so that no numerical differentiation is required.

3. RESULTS FROM EXISTING PROGRAMS

3.1 The scope of the programs. Two special cases of the general iron free problem formulated above have been coded in order to assess the practicability of the method. Both are two-dimensional in the sense that no variation in the Z direction is allowed either for field variables or conductor cross-sections and the conductors extend to $\pm\infty$ in the Z direction.

The first program, called EDDY ONE, allows for only one component of A and J, parallel to the Z axis. For this case there is no ϕ since the electric field is everywhere parallel to the surface. Therefore (2.2.4) reduces to:

$$G_A \left[\partial A/\partial t\right] = \left[A_o - A\right]$$

There is also no mismatch problem (Section 2.2) for this case.

The second program, called EDDY TWO, allows for A_x, A_y, J_x, J_y, but no Z components. For this case the eddy current field is zero outside the conductors. Results from both programs are compared with analytic solutions[7] calculated by applying the Laplace transform method for simple geometries and a uniform step function driving field of 1 Tesla.

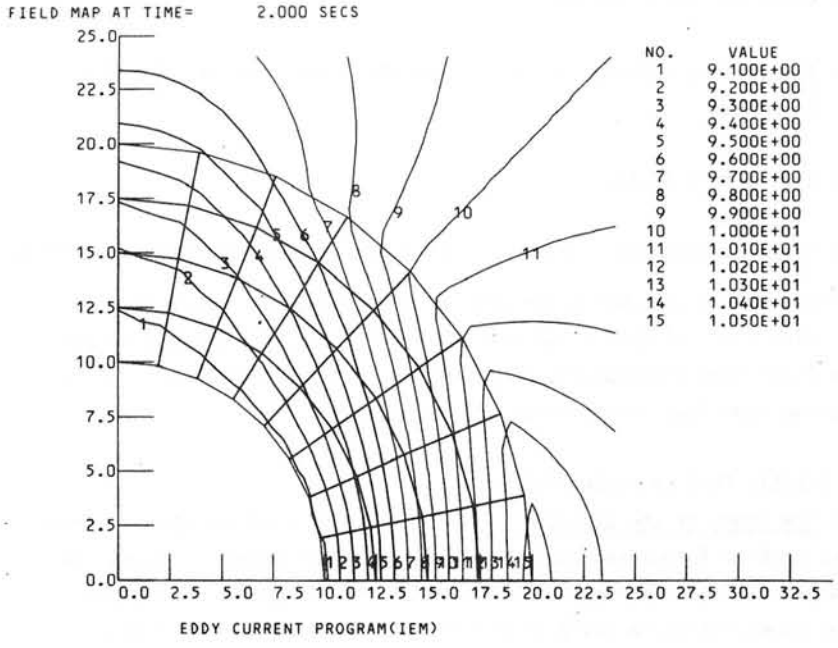

FIGURE 3.2.1 - ELEMENT STRUCTURE AND FIELD LINES IN HOLLOW CYLINDER

3.2 Results from EDDY ONE. Here the analytic comparison is with a hollow cylinder. The cross-section and element structure used by EDDY ONE for one quadrant are shown in Figure 3.2.1, symmetry being exploited to imply the other three quadrants. Figures 3.2.2 to 3.2.4 show the error as a function of time for varying numbers of elements at 3 points: respectively inside the hollow, in the conductor and outside. In all cases the elements were of roughly uniform size including those near the surface so

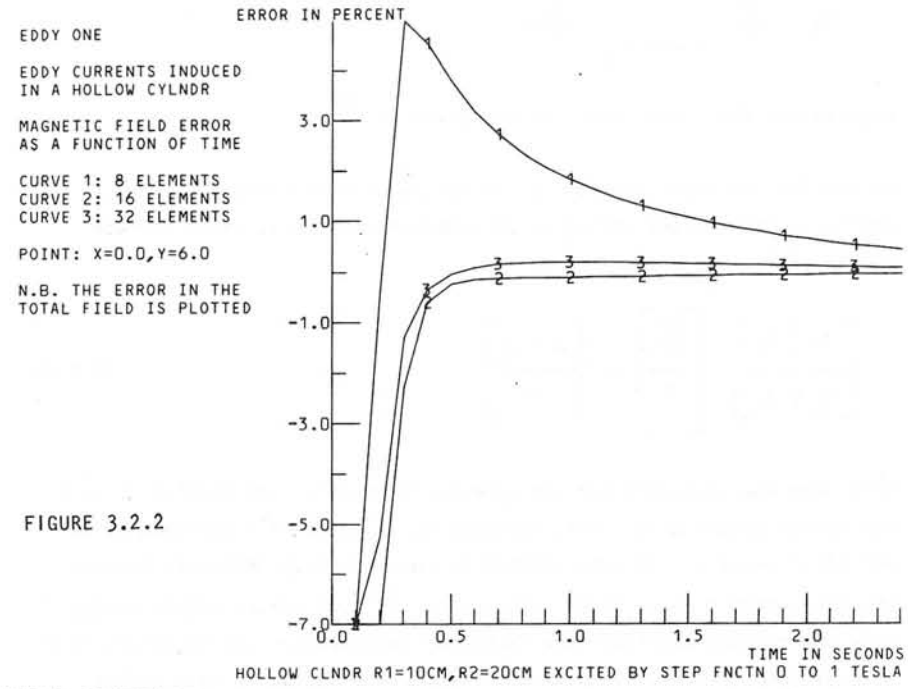

FIGURE 3.2.2

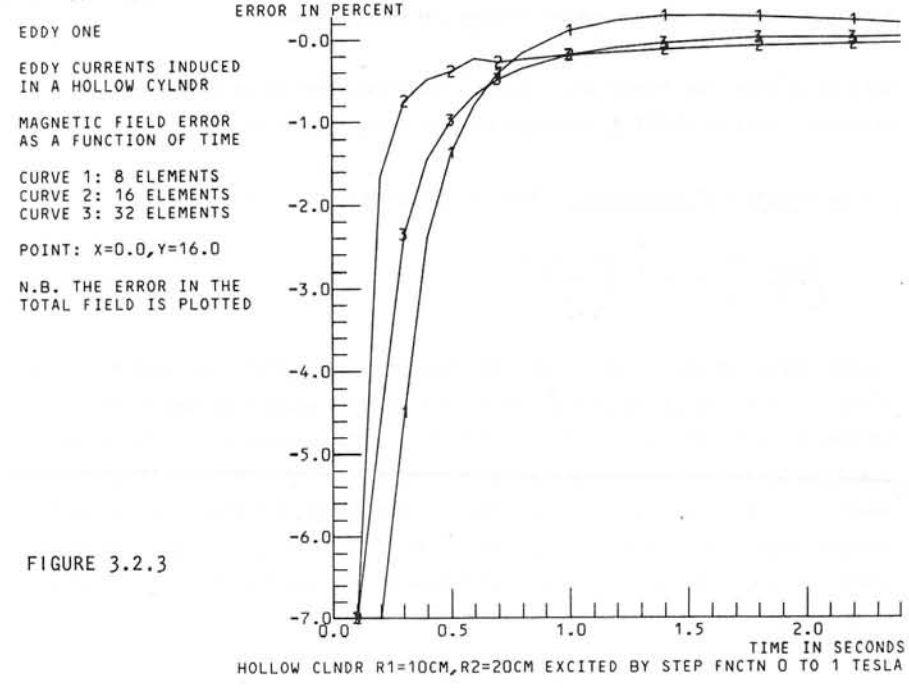

FIGURE 3.2.3

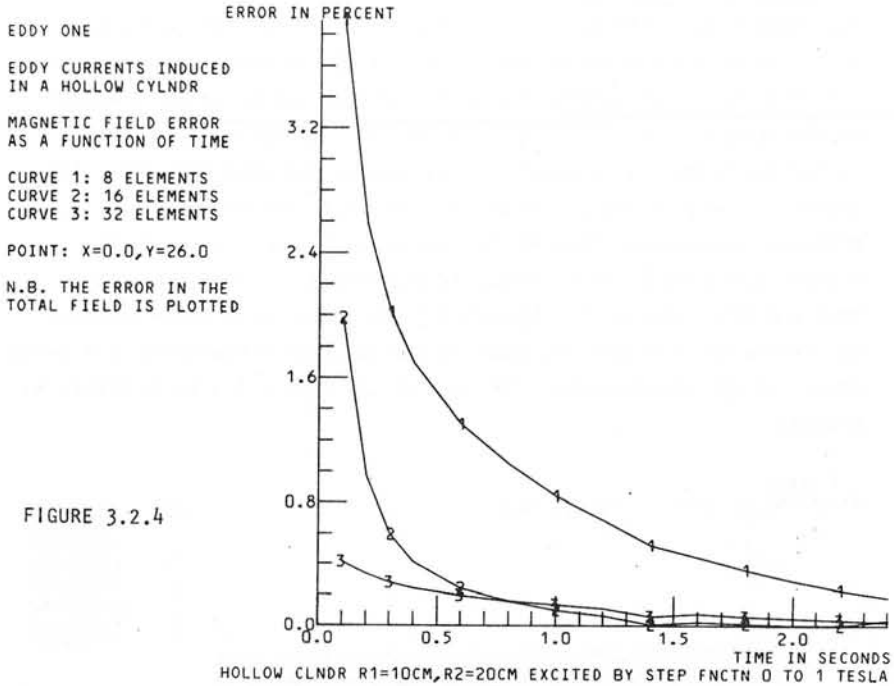

FIGURE 3.2.4

that the element structure is not exploiting knowledge of the skin effect. Convergence for increasing numbers of elements is apparent and the rather greater error for the point within the conductor is to be expected since the further away from the elements the field point is, the less the error introduced by the assumption of constant $\partial A/\partial t$ and $\emptyset$.

Figure 3.2.5 shows another configuration, with the driving field provided by a 50 Hz current (for t > 0) in the 4 outer bars and the penetration of flux into the rectangular tube is illustrated at different times in Figures 3.2.5 to 3.2.7, the latter showing the flux of the eddy currents alone as the driving field crosses the zero axis. The transient eddy current response in one element is shown in Figure 3.2.8.

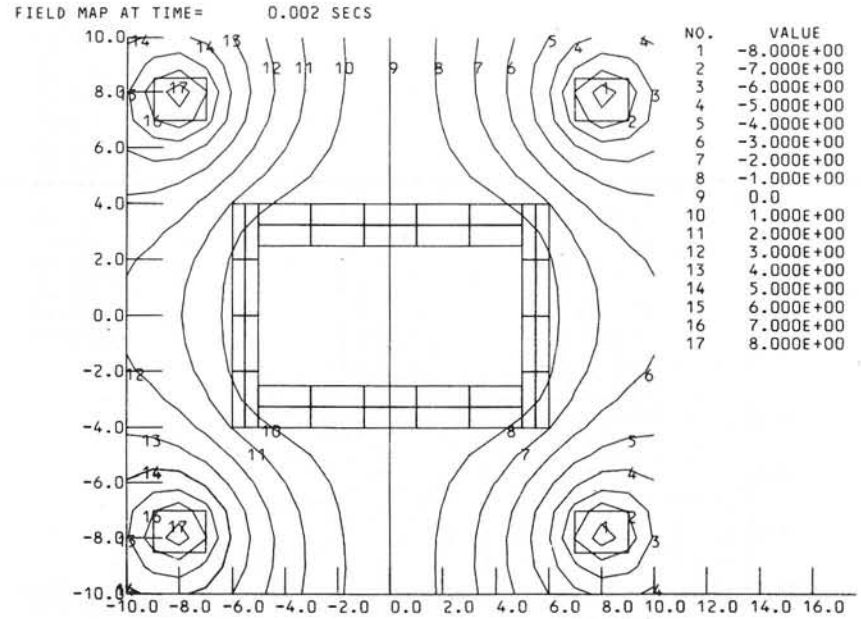

FIGURE 3.2.5 - FLUX PENETRATION INTO RECTANGULAR TUBE,AFTER 0.002 SECS

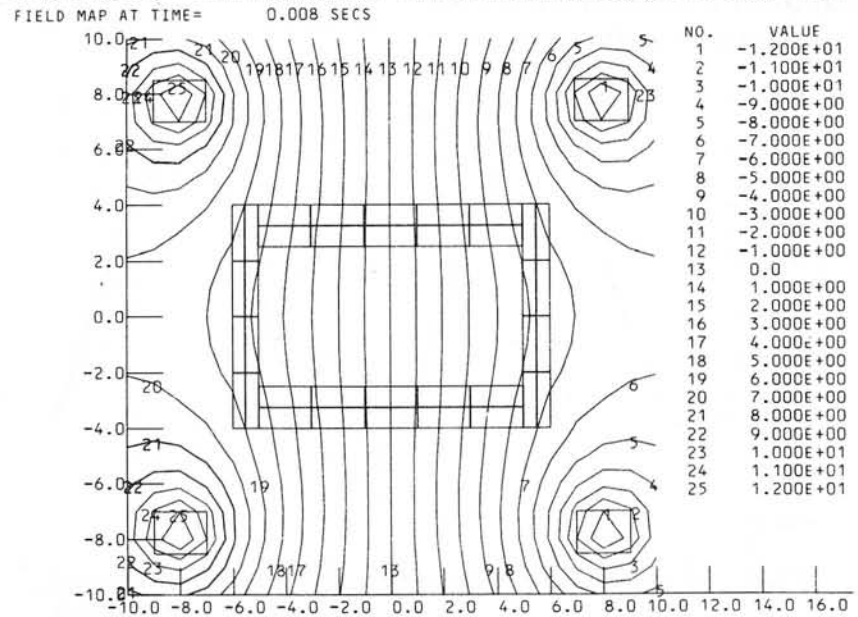

FIGURE 3.2.6 - FLUX PENETRATION INTO RECTANGULAR TUBE,AFTER 0.008 SECS.

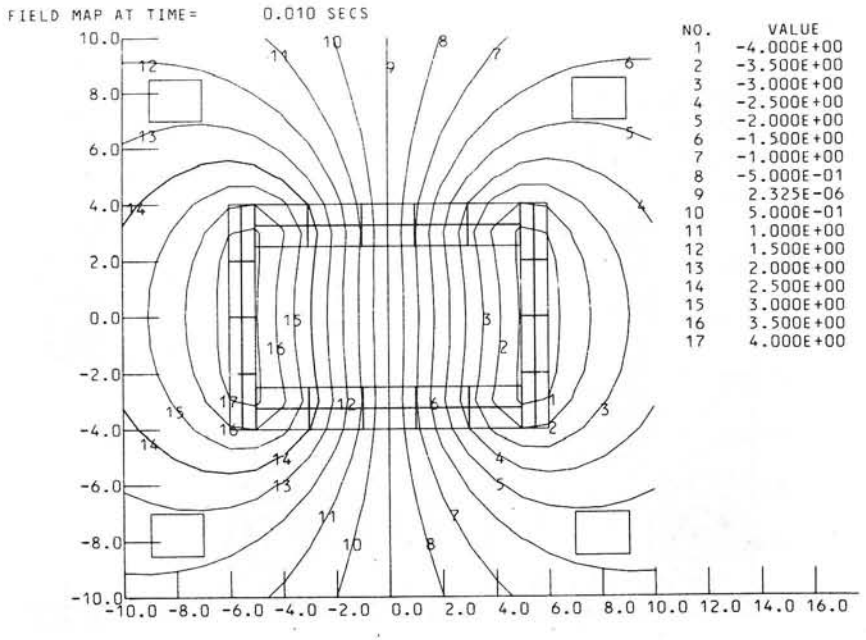

FIGURE 3.2.7 - FLUX MAP AT ZERO OF DRIVING FIELD

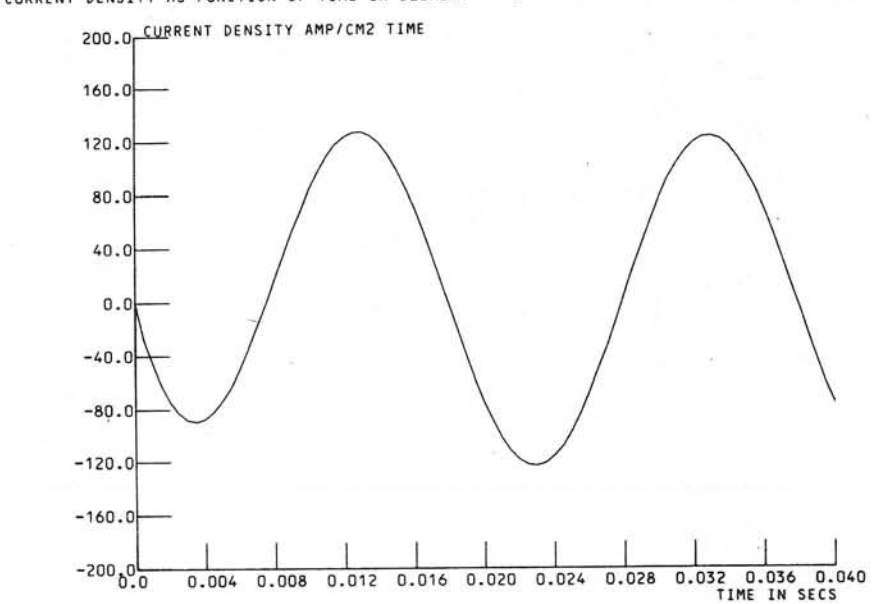

FIGURE 3.2.8 - TRANSIENT EDDY CURRENT RESPONSE TO SINUSOIDAL DRIVE

3.3 Results from EDDY TWO. Here the analytic comparison is with a rectangular bar. The calculated response is illustrated by Figure 3.3.1 the arrows indicating both direction and magnitude of the current. The errors are shown graphically at 3 different points on the diagonal of the rectangle in Figures 3.3.2 to 3.3.4. The convergence with increasing numbers of elements is less happy than with EDDY ONE. The effect of the position of the field relative to the element mesh is probably responsible. Thus at the centre, Figure 3.3.2, in the 96 element model the point is common to 8 elements but to 4 elements in both the other cases. In Figure 3.3.3 the point is in all 8 cases at the centre of an element boundary so the observed convergence to a wrong answer is not unreasonable. The best point, Figure 3.3.4, is within an element.

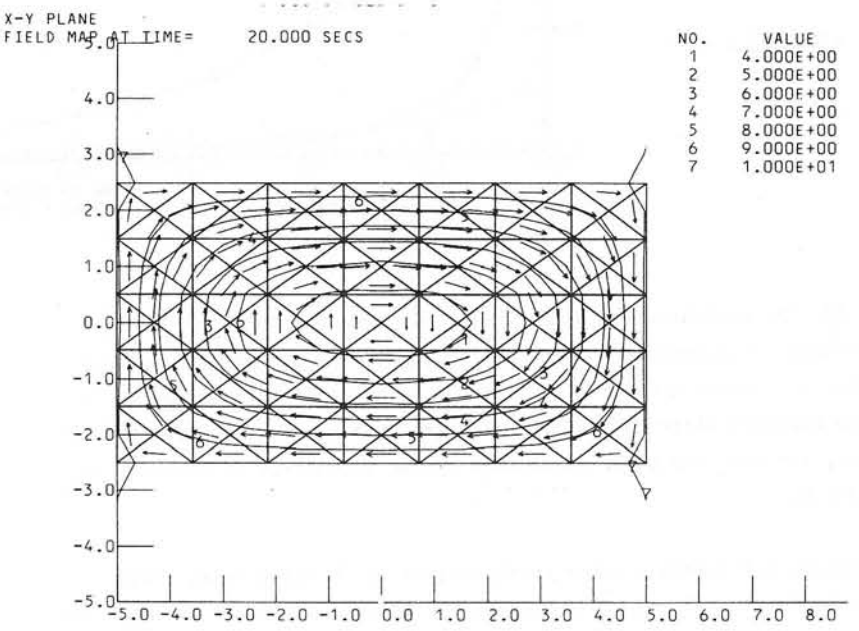

FIGURE 3.3.1 - ELEMENT STRUCTURE, FIELD LINES AND ARROWS REPRESENTING EDDY CURRENTS IN RECTANGULAR BAR

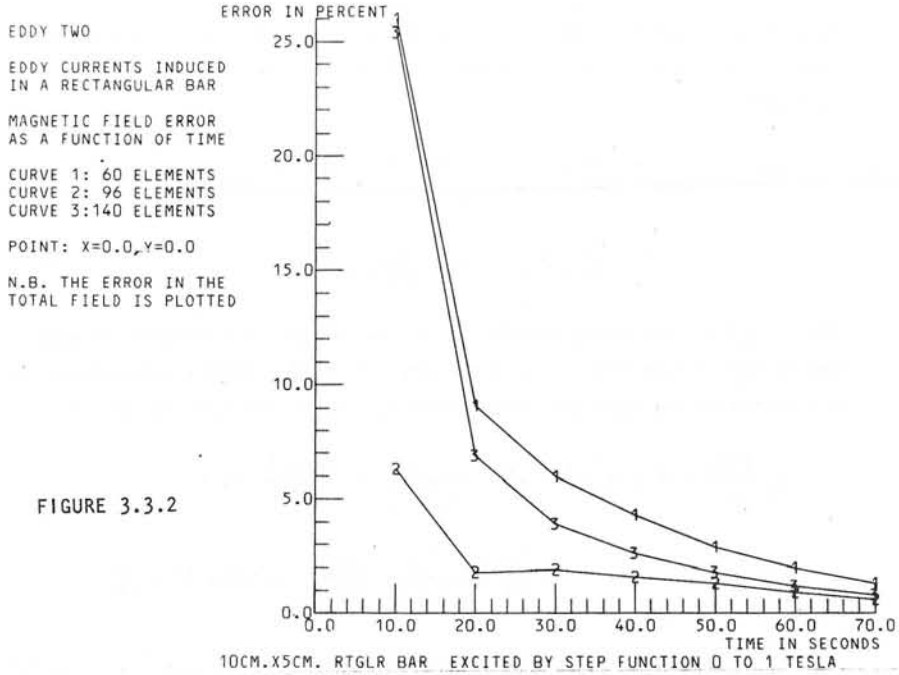

FIGURE 3.3.2

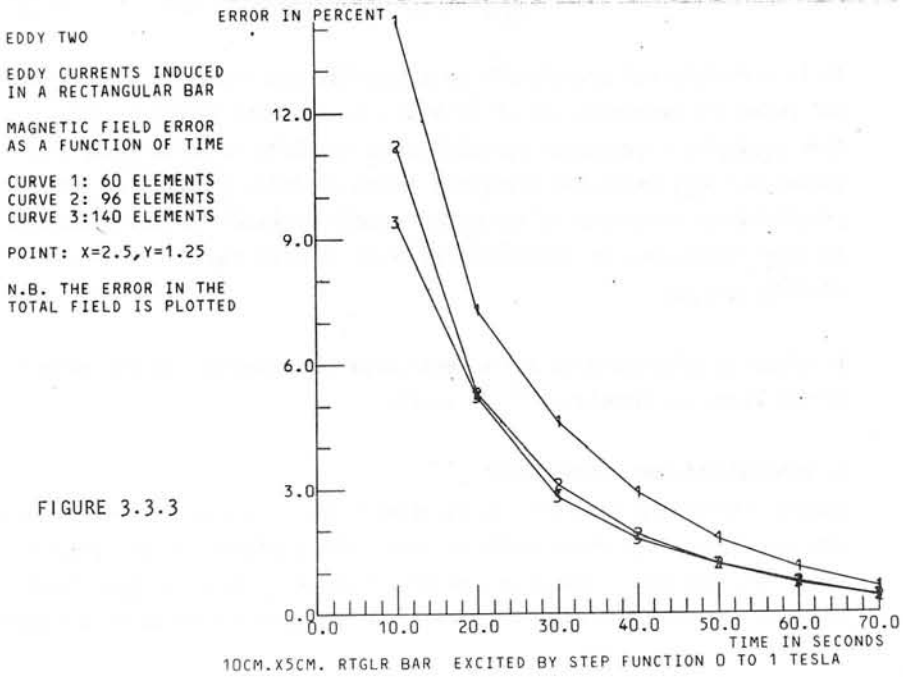

FIGURE 3.3.3

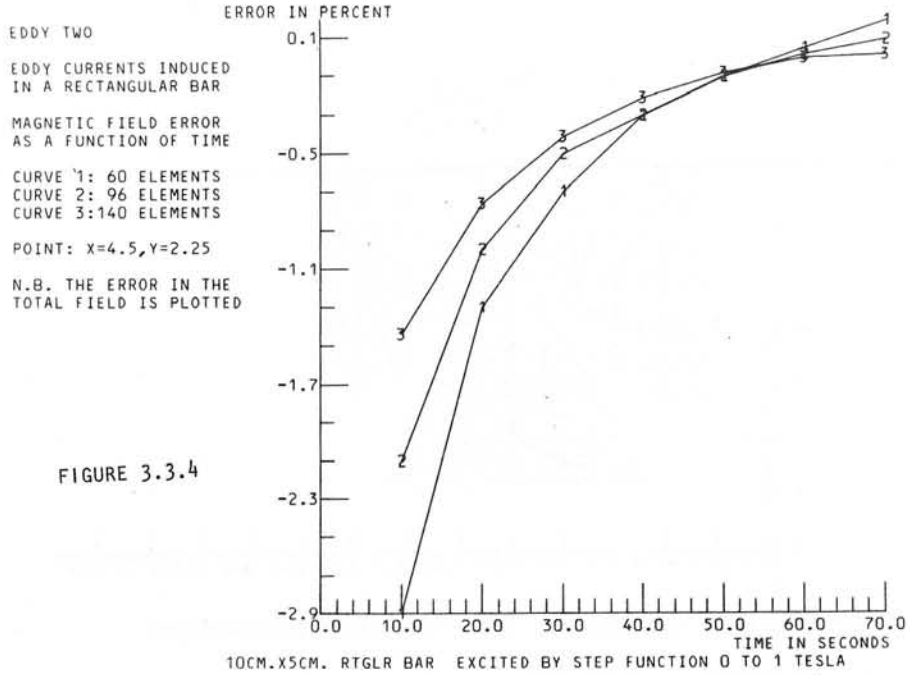

FIGURE 3.3.4

Though the field contours follow the boundary almost perfectly for the case of a rectangle, the final illustration, Figures 3.3.5 and 3.3.6, show the breakdown of this for a more complex shape, and the current direction in the corner is clearly wrong. Hopefully this is due to mismatch error.

4. INCLUSION OF IRON REGIONS

The method could be extended to include regions of magnetically permeable

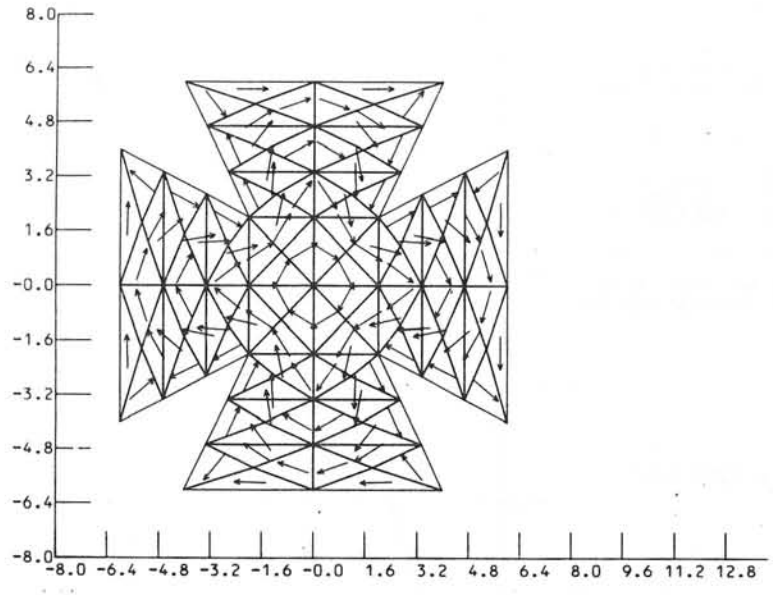

FIGURE 3.3.5 - EDDY CURRENTS IN BAR WITH CROSS SECTION SHOWN

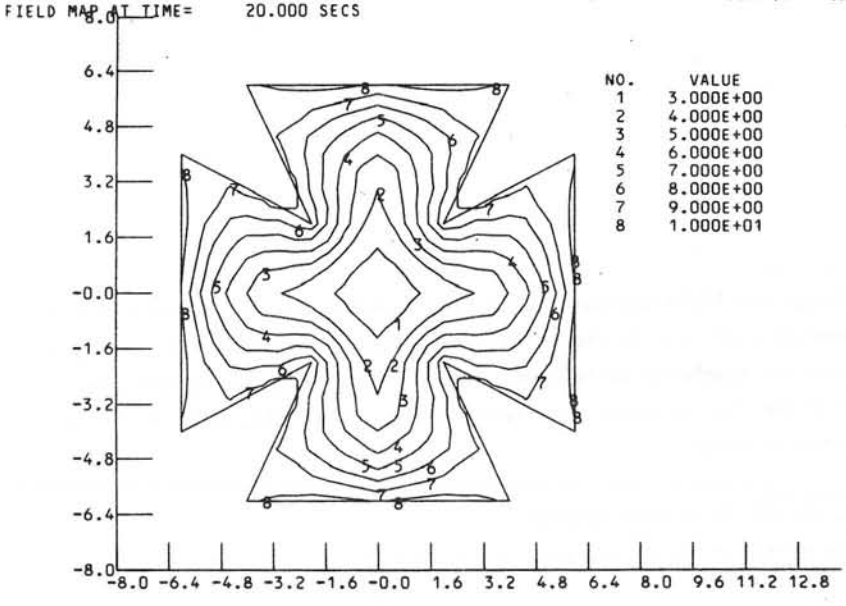

FIGURE 3.3.6 - FIELD LINES IN BAR WITH CROSS SECTION SHOWN

materials by adding a term for the vector potential due to the magnetised region to the integral equation (2.1.12) which becomes (for constant σ):

$$A(\underline{r}) = A_o(\underline{r}) - \frac{\mu_o}{4\pi}\int \frac{\sigma}{|\underline{r}-\underline{r}'|}\left(\frac{\partial A(\underline{r}')}{\partial t} + \nabla\phi(\underline{r}')\right) dV + \frac{\mu_o}{4\pi}\int M(\underline{r}') \times\nabla\left(\frac{1}{|\underline{r}-\underline{r}'|}\right) dV \qquad (4.1)$$

where $M(\underline{r})$ is the magnetisation at $\underline{r}'$ and the second integral is over the volume of the iron. The ϕ equation (2.1.13) remains unchanged, and the constitution equation is obtained by taking the curl of (4.1):

$$\mu_o \frac{M(\underline{r})}{\chi} = \nabla \times A_o(\underline{r}) - \frac{\mu_o}{4\pi}\int \left\{\frac{\sigma}{|\underline{r}'-\underline{r}|}\nabla\times\frac{\partial A(\underline{r}')}{\partial t}\right\}dV + \frac{\mu_o}{4\pi}\int \left\{\frac{\sigma}{\underline{r}'-\underline{r}}\frac{\partial A(s')}{\partial t} + \nabla\phi(s')\right\} \times \underline{dS} + \frac{\mu_o}{4\pi}\int \left\{(M(\underline{r}').\nabla)\,\nabla\left(\frac{1}{|\underline{r}'-\underline{r}|}\right)\right\} dV \qquad (4.2)$$

It is certainly not practicable to discretise the iron into M elements and solve the resulting set of 3N + 3M + L equations simultaneously. Some predictor - corrector approach seems feasible in which (4.2) is solved for $M(\underline{r})$ using the predicted values of $\partial A/\partial t$ and $\nabla\phi$, the same problem which is solved by the magnetostatic program[1]. The solutions for $M(\underline{r})$ could then be substitued in (4.1) to find the corrected values of $\partial A/\partial t$ and $\nabla\phi$.

It might be preferable to use a magnetostatic potential for the effect of the iron, as formulated[8] by Iselin.

5. CONCLUSIONS AND FUTURE WORK.

Having established that this formulation leads to a useful program there are some extensions which could be made. The exploitation of symmetry would considerably increase thd detail in which symmetrical geometries could be mapped. Improved accuracies can be hoped for by using a higher

order basis for the variation within elements, and also by using a more suitably distributed element mesh within the conductors. The coupling coefficients in (2.2.1) to (2.2.3) can be evaluated in a general three-dimensional element[6]. Collectively this should result in a general three-dimensional program for iron free problems.

The major task is to bring the induced current and magnetisation formulations of the Integral Equation Method together and to compare the result with the Finite Element Method, or with a Boundary Integral Method. Any very general program along these lines may be prohibitively expensive and there is clearly a place for steady state versions or, for linear problems, a Fourier transform version.

6. ACKNOWLEDGEMENTS

The authors would like to express their thanks to all the staff of the Rutherford Laboratory who have helped in this work, especially Dr D B Thomas for his encouragement and Mrs E Dawson for her patience with the manuscript.

7. REFERENCES

1. A G A M Armstrong et al. New Developments in the Magnet Design Program GFUN. RL-75-066.

2. C J Carpenter. Computation of Magnetic Fields and Eddy Currents. Proc. 5th Int. Conf. on Magnet Technology, Frascati, 1975.

3. R Stoll. Analysis of Eddy Currents, page 4. Clarendon Press, Oxford, 1974.

4. G T Symm. Potential Problems in Three Dimensions. Numerical Solution of Integral Equations, Ch. 24. Clarendon Press, Oxford, 1974.

5. J Simkin, C W Trowbridge. Magnetostatic Fields using an Integral Equation derived from Green's Theorems. Proc. COMPUMAG Conference on the Computation of Magnetic Fields, Oxford, 1976.

6. C J Collie. Magnetic Fields and Potentials of Linearly Varying Current or Magnetisation in a Plane Bounded Region. Proc. COMPUMAG Conference on the Computation of Magnetic Fields, Oxford, 1976.

7. J C Jaeger. Magnetic Screening by Hollow Circular Cylinders. Phil.Mag. Vol.29, 1940.

8. Ch. Iselin. A Scalar Integral Equation for Magnetostatic Fields. Proc. COMPUMAG Conference on the Computation of Magnetic Fields, Oxford, 1976.

Discussions following paper:

(Becker, University of Texas) 1. Experience with boundary integral equation methods in stress analysis problems has shown that the use of linear (or higher) variation within elements can increase the accuracy per unit of computing cost tremendously. Have you considered the use of higher order elements in GFUN?

2. In our finite element method for transient field problems we have included interfaces between a) different materials.
b) moving and stationary media
Would these present difficulties in the integral formulation?

(Collie) 1. We certainly intend to put in linear variation as soon as possible; the present constant variation technique was adopted simply for speed of implementation, given the existing GFUN coding and is not recommended.

There are problems in introducing higher order variations into the magnetisation routines in GFUN because of singularities on the element corners, these do not occur in the eddy current problem.

2. a) Different materials present no problem, though we should need surface elements over the interfaces between regions.
b) We have not given moving media serious thought. If the media is providing the driving field it should be OK, otherwise we need to do some thinking.

(Yeh) Would you please comment on the amount of computer time needed for solving the transient?

(Collie) Most of the pictures shown took about 1 minute on a 360/195. The present version of EDDY TWO makes no use of symmetry, and when we put this in it should take a few seconds only.

(Newman) To people familiar with finite difference techniques you appear to achieve impressive results with elements whose size is comparable with the dimension of irregularities in the boundary. Is this a feature of the integral equation method?

(Collie) Integration is an intrinsically accurate process numerically, so that for example the constant variation assumption gives a very reasonable average for the effect of 1 element, especially a few element sizes away. However, we pay for our small matrix by having it dense and non-symmetrical.

(Miller) The method appears to solve for four dependent variables, although these are not independent of one another. I would like to know whether there is any special physical significance in the use of the scalar potential ϕ, and whether the problem could in fact be solved solely with the three components of A?

(Collie) ϕ certainly has a simple physical interpretation: charges build up on the conductor surface until their field, $-\Delta\phi$, forces the currents to flow parallel to the surface. This provides the dependence between ϕ and the vector potential.

Mathematically, the integral equation formulation seems tied to the Coulomb gauge, since only then does

$$Ai = \int \frac{j_i}{r} \text{ hold .}$$

A PERTURBATION EXPANSION WITH SEPARATED TIME DEPENDENCE FOR EDDY CURRENT CALCULATIONS*

K. H. Carpenter and H. T. Yeh

Oak Ridge National Laboratory
Oak Ridge, Tennessee 37830 USA

Abstract

A particular solution to the eddy current integro-differential equations is found in the form of a perturbation expansion with separated time dependence. No reference to field values outside the conductor is required and a full three-dimensional treatment is maintained. Transient behavior of the eddy currents is obtained by this method through the technique of fitting the time variation of the driving field with a polynomial in time. As an example, the case of a thin plate of constant conductivity is studied. The eddy current distribution is obtained as a function of time for the external magnetic field of a dipole having ramp time dependence, and with the dipole axis perpendicular to the plate. The effects of the boundary charges in modifying the eddy current pattern are illustrated.

Introduction

Design of structures where pulsed magnetic fields of high magnitude are encountered (e.g., in tokamak fusion reactors[1]) requires knowledge of the eddy currents the fields will produce. Further, because most such systems are quite complex, it is desirable to adopt an integral formulation for the eddy current problem.[2] In the integral formulation, the field values need to be determined only for points in the conductor, but the total external field must be known in advance. This is usually the case. (In the tokamak example the fields due to magnets and plasma are known since the charging and discharging of these currents are programmed or controlled. During quench of a superconductor, although the currents are not programmed, they follow approximately the solutions of the lumped circuit equations, provided the coupling between the induced eddy current and the magnets and plasma is not strong.) Any nearby conductors whose eddies couple strongly to the region of interest need to be treated as a part of the region included in the integral formulation.

Furthermore, in nearly all cases the external vector potential imposed on the conductor can be presented as a finite sum of terms of the form $\underline{\alpha}_o(\underline{r})f(t)$. Thus provided that the conductor is linear (conductivity and permeability independent of field), it is natural to separate out the time dependence from the integral equation by making a perturbation expansion in terms of f and its derivatives.[3] This method still allows for arbitrary time dependence in the external field but avoids the need for introducing a time stepping numerical technique with its related stability problems.

In the following we will develop a perturbation expansion that separates the time dependence from the space dependence of an integral formulation of the potential equations for a linear conducting medium. We will then discuss the convergence of the expansion and show how it can be applied to cases where transient behavior is important by making polynomial fits to the time variation of the exciting fields. Several examples will be presented.

Derivation of Expansion

A. Basic Equations

The basic differential equations for the magnetic vector potential $\underline{A}$ and the electrostatic vector potential ψ in Coulomb gauge inside a linear homogeneous and isotropic conducting medium are

$$\nabla^2\underline{A} = \mu_o\left(\sigma\frac{\partial\underline{A}}{\partial t} + \sigma\nabla\psi - \nabla \times \underline{M}\right) \tag{1}$$

$$\nabla^2\psi = -\frac{\rho}{\varepsilon} \tag{2}$$

$$\frac{\partial\rho}{\partial t} + \frac{\sigma}{\varepsilon}\rho = 0 \tag{3}$$

(All equations are in mks units, and symbols are defined at the end of the paper.) Eq. (3) shows that for typical conductors for which σ/ε is large, ρ will be zero except for charges on the conductor surfaces. Surface charges will require ψ to be nonzero if $\nabla\cdot\underline{A} = 0$ is maintained.

*Research sponsored by the U.S. Energy Research and Development Administration under contract with Union Carbide Corporation.

The integral formulation of Eq. (1) is

$$\underline{A}\ (\underline{r},t) = \underline{A}_o\ (\underline{r},t) - \frac{\mu_o \sigma}{4\pi}\int \frac{\frac{\partial \underline{A}\ (\underline{r}',t)}{\partial t} + \nabla'\psi\ (\underline{r}',t)}{|\underline{r} - \underline{r}'|}\ d^3r'$$

$$+ \frac{1}{4\pi}\left(1 - \frac{\mu_o}{\mu}\right)\int \frac{\left(\nabla' X \underline{A}\ (\underline{r}',t)\right)\ X\ (\underline{r} - \underline{r}')}{|\underline{r} - \underline{r}'|^3}\ d^3r', \qquad (4)$$

where integration is over the region occupied by the conducting medium and $\underline{A}_o$ is the part of $\underline{A}$ due to all sources external to this region. Since $\frac{\sigma}{\varepsilon}$ is large, equations (2) and (3) are replaced by

$$\nabla^2\psi = 0 \qquad (5)$$

$$\frac{\partial \psi}{\partial n} = -\frac{\partial A_n}{\partial t} \qquad (6)$$

Eq. (6) is the boundary condition forcing the normal component of the current density to be zero at the surface of the conductor.

As mentioned in the introduction, linearity makes it sufficiently general to consider the case where $\underline{A}_o$ has the form of $\underline{\alpha}_o f$. In order to obtain a dimensionless form in the expansions to follow we shall normalize the space coordinates of $\underline{\alpha}_o$ by some characteristic length L of the conductor region, and normalize the time argument of f to some characteristic time t_o. Thus all succeeding equations will be in normalized variables.

$$\underline{x} = \frac{\underline{r}}{L} \text{ and } \tau = \frac{t}{t_o} \qquad (7)$$

B. Perturbation Series

One can obtain a particular solution for $\underline{A}$ in terms of the external driving field $\underline{A}_o$ by expanding $\underline{A}$ and ψ in a perturbation series in terms of the derivative of f, with expansion parameter Γ.

$$\Gamma = \frac{\mu_o \sigma}{4\pi}\frac{L^2}{t_o} \qquad (8)$$

The result is

$$\underline{A}\ (\underline{r},t) = \sum_{m=o} \underline{a}_m\ (\underline{x})\ (-\Gamma)^m \frac{d^m f}{d\tau^m} \qquad (9)$$

$$\psi\ (\underline{r},t) = \frac{L}{t_o}\sum_{m=1} \zeta_{m-1}\ (\underline{x})\ (-\Gamma)^{m-1}\frac{d^m f}{d\tau^m} \qquad (10)$$

where the $\underline{A}_m$, ζ_m are recursively related by ($m \geq 0$),

$$\underline{a}_m\ (\underline{x}) = \underline{\alpha}_m\ (\underline{x}) + \frac{1}{4\pi}\left(1 - \frac{\mu_o}{\mu}\right)\int \frac{\left(\nabla_x' X \underline{a}_m\right)\ X\ (\underline{x} - \underline{x}')}{|\underline{x} - \underline{x}'|^3}\ d^3x', \qquad (11)$$

$$\nabla^2\zeta_m = 0 \qquad \text{with} \qquad \text{B. C.} \quad \frac{\partial \zeta_m}{\partial x_n} = -\ (\underline{a}_m)_n \qquad (12)$$

$$\underline{\alpha}_{m+1}\ (\underline{x}) = \int \frac{\underline{a}_m\ (\underline{x}') + \nabla_x'\zeta_m}{|\underline{x} - \underline{x}'|}\ d^3x', \qquad (13)$$

For magnetic conductors ($\mu \neq \mu_o$) recursion relation Eq. (11) is itself an integral equation. Solution of Eq. (11) could perhaps be approached in a manner similar to that of Karmacher & Robertson[4]. We shall restrict ourselves here to non-magnetic case ($\mu = \mu_o$) in which Eq. (11) is eliminated and $\underline{\alpha}_m \equiv \underline{a}_m$. Thus, given $\underline{\alpha}_o$ and f, solution for $\underline{A}$ and ψ reduces to a sequence of solvings of the Laplace's equation with Neumann boundary conditions inside the conductor, and integrations over the volume of the conductor.

The eddy current density and the total field may then be obtained as

$$\underline{j}\ (\underline{r},t) = -\frac{\sigma}{t_o}\sum_{m=0}\ (-\Gamma)^m\left[\underline{a}_m(\underline{x}) + \nabla_x\zeta_m\right]\frac{d^{(m+1)}f}{d\tau^{m+1}} \qquad (14)$$

$$\underline{B}\ (\underline{r},t) = \frac{1}{L}\sum_{m=0}\ (-\Gamma)^m\left\{\nabla_x X\left[\underline{a}_m(\underline{x}) + \nabla_x\zeta_m\right]\right\}\frac{d^m f}{d\tau^m} \qquad (15)$$

C. Convergence of Series and Handling of Transients

In general, the convergence of an expansion such as Eq. (4) requires successive terms to be smaller in magnitude. If the normalization conditions L and t_o are chosen properly this reduces to a requirement $\Gamma < 1$. This condition is similar to that encountered in previous power series solutions of magnetic field problems.[5] Further, as noted above, the solution for $\underline{A}$ provided by Eq. (9) vanishes when $\underline{\alpha}_o$ vanishes and hence is only the particular solution to the (time-dependent) differential equation and not the complete solution.

Choice of the proper characteristic length L to make $\Gamma < 1$ the convergence criterion depends on both the conductor geometry and the distribution of the source field $\underline{A}_o$ in the conductor. Note that for conductors which are thin surfaces, the successive integrations of Eq. (13) each introduce a factor of $(\Delta L/L)$ in addition to a factor of L^{-2} times the mean of the area weighted by the integrand. Thus, the choice of L should be $L = (\Delta L \times \text{mean area})^{1/3}$ to cause successive α_m's to be of the same order of magnitude for thin (non-magnetic) conductive surfaces. Hence, for very thin surfaces L is small and so $\Gamma << 1$ - which yields an eddy current $\underline{j}$ that is essentially the first term in Eq. (14).

The solutions to Eq. (4) with $\underline{A}_o = 0$ will be combinations of exponential decays with time constants proportional to Γt_o. Thus, for small Γ, transient effects die out quickly and $\underline{j}$ is proportional to $\frac{df}{d\tau}$. However, for the case of $\Gamma \lesssim 1$, transient effects cannot be ignored. One way to include them is to replace any discontinuous time functions $f(\tau)$ with an analytic approximation which is valid over a time interval that extends to several times the longest transient decay time constant prior to the time for which Eq. (9) is to be evaluated. Thus any transient effects that are introduced at the beginning of the time interval become negligible by the time we reach the instant for evaluation. Further, if the analytic function used to approximate $f(\tau)$ is a polynomial in τ the series in Eq. (9) terminates, eliminating, technically at least, the convergence question.

In the following examples we use the technique of approximating f by a finite polynomial in τ, assuming that if the polynomial approximates f closely, the results for $\underline{j}$ are also approximated in the same sense. This indeed seems to be the case when the method is applied to an analogous one-dimensional problem where the problem can also be solved analytically.[3]

Examples

A. Numerical Method

We shall illustrate the above method with examples of eddy currents induced in a thin plate by an external dipole, which has a ramp time dependence ($f = 0$, $\tau < 0$; $f = \tau$, $\tau > 0$) in the dipole strength. Numerical calculations were carried out using a PDP-10 computer. f was approximated over a specified range of t by an unweighted least squares fit to a polynomial. (Both α_o and f could be modified by changing the appropriate numerical subroutines). ζ_m of Eq. (12) was determined to within an unknown constant by a standard numerical program for the Poisson equation.[6] $\nabla\zeta_m$ was calculated by central differences. The integration in Eq. (13) was carried out by a two-dimensional trapezoidal rule, with special handling of the element containing the singularity of the integrand.

The numerical method settled quickly to a unique solution as the number of mesh point was increased. Checks on a typical case showed results from a 7 × 7 grid deviated from those of a 21 × 21 grid by less than 4%.

B. Results when $\Gamma << 1$

The first case to consider is for the expansion parameter $\Gamma << 1$. For this case, transients will die away almost immediately following the external excitation, hence $\underline{j}$ is given by the first term of Eq. (14) and no approximation for f is needed.

For the example of a linear ramp, $\frac{df}{d\tau} = 1$ and $\frac{d^m f}{d\tau^m} = 0$, $m \neq 1$. For such a linear ramp there is no time t_o that can be considered a "natural" normalizing value. Instead t_o is chosen to set the time scale to show the amount of detail in t desired while the interval used for τ is fixed — say at $-1 < \tau < 1$. Thus t_o can always be made large, forcing Γ to be small and hence yielding information about only the equilibrium condition. Fig. 1 shows the resulting equilibrium solution for eddy current $\underline{j}$ induced by a dipole of ramp time dependence located half the width of a square plate from the plate with dipole axis perpendicular to the plate and passing through the center of the plate. (If the plate has width 2 m and values of $\sigma = 1.4 \times 10^6\ \Omega^{-1}m^{-1}$, $\mu = 4\pi \times 10^{-7}$ H/m, and $\Delta L = 0.0\ 1$ m are chosen, corresponding to a stainless steel at 4 K, the effective value of the expansion parameter is $\Gamma = 6.5 \times 10^{-3}$ for $t_o = 1$ sec and effective area assumed to be 1 m^2.)

Fig. 2 compares the current density for points along the line connecting the center of the plate to the midpoint of one side for the case above and for the case where the plate is of infinite area and the case where a lumped circuit approximation is used. j_b corresponds to the square plate case of Fig. 1. j_a corresponds to an infinite plate (no edge charge effect), and j_c corresponds to the lumped circuit approximation of a round plate of radius 1.05 m, divided into eleven concentric circular rings each of width 0.1 m. We see that j_c follows j_b closely, passing

through a peak near 0.7 m away from center, while j_a increases monotonically as we move away from the center.

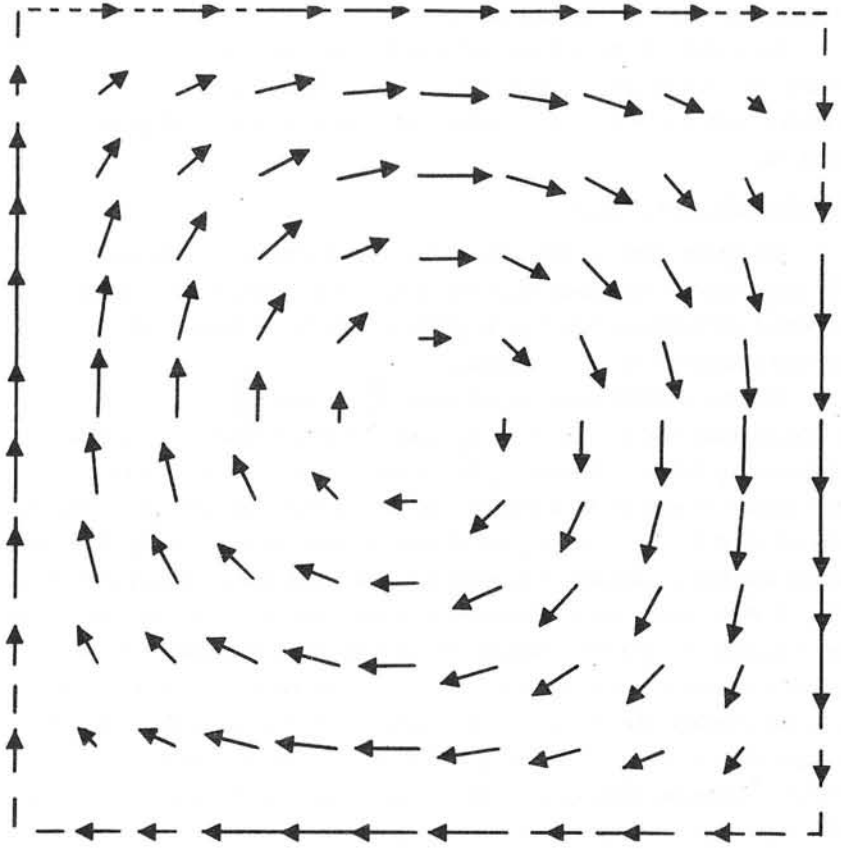

Fig. 1 Eddy current induced in a square plate by a dipole pointing toward the center.

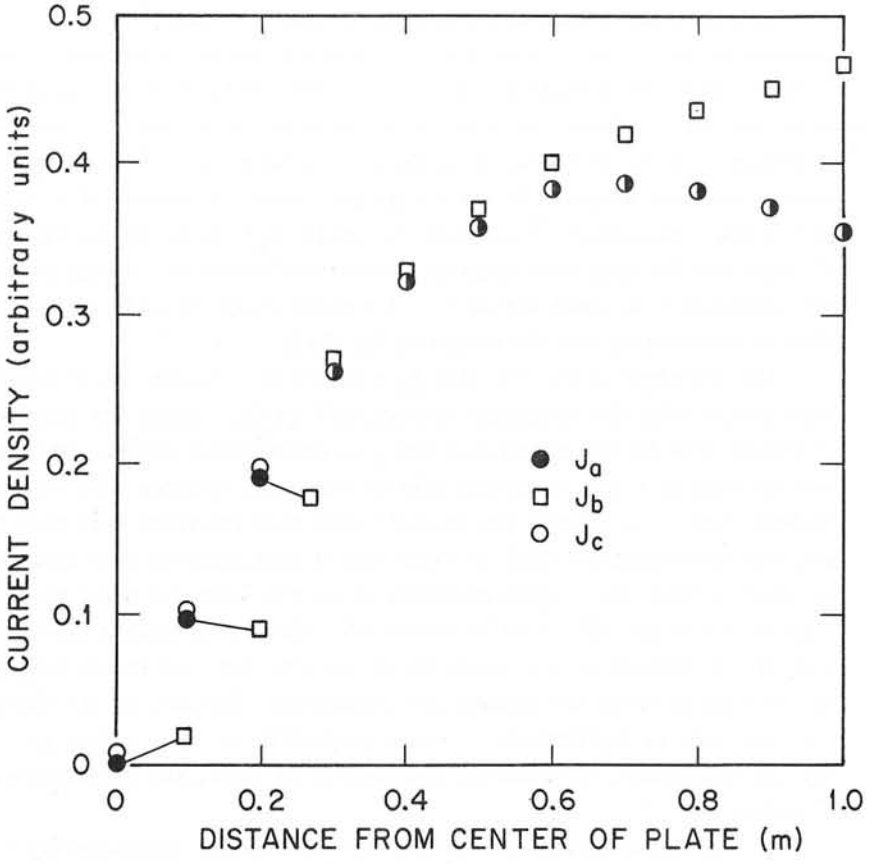

Fig 2 Induced eddy current density along line from center outward of a thin plate for: j_a - infinite plate by perturbation series method; j_b - finite square plate by perturbation series method; j_c - round plate by lumped circuit method.

Another illustration of the edge effect is given in Fig. 3, where the eddy current pattern is shown for the upper right quadrant of the plate in Fig. 1, assuming that the rest of the plate is cut away. We notice that the new boundary significantly modifies the eddy current flow pattern.

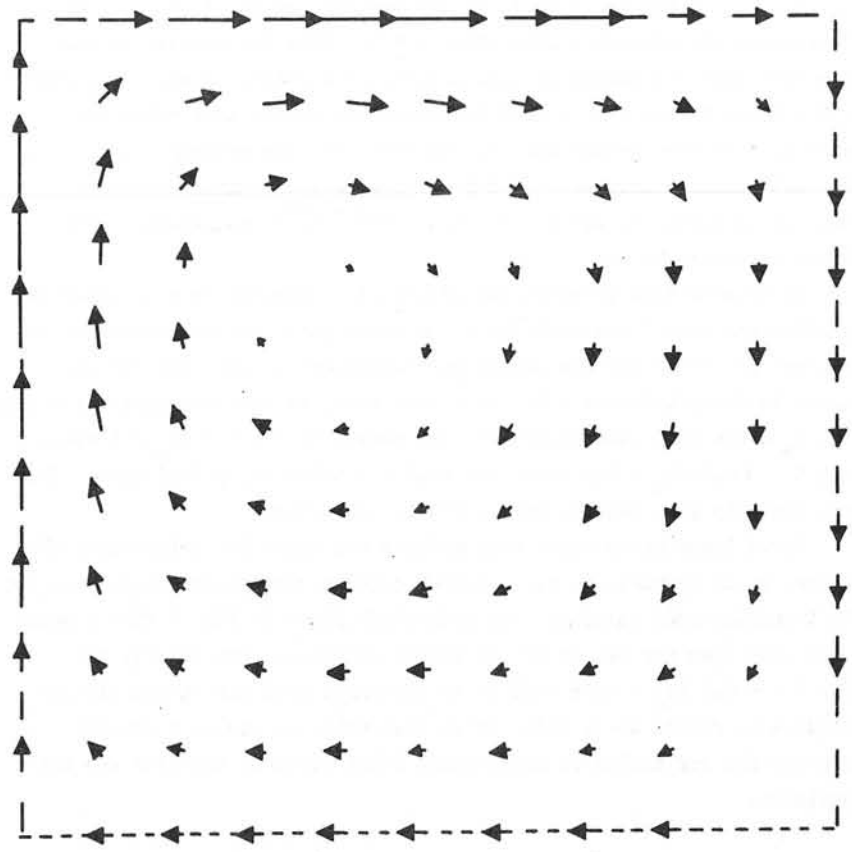

Fig. 3 Eddy current induced in a square plate with dipole pointing at one corner.

C. Transient Effects

We have also evaluated $\underline{j}$ for the case of Fig. 1 by fitting $f(\tau)$ by a 10th order polynomial f_a in the range $-1 < \tau < 1$, and taking $\Gamma = 6.5 \times 10^{-3}$. For those instants for which $\frac{df_a}{d\tau} = 1$, the results agree with the equilibrium solution. This is not surprising, since the sume in Eq. (14) is dominated by its first term for $\Gamma << 1$. Hence the accuracy of the method is largely dependent upon the accuracy of the factor $\frac{df_a}{d\tau}$. The more terms used in f_a, the better approximation it gives for $\frac{df_a}{d\tau}$. To reduce the deviation of $\frac{df_a}{d\tau}$ from $\frac{df}{d\tau}$ to less than 10% for most of the range of interest $(0 < \tau < 1)$, an eleven term polynomial is satisfactory. The fits of f_a and $\frac{df_a}{d\tau}$ are illustrated in Figs. 4 and 5.

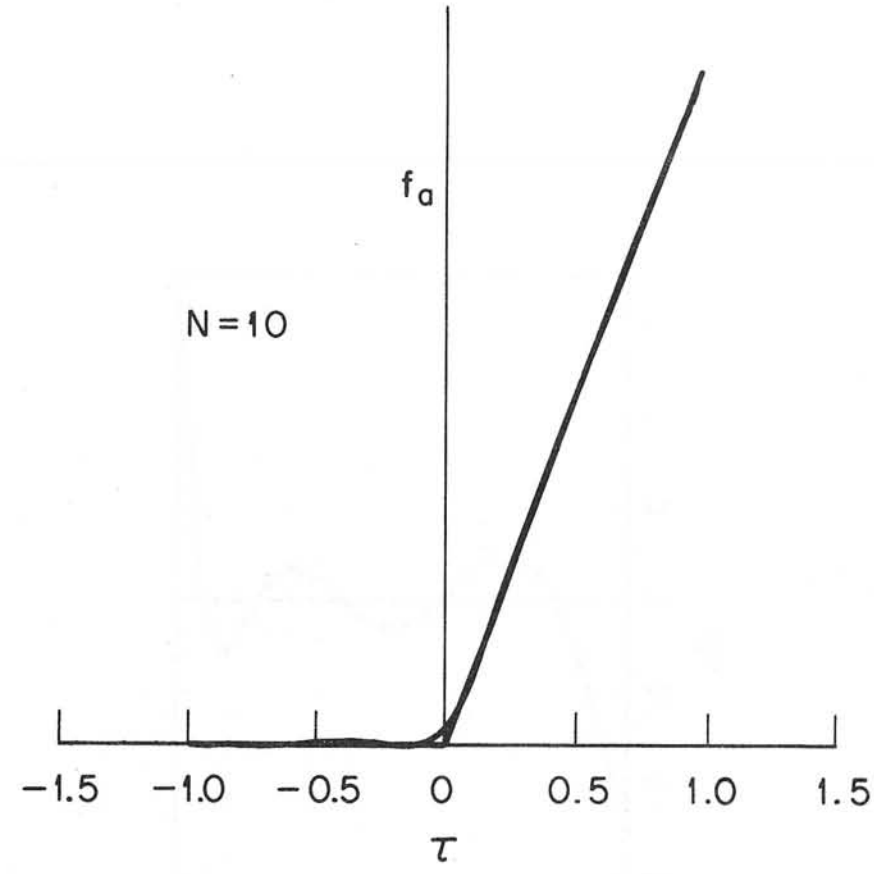

Fig. 4 The fitting of a linear ramp by a 10^{th} order polynomial over the range $-1 < \tau < 1$.

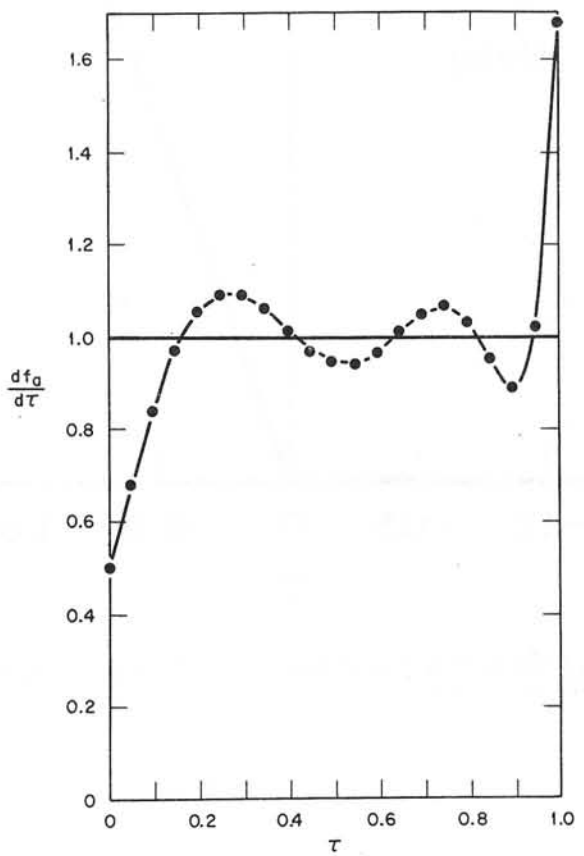

Fig. 5 Comparison of $\frac{df}{d\tau}$ (=1) with $\frac{df_a}{d\tau}$ for a 10^{th} order polynomial fit over the range $0 < \tau < 1$.

Having established a limit on the goodness of fit of f_a to f we next investigate the transient case where $\Gamma \lesssim 1$. From the results of Fig. 2, we expect that the lumped circuit solution for points close to the center of the plate should give a good approximation to the true transient behavior. We have solved the problem with the same geometry as Fig. 1, but with larger values of Γ (which correspond to changing the plate material to copper at 150 K - $\sigma = 1.4 \times 10^7 \Omega^{-1} m^{-1}$) and giving t_o the values indicated below.

It is necessary to shift the origin of τ relative to t in order to optimize the detail obtained for $t > 0$ while still leaving enough of an internal for $t < 0$ for the transients introduced at the time the fit begins to decay before $t = 0$. As a test case, we have successively fitted f by f_a a ten term polynomial over the ranges $-1 < \tau < 1$ ($t_o = 1$ sec), $-1.6 < \tau < 0.4$ ($t_o = 0.5$ sec), and $-1.2 < \tau < 0.8$ ($t_o = 0.25$ sec). The last two fits give results very close to each other.

For a large plate where edge effects are small for points near the center, it is possible to use a lumped circuit approximating solution for the transient eddy current. The comparison given in Fig. 6 (for a point 0.5 m away from the center of the plate) indicates that the fit for $-1.2 < \tau < 0.8$ ($t_o = 0.25$ sec) is in agreement with the lumped circuit solution to within about 15%. It is reasonable to assume a similar accuracy for our method in cases where other means of solution are not available.

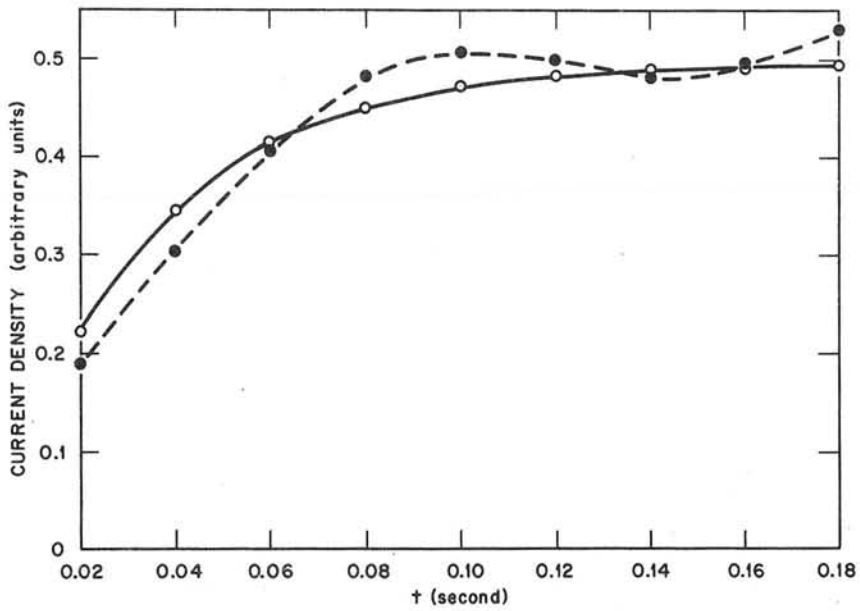

Fig. 6 Comparison of the eddy current transient behavior as calculated by lumped circuit (O) and by the perturbation expansion method (●).

Conclusion

The method of eddy current calculation using the perturbation expansion of the integral equations has been shown to give reasonable results for the equilibrium cases tested. These results agree with lumped circuit approximations and analytic solutions when these are available.

The transient solution for a linear ramp excitation can be obtained by fitting a polynomial to the ramp function over an appropriate interval. In principle, the expansion parameter Γ can always be made small by choosing a very large t_o. Then one must use enough terms in the polynomial fit to show the desired detail in the transient region.

There appears to be no fundamental difficulty in applying the above method to three-dimensional materials or linear magnetic materials. We intend to extend our work to these cases. We are also investigating alternative schemes for fitting f to f_a (such as fitting $\frac{df}{d\tau}$ directly) which should improve the numerical accuracy of $\underline{j}$ for a given order polynomial.

References

1. M. Roberts and E. S. Bettis, "Oak Ridge Tokamak Experimental Power Reactor Study — Reference Design," ORNL-TM-5042, Oak Ridge National Laboratory, Oak Ridge, Tenn. (Nov. 1975).

2. C. J. Carpenter, "Computation of Magnetic Fields and Eddy Currents," Int. Conf. on Magnet Tech., Vol. 5 (1975).

3. The approach of using perturbation expansion with separated time dependence in diffusion equation type problems is derived and verified in: K. H. Carpenter, "Solution of the Diffusion Equation by a Perturbation Approach with Polynomial Approximations to the Driving Term," to be published.

4. H. C. Karmaker, S.D.T. Robertson, "Integral Equation Formulation for the Solution of Magnetic Field Problems, Part II, Magnetization Vector Approach," Trans. IEEE, PAS 92, 815 (1973).

5. R. L. Stoll, J. Muhlhaus, "Power-Series Method of Calculating Eddy Currents in Non-magnetic Conductors," Proc. IEE, 119, 1616 (1972).

6. P. Swarztrauber and R. Sweet, "Efficient FORTRAN Subprograms for the Solution of Elliptic Partial Differential Equations," NCAR-TN/1A-109, National Center for Atmospheric Research, Boulder, Colorado (July 1975).

Symbols

$\underline{A}$, $\underline{A}_o$	Magnetic vector potential
$\underline{\alpha}_o$	Spatial part of the external vector potential
$\underline{\alpha}_m$, $\underline{\alpha}_m$	m^{th} order term of the spatial part of the vector potential
$\underline{B}$	Magnetic Induction
ε	Dielectric constant
f	Time-dependent part of the external vector potential
f_a	Polynomial approximation to f
Γ	Perturbation expansion parameter
$\underline{j}$	Current density
L	Characteristic length of the conductor
ΔL	Thickness of the conductor
M	Magnetization vector

Symbols (cont.)

μ_o (μ)	Magnetic permeability in vacuum (conductor)
n	Subscript to indicate normal component
ψ	Electrostatic scalar potential
$\underline{r}$, $\underline{r}'$	Spatial variables
ρ	Charge density
σ	Conductivity of the conductor
t	Time
t_o	Characteristic time of f
τ	Dimensionless Time (t/t_o)
$\underline{x}$, $\underline{x}'$	Dimensionless spatial variables ($\underline{r}/L$, $\underline{r}'/L$)
ζ_m	m^{th} order terms of the spatial part of the scalar potential

The Solution of Transient Fields by the Nodal Method

A.Y. Hannalla & D.C. Macdonald
Ain Shams University Cairo & Imperial College London

Abstract

The transient field in a machine cross-section is obtained numerically in terms of vector potential, full account being taken of saturation and eddy currents in a manner akin to that of the finite element method. Oscillations in the transient solution which are very pronounced in a solid rotor are avoided by making the first time at the start of a transient a special case. Accurate solutions are obtained for simple transients although the computing/real time ratio is approximately 10^4. As it stands the method is a means to a better understanding and a design tool.

1. Introduction

Magnetic field problems have been studied by finite difference and finite element techniques under steady-state conditions. The ability of the finite element method to accommodate awkward geometries without a very large number of nodes makes it preferable. The nodal method[1] has all the advantages of the first-order finite element method, but gives a more accurate distribution of current to nodes. It also indicates that obtuse-angled triangles give a poor representation. When applied to rectangular elements it has been shown to have the same approximation as that of the finite difference method. In transient conditions the nodal method, being an application of Ampere's law is unquestionably valid. It is therefore an attractive approach, for the derivation through the calculus of variations requires careful justification.

Here the nodal method is used to establish equations for the values of vector potential (A) at nodes in an alternator cross section. In the steady state these are similar to those obtained by the first-order finite element approach. The steady state equations are solved by the Newton-Raphson method for the initial current distribution - here constant field current. The field decrement test is then simulated, the field supply voltage being short-circuited, the stator winding being open. A transient solution of the field is obtained and the field current decrement calculated compares well with measured values when the effect of field winding end-leakage is included.

The transient solution requires a good representation of the conducting paths in the machine cross-section and this is obtained with a conductivity matrix. The current induced in a multi-turn winding is made dependent on the values of $\frac{\partial A}{\partial t}$ over all of its cross-section. The Newton-Raphson method is used to provide the solution at each time instant for the augmented equations including time effects, reluctivity being iterated at the same time.

Solutions have been obtained for field current decrement for a 3 kVA micro-alternator and a 325 MVA 4-pole solid rotor machine. The solution for the latter indicates that eddy currents in the solid rotor may have both positive and negative values which may be explicable in terms of higher modes of oscillation.

Equations have also been formulated for a loaded machine, including rotational voltages. This requires representation over a full pole-pitch and very large computing times would be involved in obtaining a solution. With the field decrement calculations over half-a-pole pitch containing 300 nodes, a computed to real time ratio of 10^4 is obtained. For the full pitch analysis 1,000 nodes are required and the ratio might well be 10^5.

The ultimate aim of the work is to find a model of a solid rotor which will represent it correctly under power system transient conditions. Thus secondary effects, such as tooth ripple, have been neglected and the rotor and stator are considered in a single position with respect to each other.

2. Governing equations

The two-dimensional field is obtained in terms of magnetic vector potential, A, normal to the plane of cross-section. J the current density is also normal to this plane and is distributed in the conducting paths presented by the machine. The field is governed by the equation

$$\nabla_{\wedge} r(\nabla_{\wedge} A) = -J + c' \frac{\partial A}{\partial t} \qquad (1)$$

where r is the reluctivity of the medium, J represents constant current density, c' is the material conductivity, and the last term represents currents induced by the changing field pattern within the machine. At a point in a closed winding the pattern is more complicated because the resultant current is dependent on the value of $\frac{\partial A}{\partial t}$ throughout the winding. Motion may also produce induced voltage and is omitted in the above.

The boundary conditions in a machine are taken to be those of Dirichlet, Neumann and periodicity. At the inner and outer bore of the

rotor and stator; flux is assumed to be completely contained (A = constant) the leakage flux being negligible. In the field decrement test the field is symmetrical about each pole and only half a pole need be considered. No flux crosses the pole axis (A = constant) and flux crosses the quadrature axis normally ($\frac{\partial A}{\partial n} = 0$). In more general transient problems in the presence of load currents a pole-pitch must be considered and a periodicity condition applied along the radial boundaries.

3. Numerical formulation

The machine cross-section is divided into acute-angled triangles (Plate 1) the sides of which lie along iron and copper boundaries. Within each triangle A varies linearly, giving uniform flux density and reluctivity and takes the much used form:

$$A = \frac{1}{2\Delta} (\text{sum of } (a_i + b_i x + c_i y) A_i),\ i=1,2,3$$

where Δ is the area of the triangle, A_i are values at the vertices, and a_i, b_i and c_i are defined typically as

$$a_1 = x_2 y_3 - x_3 y_2$$
$$b_1 = y_2 - y_3$$
$$c_1 = x_3 - x_2$$

the remainder being obtained by cyclic permutation.

Equation 1 is the infinitesimal representation of Ampere's law and here in the nodal method, Ampere's law is used along the orthogonal grid shown in Fig 1 around each internal node and those on the interpolar boundary. This immediately relates the value of current within the contour and associated with the node, with the values of A at the node and at surrounding nodes. The matrix equation obtained is thus

$$S A = c \frac{\partial A}{\partial t} - I \qquad (2)$$

where the elements of S on the diagonal are:

$$S_{pp} = \frac{1}{4} (\text{sum of } r_j (b_{1j}^2 + c_{1j}^2)/\Delta_j)\ j=1, m \qquad (3)$$

and on the pth row of the kth column

$$S_{pk} = \frac{r_j}{4\Delta_j} (b_{1j} b_{3j} + c_{1j} c_{3j}) + \frac{r_{j+1}}{4\Delta_{j+1}} (b_{1_{j+1}} b_{2_{j+1}} + c_{1_{j+1}} c_{2_{j+1}}) \qquad (4)$$

where b_{1j} and c_{1j} are the b_1 and c_1 of the jth triangle, and node k is coupled to node p by the common side of the j and (j+1)th triangles around node p. I represents a vector of constant currents.

S is symmetrical and has n rows (n = no. of active nodes). The inactive nodes on the Dirichlet boundaries are set to zero.

The right-hand side of equation (2) is zero at nodes where there is no conducting path, i.e. in air and laminated material. In the field winding, current may flow and the conductivity matrix has the form

$$c = \begin{bmatrix} 0 & 0 & 0 \\ 0 & c_1 & 0 \\ 0 & 0 & c_2 \end{bmatrix} \qquad (5)$$

The sub-matrices c_1 and c_2 represent the damping circuits and the field circuit. In the damping circuits current point is dependent on the value of $\frac{\partial A}{\partial t}$ at each node, and c_1 is a diagonal matrix of elements representing conductivity x area for each node. c_2 is a full matrix by which the current concentrated at any node is related to the values of $\frac{\partial A}{\partial t}$ at all nodes within the field winding cross-section and the resistance of the field circuit:

$$c_2 = \frac{c' N}{\Delta_s k_s k_i n_f} W W^T \qquad (6)$$

where W is the column vector of areas associated with the n_f nodes in the field winding cross-section over half a pole of total area Δ_s. N is the no. of turns/pole, k_s is the field winding space factor and k_i the mean length of turn/2 x rotor effective length.

The two parts of the conductivity matrix are kept distinct by ensuring that conducting regions are separated by a set of small non-conducting elements.

4. Time approximations

An implicit method is used to obtain $\frac{\partial A}{\partial t}$ at the end of each time step, dt:

$$\left.\frac{\partial A}{\partial t}\right|_{t+t} = - \left.\frac{\partial A}{\partial t}\right|_{t} + \frac{2}{dt} (A_{t+dt} - A_t) \qquad (7)$$

The error starts from the third derivative and the time interval is independent of the size of the elements. The initial time step has to be considered separately.

5. Initial values and the first time-step

At nodes in non-conducting regions $\frac{\partial A}{\partial t}$ does not give rise to current and may be allowed to vary freely from zero at the start of the transient.

The solution of equation (2) at the end of the first time step requires a value of $\frac{\partial A}{\partial t}\Big|_{dt}$, or, more exactly, $c\frac{\partial A}{\partial t}\Big|_{dt}$. Equation (7) would appear to give this if $c\frac{\partial A}{\partial t}\Big|_{o}$ is known. In conductors initially carrying current immediately following the transient, current is maintained by $\frac{\partial A}{\partial t}$, i.e.

$$c\frac{\partial A}{\partial t} = I_o$$

However the use of equation (7) at t=0 gives rise to oscillations in the solution (Fig.2 & 3) as was also found by Flatabo[2] in a thermal diffusion problem.

In conducting paths not initially carrying current, currents rise from zero at t=0 and therefore $\frac{\partial A}{\partial t}\Big|_{o} = 0$. For a short time after the start of the transient $\frac{\partial A}{\partial t}$ remains constant, changing by dA in successive time steps dt. Using equation (7) at the end of the first time step:

$$\frac{\partial A}{\partial t}\Big|_{dt} = 0 + \frac{2}{dt}(dA)$$

$$= 2\frac{dA}{dt}$$

which is clearly wrong and at the next instant gives $\frac{\partial A}{\partial t}\Big|_{2dt} = 0$.

A better solution is obtained if in the first time step a first-order approximation is used for $\frac{\partial A}{\partial t}$

$$\frac{\partial A}{\partial t}\Big|_{dt} = \frac{1}{dt}(A_{dt} - A_o),$$

with a very small value for dt.

A further difficulty occurs if nodes are situated on a common boundary between two conducting regions, one of which is initially carrying current (the field winding) and the other is not (the damper winding or solid iron). When driving voltage is suddenly removed (from the field circuit) current is maintained constant by $\frac{\partial A}{\partial t}\Big|_{t=0}$. However in the conductor that is initially dead $\frac{\partial A}{\partial t}\Big|_{t=0} = 0$ for current rises from zero. If no special provision is made the latter condition is not satisfied and current is calculated in the damping circuits at t=0. A full consideration of this situation would have to include the effect of the end leakage of the field winding for it must be the change of flux linkage there which initially contributes to the maintenance of current at the boundary.

However ignoring end effects a solution may be obtained when the field winding consists of many small conductors connected in series. The initial distribution of $\frac{\partial A}{\partial t}$ may then be obtained by assuming uniform rate of change of current density, which gives rise to $\frac{\partial A}{\partial t}$. The total voltage induced is at t=0

$$c_2\frac{\partial A}{\partial t} = I_o.$$

$\frac{\partial A}{\partial t} = 0$ is also satisfied at the common boundary. If the field conductors are large a better approximation would probably be to keep the total conductor current constant.

Here these difficulties have been avoided by putting a set of small non-conducting elements between conducting regions and by allowing $\frac{\partial A}{\partial t}\Big|_{o}$ to have a uniform value over conductors initially carrying current.

6. Choice of Grid

The nodal method allows for triangles or rectangles to be chosen as elements. Rectangles have been used in stator slots (Plate 1) where permeability is constant, and flux distribution is of minor importance in field decrement conditions. Many small elements have been used where gradients of flux density are large, but the overall aim is to use few, large elements, so as to minimise the number of nodes. In transient conditions Carpenter has shown that the surfaces of magnetic material must have at least one layer of elements in the depth of penetration if serious error is to be avoided. Here under transient conditions penetration depth does not have a clear meaning and the grid used has been laid out rather arbitrarily with a coarse grid and with smaller elements towards the air gap surface. As is shown later, higher modes of oscillation appear to be excited by the sudden transient and clearly the representation will limit the modes which can appear in the solution.

The choice of elements in the rotor slots requires to be sufficiently detailed to represent the distribution of $\frac{\partial A}{\partial t}$ over the conductor. Six nodes have been used in each slot and are about the minimum necessary to obtain the distributions shown for t=0 and after the first time step in Fig.2.

Nodes are numbered as far as possible so that the s-matrix has a strip of elements about its leading diagonal, i.e. the numbers of adjacent nodes are kept as near together as possible. There are exceptions to this rule in respect of:

inactive boundary nodes
nodes within the field winding cross-section
nodes within the damper winding cross-section, or in solid iron,

These are numbered in three groups within each of which numbers follow consecutively.

7. The iterative method

The initial values having been obtained by Newton-Raphson successive iteration, time steps are made in the same way with augmented equations. However, the solution to be obtained at the next instant involves $\frac{\partial A}{\partial t}$ and the value given by equation (7) is used save at the first instant. The vector of errors G is given by

$$G = S A + I - c \frac{\partial A}{\partial t}$$

and the solution is obtained for minimal G. The starting values of A at the instant t+dt are those at t, and at the (j+1)th iteration are

$$A_{j+1} = A_j - H_j^{-1} G_j$$

where H_j is the first order derivative of G_j with respect to A. Thus at

$$G_j = S_j A_j + 2 \frac{c}{dt} (A_j - A_t) + I_t$$

and

$$H_j = H_s + \frac{2}{dt} c .$$

H_s is the differential of S as given by Silvester[3]. At the first time step in a transient the first order approximation gives

$$H_j = H_s + \frac{c}{dt} .$$

Jennings[4] sparsity techniques are used and very good solutions are normally obtained in under ten iterations. The values of reluctivity are adjusted at each iteration and the method is unconditionally stable, the size of time step being restricted by the accuracy sought, not by stability.

Applications

The method has been successfully applied to the calculation of simple transients, the field decrement test. The first machine, a 3kVA micro-alternator, has a laminated stator and rotor, damping currents occurring only in the cage damper winding. Fig.3 shows the growth of damper current following the short-circuiting of the field supply voltage. It will be seen that the current density increases fastest at A nearest to the field winding.Current at point B is slightly slower and is followed by the current at the top of the bar (c). Damper current density having reached a maximum uniform value, the damper and field currents decay away together. The fast rise in damper current shown is associated with the initial swift drop in field current.

Fig.3 also shows the oscillation in the solution associated with the use of the second-order approximation throughout.

A typical solution for the solid rotor 4-pole machine are shown in Plate II. The field current decrement is shown in Fig.4. Curves C ann D show the oscillations obtained using the second order approximation throughout. E shows the effect of using the first order approximation at t=0 and taking full account of the switching operation (current in the discharge resistor was initially in the reverse direction), and F allows for the effect of field leakage reactance at the ends of the machine.

Fig.5 gives the eddy current density at the centre of a tooth at successive instants. A negative current is clearly indicated towards the front of the tooth and in the rotor body. These may be thought of as evidence of excitation of the higher natural modes of oscillation of the rotor, and several other explanations have been considered which would tend to confirm what at first was a surprising result. It would be interesting to confirm these results by measurements.

Conclusions

It has been shown that general transient conditions may be calculated with due regard to eddy currents, varying permeability and awkward geometry. The method is limited at the moment by the poor computing/real time ratio, and this must inhibit its use. If the time of calculation is reduced substantially the method may have a very wide significance. As it

is, it is an interesting tool giving considerable insight and holds promise as a means of devising more approximate machine models.

Acknowledgement

Thanks are due to A.B.J. Reece of GEC Power Engineering Ltd. who supplied the data of the solid rotor machine.

References

1. Hannalla, A.Y and Macdonald, D.C. 'A nodal method for the numerical solution of transient field problems in electrical machines', IEEE Trans on Magnetics, September 1975, pp.1544-46.
2. Flatabo, N. 'Transient heat conductance problems in power cables solved by the finite element method', IEEE Trans. PAS-92 1973 pp.56-63.
3. Silvester, P., Cabayan, H.S. and Browne, B.T. 'Efficient techniques for finite element analysis of electrical machines', IEEE Trans. on Power App. & Syst. Vol. PAS-92, 1973, pp.1274-81.
4. Jennings, A. 'A compact scheme for the solution of symmetric linear simultaneous equations', Computer Journal 1966, pp.281-5.

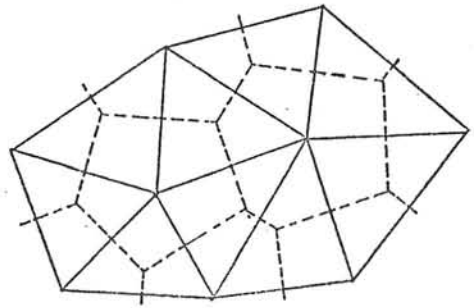

Figure 1 Orthogonal grid

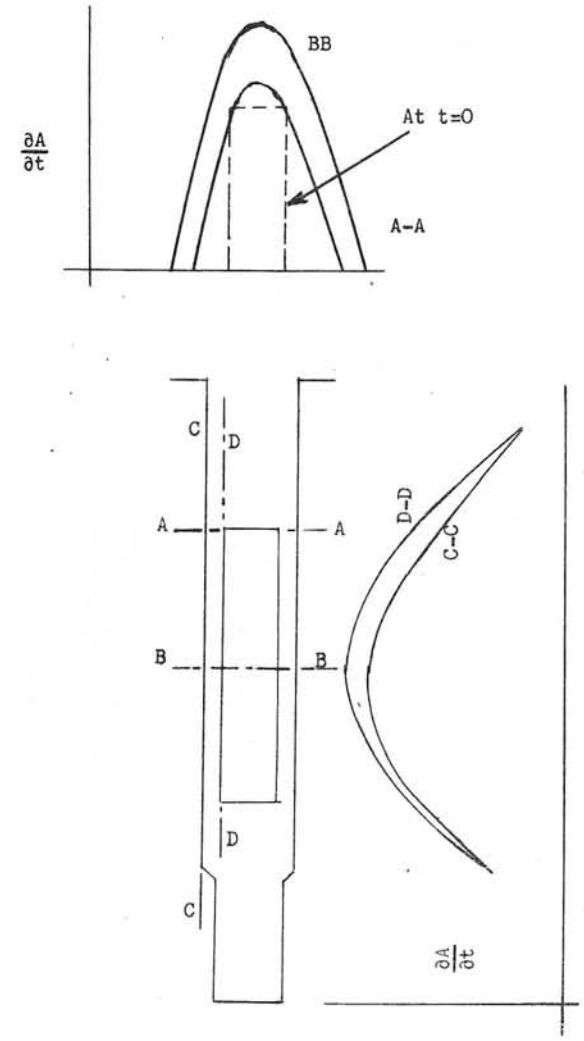

Figure 2 Distribution of $\frac{\partial A}{\partial t}$ in a rotor slot after the first time step

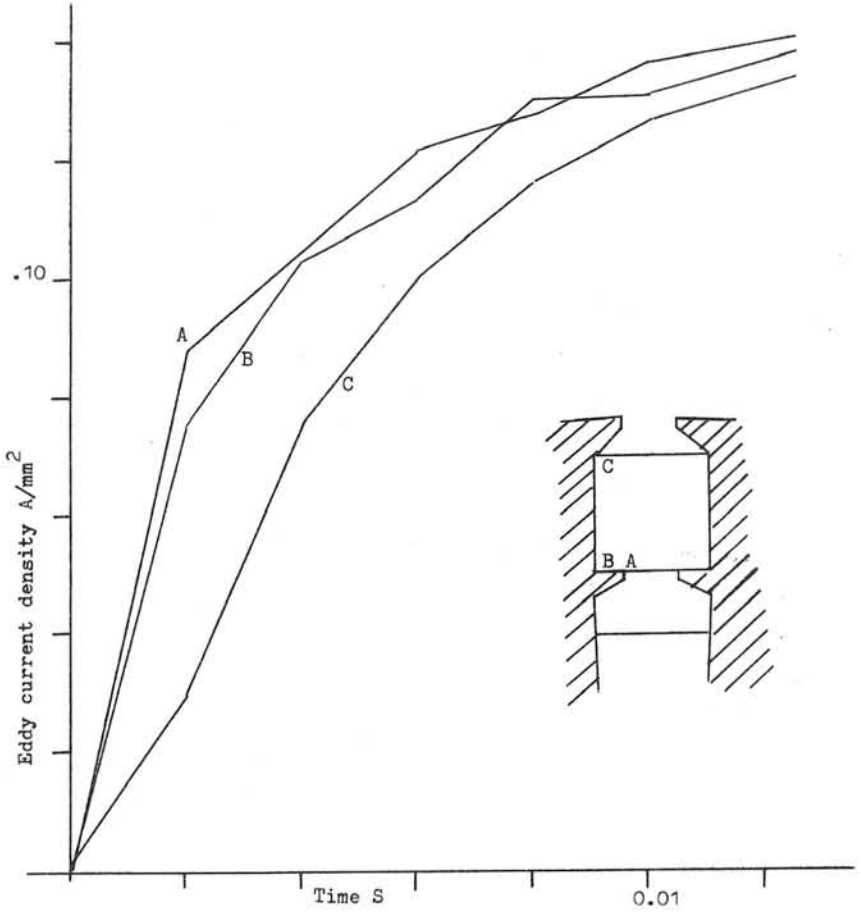

Figure 3 Growth of current in a rotor damper winding

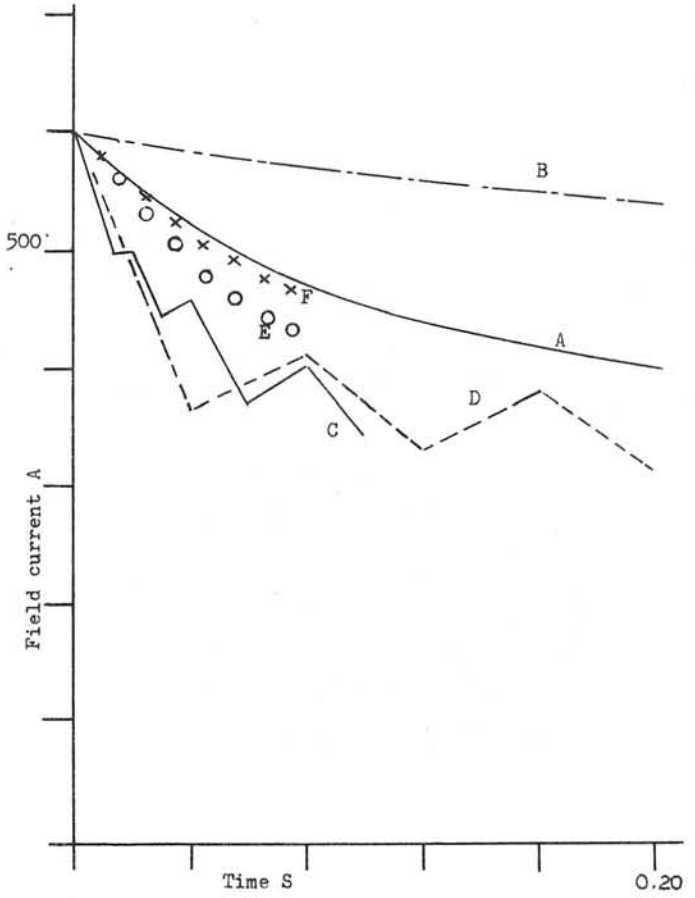

Figure 4 Field current decrement of a solid rotor machine

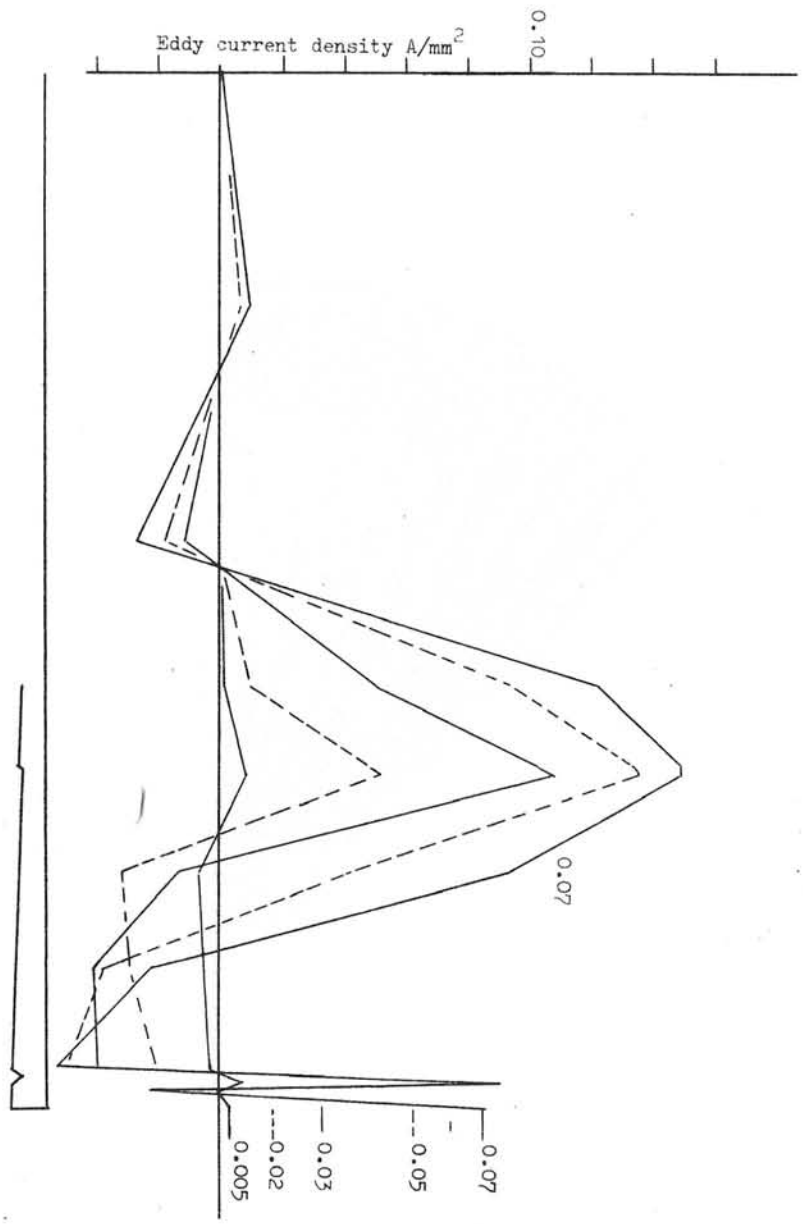

Figure 5 Growth of current along the centre line of a tooth at times from .005 - .075.

Correction Fig.5 shows values of current density scaled from $\frac{\partial A}{\partial t}$ values at nodes directly. These are not correct for in the consideration of the solid pole work current taken to act at a node is also dependent on $\frac{\partial A}{\partial t}$ values at adjacent nodes. When this process is followed only positive values of current density occur.

A.Y.H. and D.C.M.

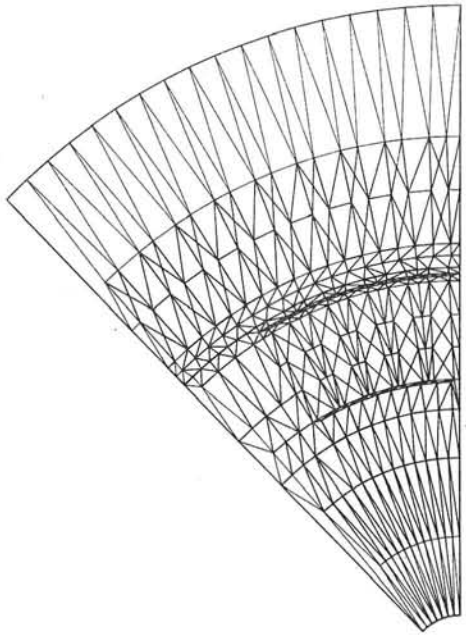

Plate 1 Grid of triangles used over half a pole pitch of a 325 MVA machine.

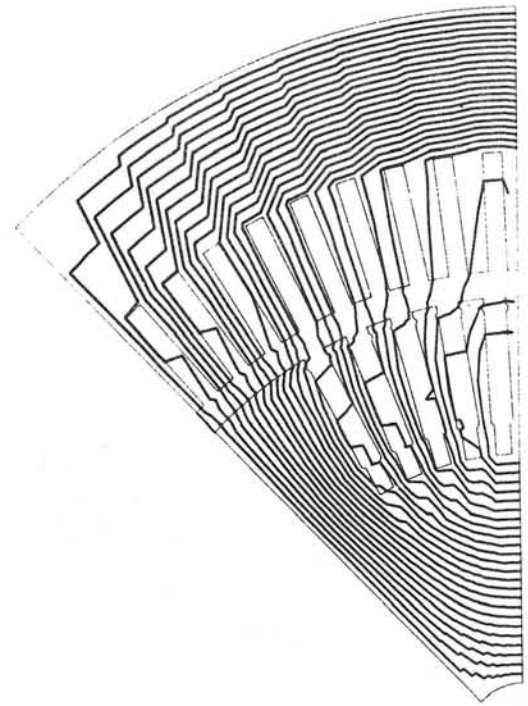

Plate 2 Flux distribution 0.035s after the start of the field decrement test.

CALCULATION OF THE DYNAMIC BEHAVIOUR OF ELECTROMAGNETIC ACTUATORS*

B. Aldefeld+

ABSTRACT

A method for the calculation of the dynamic behaviour of electromagnetic actuators is described which uses finite difference techniques and solves the magnetic field equation for successive time steps. Results of numerical investigations of the convergence of the SLOR method are discussed. As an application the dynamic behavior of a print needle actuator is shown.

INTRODUCTION

Electromagnetic actuators are found in a variety of technical devices e.g. in printers or paper tape and punch card equipment. They are used to provide mechanical energy at a given stroke and in a given time interval. Strokes of the order of 1 mm and times of action in the ms range are typical for many applications. For the excitation usually a voltage pulse of short duration is applied.

In the design and optimization of these devices requirements have to be met as to power consumption, magnetic force, mechanical energy, and speed of action. From the mathematical point of view, the main problem is the solution of Maxwell's field equations for time-varying excitation and moving media taking non-linear magnetization characteristics into account. Because of the dynamic nature of the problem a large number of field distributions for successive time steps have to be calculated, and it is of major importance that efficient methods of solution are used.

*Work supported by the Bundesministerium für Forschung und Technologie of the Federal Republic of Germany.

+Philips GmbH Forschungslaboratorium Hamburg, 2 Hamburg 54

The work of which some aspects will be described in this paper is aimed at a complete digital simulation of electromagnetic actuators. As yet, only magnets with rotational symmetry have been taken into consideration and eddy currents have been neglected. However, the eddy current effect is considered to be important, and the methods have been chosen with respect to include this effect at a later time.

METHOD

The dynamic behaviour of an electromagnetic actuator is described by three differential equations, which in common notation read

$$iR = U - \frac{d}{dt}(Li) \qquad (1)$$

for the calculation of the current in the coil,

$$m\frac{d^2z}{dt^2} = \text{magnetic force} + \text{spring force} + \text{frictional force} \qquad (2)$$

for the displacement of the armature, assuming that only one mass and one spring are present, and

$$\frac{\partial}{\partial r}\left(\frac{1}{r\mu}\frac{\partial}{\partial r}(rA)\right) + \frac{\partial}{\partial z}\left(\frac{1}{r\mu}\frac{\partial}{\partial z}(rA)\right) = -j \qquad (3)$$

for the vector potential, which has only a tangential component in rotationally symmetrical geometries.

The basic principle used in this paper for the solution of these differential equations is shown in the simplified flowchart Fig. 1. The magnetic force and the inductance can be obtained by simple integrations from the magnetic field distribution[1,2], and the ordinary differential equations (1) and (2) can be solved by standard methods. The main problem is the solution of the non-linear partial differential equation (3), which will be discussed in more detail in the following.

The finite difference approach is used applying similar techniques as described by Erdélyi[3]. This method allows for sufficiently accurate discretization for the geometrical con-

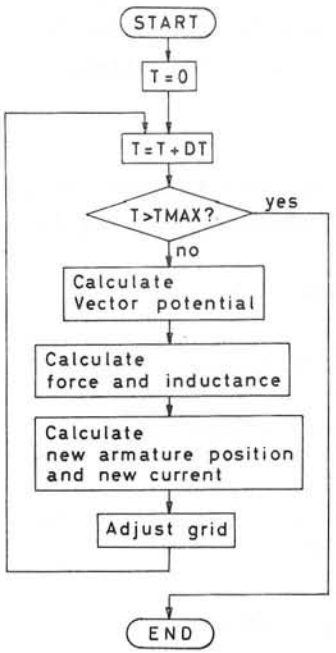

Fig.1 Simplified Flowchart for Calculation of Dynamic Behaviour

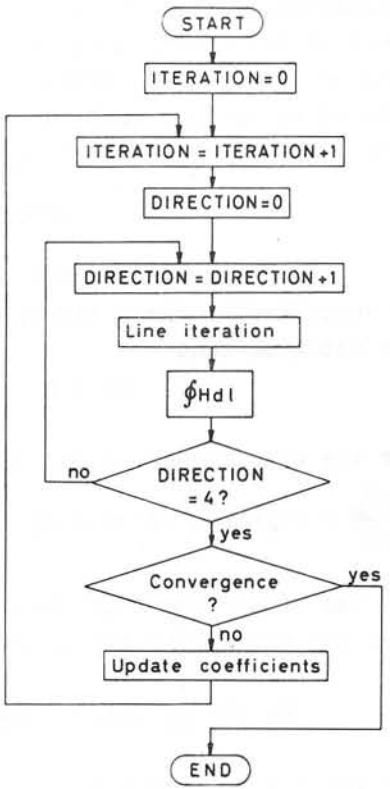

Fig.2 Flowchart of Iteration Method

figurations considered here, and the generation of the grid and its adaption to the time-varying geometry is easy to perform.

The iteration procedure consists of an inner and an outer cycle (Fig. 2). In the inner cycle new vector potentials are calculated by successive line iteration using the Thomas algorithm for the solution of the tridiagonal systems.

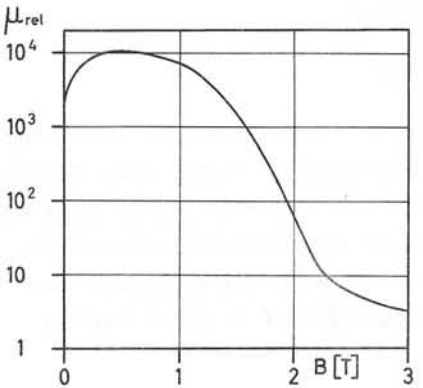

Fig.3 Magnetization Curve

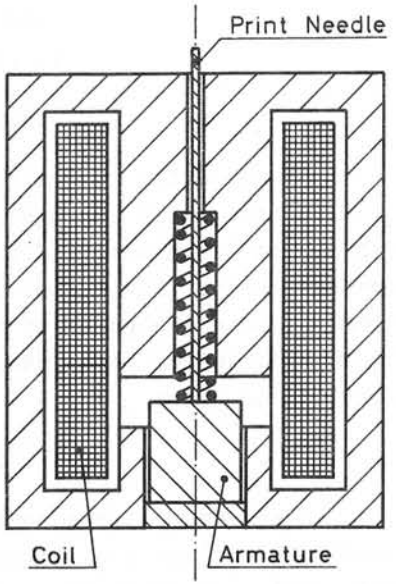

Fig.4 Print Needle Actuator

The vector potentials $A_{J,K}$ are overrelaxed according to

$$A_{J,K}^{(M)*} = A_{J,K}^{(M-1)} + ORF\ (A_{J,K}^{(M)} - A_{J,K}^{(M-1)}) \qquad (4)$$

where J,K refer to the nodes of the grid, M denotes the number of completed iterations of the inner cycle, and ORF is the overrelaxation factor. Additional acceleration of convergence is obtained by the multiplicative method based on Ampere's law, which has been described by Ahamed[4].

The outer iteration cycle consists of four inner cycles performed in alternating directions followed by updating the coefficients. The reluctivities $\nu_{J,K}$ are calculated from the flux density and the magnetization curve and underrelaxed according to

$$\nu_{J,K}^{(I)*} = \nu_{J,K}^{(I-1)} + URF\ (\nu_{J,K}^{(I)} - \nu_{J,K}^{(I-1)}) \qquad (5)$$

where I denotes the number of completed iterations of the outer cycle and URF the underrelaxation factor.

The initial values for the start of the iterative procedure are obtained from the field distribution of the previous time step, except for the first field calculation, which starts from $A_{J,K} = 0$. The convergence of the solution is monitored by three quantities:

- Percentage change in the magnetic force in two successive iterations
- Deviation of $\frac{1}{Ni} \oint Hdl$ from 1
- Euclidean norm of the difference vector divided by the average vector potential.

NUMERICAL INVESTIGATIONS

In several publications the convergence of iterative solutions has already been discussed. However, the results obtained by different authors, e.g. as to optimum relaxation factors, indicate that there is a strong dependence on the special problem and the method used. Additional investigations have therefore been carried out. The convergence of the solution for a number of different electromagnets, including open magnets (without flux return yoke), has been examined for low and high excitation currents and the magnetization curve shown in Fig. 3. Also the influence of the position of the integration path for the evaluation of $\oint Hdl$ has been investigated. The number of cells was chosen between 650 and 1500, which gives sufficient accuracy for the design applications under consideration. The following results have been obtained.

The position of the path of integration is not critical and the convergence is at least five times more rapid than without this acceleration.

On the relaxation factors there is a significant dependence. The underrelaxation factor had to be chosen lower than 0.12 and the overrelaxation factor lower than 1.8 to avoid instabilities in the solution. Suitable values were found to be 0.1 and 1.7 respectively, for which convergent solutions were obtained for all configurations and currents. Figures 5 and 6 illustrate the typical convergence of magnetic force and $\oint Hdl$ for different overrelaxation factors and an underrelaxation factor of 0.1. The test sample is the magnet shown in Fig. 4 subdivided into 1500 cells.

Fewer iterations are needed at very high excitation when the flux density in large parts of the magnetic circuit exceeds two Tesla. This is obviously due to the facts that at high saturation the differences between the permeabilities in air and iron are reduced and that the slope of the magnetization curve becomes less steep.

The number of iterations required to reach sufficient convergence in each time step is strongly dependent on the rate of change of armature position and current. Typical curves are given in Fig. 7. They apply to the dynamic characteristic shown in Fig. 8a (magnet Fig. 4 subdivided into 650 cells, time increment 0.05 ms). The thresholds for the termination of the iterations were preset to give an accuracy of the numerical solution of about 3 per cent: change in the magnetic force < 0.005, norm of the difference vector divided by the average vector potential < 0.05, $|\frac{1}{Ni} \oint Hdl - 1| < 0.005$.

The shape of the curves in Fig. 7 can be characterized, somewhat simplified, as follows:

- Many iterations at the beginning where the iterative process starts from $A_{J,K} = 0$
- Few iterations where the field distribution varies slowly because the armature is not yet moving
- Many iterations where the field distribution varies rapidly because both the position of the armature and the current change.

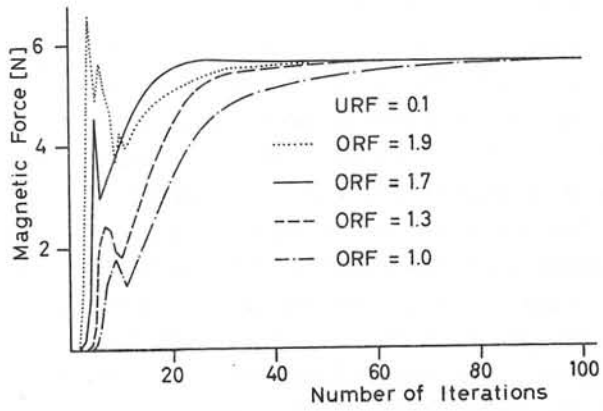

Fig.5
Convergence of Magnetic force

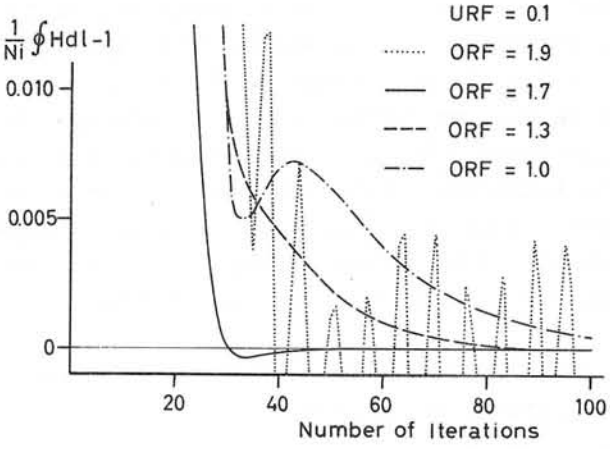

Fig.6
Convergence of $\oint$ Hdl

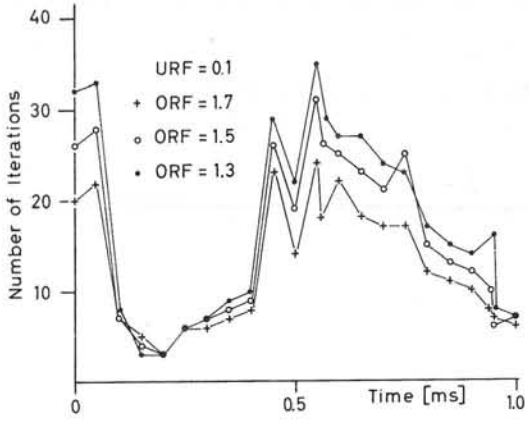

Fig.7
Number of Iterations as a Function of Time

For smaller time increments fewer iterations are required per time step because successive field distributions are more similar. For the example in Fig. 7 the average number of iterations per time step decreased from 14 to 10 (for ORF = 1,7) when an increment of 0.025 ms was chosen instead of 0.05 ms. For the determination of a suitable time increment no general rule can be given because there is a strong dependence on the special shape of the curves that describe the dynamic behaviour. On the one hand, the increment should be chosen as great as possible to keep the total number of iterations low, on the other hand, the increment should be chosen small enough to ensure that the magnetic force and the inductance can be interpolated with sufficient accuracy between the points of calculation.

APPLICATION

A computer programme has been developed on the basis of the techniques described and is used currently to assist the design of print needle actuators. The programme produces curves of magnetic force, armature displacement, velocity, mechanical energy, current, and inductance as functions of time and allows for taking 'snapshots' of vector potential, flux density, and flux lines at any time step.

An example is given in Fig. 8 showing the displacement of armature and print needle of the magnet in Fig.4. Fig. 8a shows the dynamic behaviour under pulse excitation at low repetition rate. Fig. 8b displays the behaviour in the case of three successive pulses at a high repetition rate which causes interference between the pulses. In Fig. 8c the behaviour for different initial positions of the armature is compared.

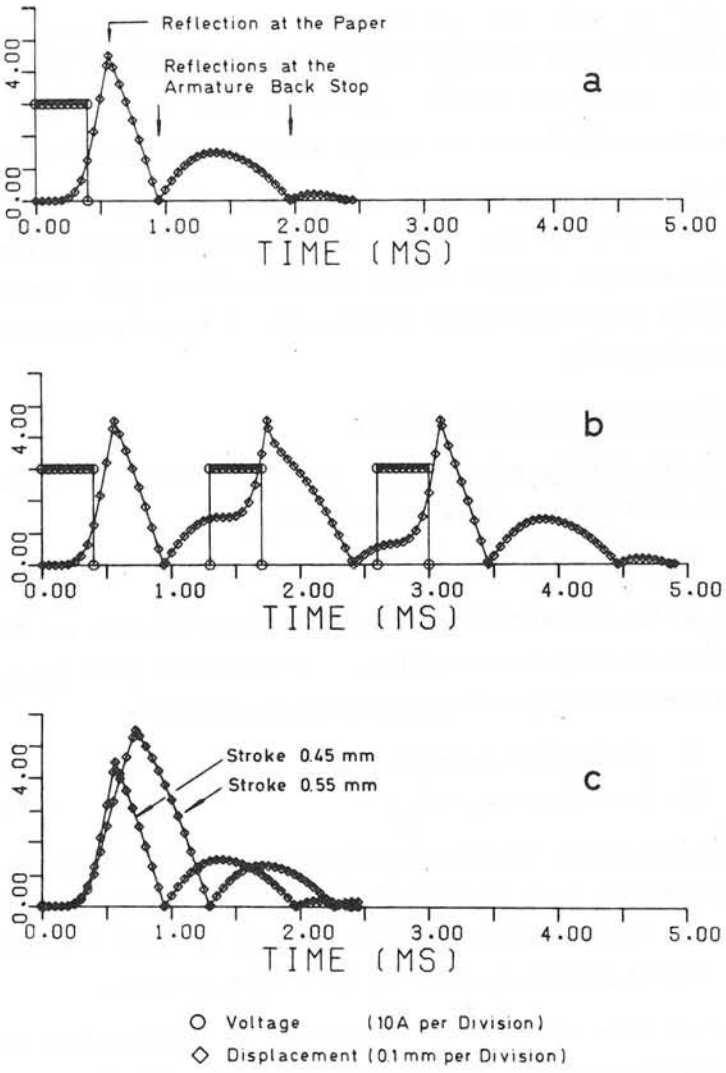

Fig.8 Dynamic Behaviour of a Print Needle Actuator

REFERENCES

1. P. Hammond, Forces in electric and magnetic fields, Bull. Electrical Eng. Educ. 25, pp. 17-28, 1960
2. R.S. Mamak and E.R. Laithwaite, Numerical evaluation of inductance and a.c. resistance, Proc. IEE 108C, pp. 252-258, 1961
3. E.A. Erdélyi and E.F. Fuchs, Nonlinear magnetic field analysis of dc machines, IEEE Trans. Power Apparatus and Systems, Vol. PAS-89, pp. 1546-1583, 1970
4. S.V. Ahamed, Accelerated convergence of numerical solution of linear and non-linear vector field problems, Computer J., Vol. 8, pp. 73-75, 1965

Discussions following paper:

(Chevalley CERN) Have you any comparisons with experimental datas? They would show the influence of neglecting the eddy current effects?

(Alderfeld) Some measurements on a print needle actuator have been performed and compared with the computations. It was found that the computed average force was too large by about 20 per cent for that electromagnet and it is supposed that this is mainly due to the eddy current effects. In order to improve the accuracy it is therefore planned to include the eddy currents in the computations.

A THREE-DIMENSIONAL ANALYTIC MODEL FOR CALCULATING EDDY-CURRENT EFFECTS APPLIED TO A TOKAMAK BLANKET AND SHIELD*

L. R. Turner, S. T. Wang, and J. R. Purcell
Argonne National Laboratory
Argonne, Illinois 60439 U.S.A.

SUMMARY

A method has been developed for calculating the induced fields due to eddy currents, in order to determine whether the conducting material is finely enough subdivided that eddy current effects do no harm. In using the method, the conducting material is divided into rectangular bricks. With suitable assumptions about the acting magnetic field, the current densities can be described by third-power equations. Consequently, the induced field from each brick can be written analytically. The method has been applied to flux penetration of the blanket and shield of Argonne National Laboratory's proposed design for a Tokamak Experimental Power Reactor.

1. INTRODUCTION

In a tokamak fusion reactor, as in other kinds of electrical machinery, time-varying magnetic fields can produce undesirable eddy currents. The eddy currents can be reduced by laminating or otherwise subdividing the metal parts; however, to make the pieces smaller than necessary may be expensive, inconvenient, or even inconsistent with their functioning. Thus it seems desirable to develop a general-purpose method of calculating eddy currents and the fields they produce, in order to determine how fine a subdivision is needed.

In a tokamak, the toroidal plasma is surrounded by a toroidal energy-absorbing blanket and radiation shield. In the Argonne design of a Tokamak Experimental Power Reactor (TEPR), these are made of stainless steel, plus non-conducting material. The blanket and shield experience both the pulsed field from the plasma current and the pulsed vertical field required to hold the plasma in equilibrium.

Eddy currents induced in the blanket and shield will produce magnetic fields which may interfere with the plasma current. In addition, those eddy currents may interact with the field from the toroidal-field coils to create large forces and torques within the blanket and shield.

In Sec. 2, below, we develop the mathematical model used to calculate eddy current effects. Section 3 is a description of the blanket and shield of a tokamak. Section 4 shows the calculation of eddy current effects in the blanket and shield. Finally, Sec. 5 describes possible extensions to the model.

2. THE MATHEMATICAL MODEL

2.1 Blocks, Fields, and Currents. The induced magnetic field due to eddy currents is given by the Biot-Savart Law:

$$B_{in} = \frac{\mu_o}{4\pi} \int \frac{J \times r}{r^3} \, dV \qquad (2.1)$$

where B_{in} is the induced field, J is the eddy current density, and r is the displacement from the source point (x, y, z) to the field point (x_o, y_o, z_o). The eddy current density is determined by two conditions:

$$J \cdot n = 0 \text{ on the conductor surface} \qquad (2.2)$$

$$\nabla \times J = -\sigma \dot{B} = -\sigma (\dot{B}_a + \dot{B}_{in}) \qquad (2.3)$$

when n is a unit vector normal to the conductor surface, σ is the electrical conductivity, B_a is the applied field, and the dot designated differentiation with respect to time. Solution of Eq. (2.1) - (2.3) is a difficult problem, and no general algorithm for their solution exists.

Let us make sufficient assumptions that the equations have convenient analytic solutions. Limitations on the applicability of the model due to these assumptions are discussed below in Sec. 2.3.

(1) The conductivity is sufficiently low that the induced field is small relative to the applied field. Thus $\dot{B}_a + \dot{B}_{in}$ may be

*Work performed under the auspices of the U.S. Energy Research Development Administration.

replaced in Eq. (2.3) by $\dot{B}_a$.

(2) All conductors can be represented as rectangular solids aligned parallel to the coordinate axes. Let a conductor be centered at the origin and have length 2a, 2b, 2c in the x, y, z directions respectively.

(3) The field B_a is everywhere in the z direction; consequently J is everywhere parallel to the x-y plane.

(4) The field B_a varies across a rectangular conductor according to

$$B_a = B_o \left(1 - \frac{x^2 + y^2}{a^2 + b^2}\right) \tag{2.4}$$

2.2 Expression for Induced Fields. Under the above assumptions, Eq. (2.2) and (2.3) are satisfied by a current density J with components

$$J_x = \sigma \dot{B}_o y \frac{a^2 - x^2}{a^2 + b^2} \tag{2.5}$$

$$J_y = -\sigma \dot{B}_o x \frac{b^2 - y^2}{a^2 + b^2} \tag{2.6}$$

Eq. (2.1) then has a z component which can then be written:

$$B_{in} = \frac{\sigma \dot{B}_o}{a^2 + b^2} \iiint \left[(y_o - y)\, y\,(a^2 + x^2) + (x_o - x)\, x\,(b^2 - y^2)\right] / r^3 \, dy\, dz \tag{2.7}$$

Substituting:

$$u = x - x_o, \quad v = y - y_o, \quad w = z - z_o,$$

and carrying out the integration, we find the following equation for the z component parallel to B_a:

$$\begin{aligned} B_{in} = -\frac{\mu_o}{4\pi} \frac{\sigma}{a^2 + b^2} \dot{B}_o \Bigg[& \tan^{-1} \frac{uv}{wr} \left\{\tfrac{1}{2} w^2 (x_o^2 - a^2 + y_o^2 - b^2) - w^4/6\right\} + \\ & + \tan^{-1} \frac{uw}{vr} \left\{v y_o (a^2 - x_o^2) + \tfrac{1}{2} v^2 (a^2 - x_o^2 + y_o^2 - b^2) + v^3 y_o + \tfrac{1}{2} v^4\right\} + \\ & + \tan^{-1} \frac{vw}{ur} \left\{u x_o (b^2 - y_o^2) + \tfrac{1}{2} u^2 (b^2 - y_o^2 + x_o^2 - a^2) + u^3 x_o + \tfrac{1}{2} u^4\right\} + \\ & + \ln(r + u) \left\{wv(b^2 - y_o^2 - 2v^2/3) - w y_o (a^2 - x_o^2 + 3v^2/2) - \tfrac{1}{2} w^3 y_o\right\} + \\ & + \ln(r + v) \left\{wu(a^2 - x_o^2 - 2u^2/3) - w x_o (b^2 - y_o^2 + 3u^2/2) - \tfrac{1}{2} w^3 x_o\right\} + \\ & + \ln(r + w) \left\{u y_o (u^2 + x_o^2 - a^2) + v x_o (v^2 + y_o^2 - b^2) + 2 x_o y_o (u^2 + v^2)\right\} + \\ & + r \left\{uvw/6 + \tfrac{1}{2} x_o vw + \tfrac{1}{2} y_o uw + 2 x_o y_o w\right\}\Bigg] \end{aligned} \tag{2.8}$$

where σ is the electrical conductivity, $r = \sqrt{u^2 + v^2 + w^2}$, and u, v, and w are evaluated at their upper and lower limits $\pm a - x_o$, $\pm b - y_o$, $\pm c - z_o$ respectively.

2.3 Limitations Due to Assumptions. Let us look at the consequences of the four assumptions listed above. For the type of application intended, subdividing the conductor to control the effects of eddy currents, assumption (1) holds definitely, in that the conductor is not adequately subdivided unless the assumption holds. Depending upon the degree of subdivision required, assumption (2) may or may not hold. In some cases, a more detailed treatment may be needed for nearby conductors, and the model used for more distant conductors. There is a class of problems for which assumption (3) is good, but certainly the model would be improved by including all three components of J and B. Assumption (4) is the most questionable; if the field B_a were actually uniform and equal to B_o, then the above expression would probably underestimate B_{in}, but by less than one third. An extension of the model to make the next approximation beyond assumption (4) is discussed in Sec. 5 below.

3. THE BLANKET AND SHIELD AND THE EQUILIBRIUM FIELD

3.1 The TEPR Blanket and Shield. In a tokamak power reactor, most of the energy is carried out of the plasma by 14 MeV neutrons. The blanket surrounding the plasma captures almost all (approximately 99%) of these neutrons and contains a circulating coolant (water or helium) to carry the energy to the generator outside. Surrounding the blanket is

the shield, designed to stop the remaining neutrons. An early design for the Argonne TEPR blanket and shield is shown in Fig. 1. It consists of a torus with alternating layers of stainless steel and boron carbide; the layers are between 5 and 15 cm thick, with a total thickness of 80 cm of stainless steel. The torus was unbroken toroidally or poloidally. After the calculations described below were performed, the design was changed to that shown in Fig. 2, which consists of thirty segments toroidally, each divided into rings of 16 blocks poloidally.

3.2 The Equilibrium Field. A tokamak must have, supimposed upon the other magnetic fields, a vertical magnetic field throughout the plasma region to keep the plasma current in equilibrium. In the Argonne TEPR, the field is 3 kG, it must be established during the one second rise time of the plasma current; and it is produced by coils outside the blanket and shield. It is this equilibrium field which produces eddy currents in the blanket and shield.

4. CALCULATING THE EDDY CURRENTS AND INDUCED FIELD

4.1 A Simpler Model. Because the blanket and shield shown in Fig. 1 consists of thin toroidal rings, it can be approximated by a toroidal shell, with toroidal and poloidal currents, but no radial currents. Furthermore, unless the aspect ratio is too low, the toroidal shell can in turn be replaced by a cylindrical shell, with the toroidal and poloidal currents replaced by axial and azimuthal currents.

If we take the equilibrium field to be vertical and perpendicular to the axis of the cylindrical blanket and shield, then when the equilibrium field changes, there will be, in the low conductivity limit, an axial current

$$J = -\sigma a \sin\theta \dot{B}_o \quad , \tag{4.1}$$

when a is the radius of the cylindrical shell, and θ is the azimuthal angle. This current will produce a field in the plasma

$$B_{in} = -\frac{\mu_o}{2} h a \sigma \dot{B}_o \quad , \tag{4.2}$$

where h is the thickness of the cylindrical shell.

4.2 Calculation of Unbroken Toroidal Shell and Modification of the Model. For the blanket and shield design shown in Fig. 1 with a rise time of one second, the induced field at the plasma as calculated by Eq. (4.2) is more than three times the applied field. This non-physical result would not actually occur; the induced fields would induce additional currents which in turn would produce fields, limiting the net induced field to a value sufficient to cancel the applied field.

Although we have not correctly calculated the field, we can draw two conclusions about what will happen if the blanket and shield are unbroken.

(1) The induced field is large (comparable to the applied field).

(2) Fields induced by the induced field are significant.

Consequently, it appears that we must break up the iron into pieces small enough so that:

(1) The induced field at the plasma is negligible.

(2) Fields induced by the induced field are negligible.

If the cylinder is broken into segments of length 2ℓ which is small compared with the diameter, the current density has components

$$J_\theta = \sigma y \cos\theta \dot{B}_o \tag{4.3}$$

$$J_y = -\frac{\sigma}{2a}(\ell^2 - y^2) \sin\theta \dot{B}_o \tag{4.4}$$

where y is measured axially from the center of the segment. The field on axis a distance y_o along the axis is given by

$$B_{in} = \frac{\mu_o \sigma h a}{8} \dot{B}_o \left[\frac{y(a^2 + y_o^2 - \ell^2)}{a^2\sqrt{a^2 + y^2}} - \ln(\sqrt{a^2 + y^2} + y) \right]_{y=-\ell-y_o}^{y=\ell-y_o} \tag{4.5}$$

4.3 Results for a Segmented Shell. For 16 segments and an applied field of 3 kG, the induced field at the plasma is calculated by Eq. (4.5) to be 566 G; for 32 segments, it is reduced to 144 G, or five percent of the applied field. Plasma physics considerations suggest that even this value is uncomfortably large; it seems safest to try to further reduce the eddy currents. To do so requires making the blanket and shield of blocks weighing a few tons each.

4.4 Results with the Brick Model. For calculating the effects of further subdivision, the design in Fig. 1 was divided into thirty segments toroidally; and each of those was divided into sixteen regions poloidally. In addition, the division into from four to six regions radially is maintained. Each segment is represented by 92 rectangular stainless steel bricks. The bricks closest to the plasma are 30 cm thick, the others are 10 cm thick. Widths vary from 112 cm to 153 cm, and lengths from 80 cm to 180 cm to correctly represent the volume of stainless steel.

A FORTRAN program, BRICK, was written to establish the vertices of the bricks in one segment, to translate and rotate the bricks to represent the other segments, and to calculate the induced field at a specified point by Eq. (2.8). The calculation shows that the maximum induced field in the center of the plasma is only 0.86% of the equilibrium field, of which the two nearest segments contribute 0.79%. The effect of repeated subdivision is shown in Table I. The induced field was judged to be sufficiently low with a subdivision of 16 cuts. The actual blanket and shield design suggested as a result of this calculation is shown in Fig. 2.

Table I. Effect of Segmenting and Subdividing the Blanket and Shield

Condition	Peak induced field on plasma axis as percent of applied field.	Calculated by
Unsegmented	325%*	Eq. (4.2)
16 segments	19%	Eq. (4.5)
32 segments	5%	Eq. (4.5)
30 segments, each with 16 cuts	0.9%	Eq. (2.8)

*Assumptions of calculation invalid in this case.

4.5 Forces and Torques. The torque on a horizontal block due to the 40 kG toroidal field can readily be found from Eq. (2.5):

$$N = \iiint J_x y B_T \, dV \qquad (4.6)$$

$$= 16 \dot{B}_o \sigma B_T a^3 b^3 c / 9(a^2 + b^2) \quad , \qquad (4.7)$$

where N is the torque and B_T the toroidal field. For one of the largest blocks, Eq. (4.7) yields a value of 36000 foot lb.

5. EXTENSIONS OF THE MODEL

5.1 Fifth-Power Equations for J. The model described in Sec. 2 can be extended in several ways. Most important, perhaps, is relaxing the condition that the field must vary across a brick according to Eq. (2.4), which was imposed so that the current density would obey the simple expression Eq. (2.5) and (2.6). If we allow fifth-power terms in the expressions for current, we get

$$J_x = \sigma \dot{B}_o y \left[a^2 - x^2 + \left\{ a^2 b^2 (a^2 - b^2) + (a^4 - a^2 b^2 + b^4) x^2 + 2 a^2 b^2 y^2 - 2 b^2 x^2 y^2 - a^2 x^4 \right\} / \left\{ a^4 + 5 a^2 b^2 + b^4 \right\} \right] / (a^2 + b^2) \qquad (5.1)$$

$$J_y = -\sigma \dot{B}_o x \left[b^2 - y^2 + \left\{ a^2 b^2 (b^2 - a^2) + (a^4 - a^2 b^2 + b^4) y^2 + 2 a^2 b^2 x^2 - 2 a^2 x^2 y^2 - b^2 y^4 \right\} / \left\{ a^4 + 5 a^2 b^2 + b^4 \right\} \right] / (a^2 + b^2) \qquad (5.2)$$

$$B_a = B_o \left[1 - \frac{a^2 x^4 + 6 x^2 y^2 (a^2 + b^2) + b^2 y^4}{(a^2 + b^2)(a^4 + 5 a^2 b^2 + b^4)} \right] \quad . \qquad (5.3)$$

Equation (5.1) - (5.3) obey

$$J \cdot n = 0 \text{ on the conductor surface}$$

and $$\nabla \times J = -\sigma \dot{B}_a \quad .$$

Moreover Eq. (5.3) approximates $B_a = B_o$ over much more of the conductor volume that Eq. (2.4) does. When Eq. (5.1) and (5.2) are substituted into Eq. (2.1) and the integration carried out, an analytic expression for B_{in} results, involving the same functions as the simpler expression in Eq. (2.8). When calculations with that expression are compared with those described above, the limitations of assumption (4) can be understood.

5.2 Other Extensions. Three other useful extensions of the model would be:

(1) Using the J_x, J_y, and B_a which approximate a linear variation of the magnetic field.

(2) Incorporating all three components of J, B_a, and B_{in}.

(3) Going beyond the low-conductivity limit by including B_{in} in

B_a, thus producing a set of linear equations to be solved for the eddy currents.

Extensions (1) and (2) in particular would be straightforward because the same kinds of expressions occur there as were determined for the equations of Sec. 2 and 5.1

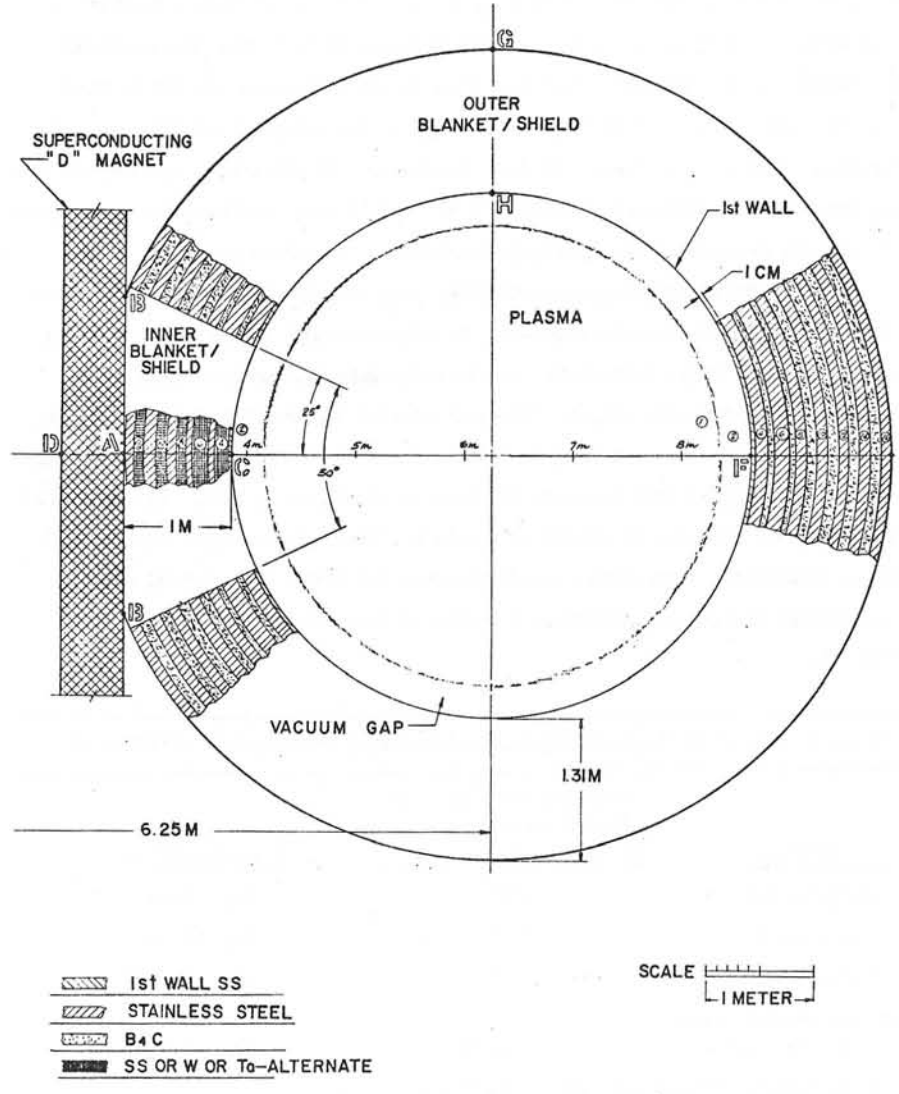

Fig. 1 Unbroken Blanket and Shield Design for the Argonne TEPR

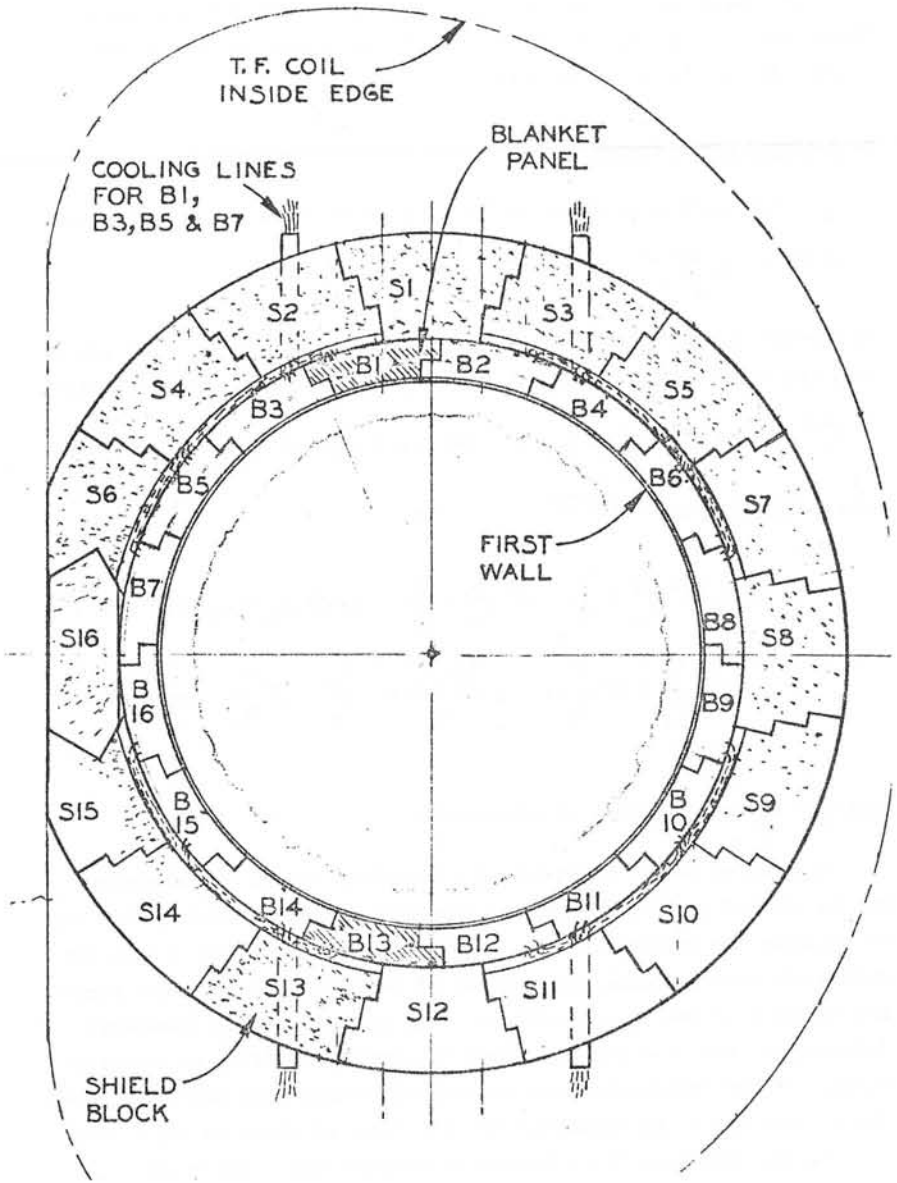

Fig. 2 Blanket and Shield Design for the Argonne TEPR, with 16 Cuts Poloidally to Reduce Eddy-Current Effects

Discussions following paper:

(Yeh) What is the duration for which the perturbing field due to eddy is comparable withVF, since eddy will dive away at flat top of pulses?

(Turner, Argonne) During the first 15 msec or so, while both the applied and induced field are less than 2 gauss.

Induction Motor Analysis and Field Calculation using Anisotropic Layer Theory

S. Williamson

Introduction

'Layer theory' is a technique of analysis that has been developed over a number of years (see introduction and bibliography of ref.1). Its chief use is for the analysis of induction machines. The basic philosophy lies in replacing the regions of a real machine by a series of separate layers. These layers may be arranged concentrically or stacked one on top of the other, depending on the geometry of the machine under analysis. The physical properties of the layers are determined by the physical properties of the regions they represent, composite regions being modelled using an averaging process. The layers are assumed to be magnetically linear, so that the principal of superposition can be evoked to enable a solution to be obtained, harmonic by harmonic. Maxwell's field equations are solved for each layer separately, matching solutions at the boundaries. This is then repeated for all significant harmonics to allow the calculation of an input impedance matrix. The solution is now essentially complete, and the various fields, forces and torques can be readily obtained.

A recent paper[1] has extended layer theory to allow the effects of both electric and magnetic anisotropy to be taken into account. This extension has become necessary with the introduction of the new transverse flux linear induction motors[2-4]. In many of these machines the path which the flux takes is governed by the direction in which the back-iron is laminated. In addition, certain flux-paths may be actively discouraged by grouping the laminations into packets, with air-spaces between. Windings have been proposed which are apt for both longitudinal-flux and transverse-flux machines[4].

The author is with the Department of Engineering, Marischal College, University of Aberdeen, Aberdeen AB9 1AS.

This paper deals with the application of the anisotropic layer-theory to the analysis of one of the new linear machines, with particular respect to the field in the airgap.

Anisotropic Layer Theory

It may readily be shown that if a harmonic solution of the form

$$e_x^{k,\ell} = \mathrm{Re}\left\{ \bar{E}_x^{k,\ell}(z) \exp(j(\omega t - ky - \ell x)) \right\} \qquad (1)$$

is assumed for all the field quantities in a region, where the x and y axes lay in the plane of motion, then $\bar{E}_x^{k,\ell}$ can be expressed in the form

$$\bar{E}_x^{k,\ell}(z) = D_1 \cosh \varepsilon_1 z + D_2 \sinh \varepsilon_1 z + D_3 \cosh \varepsilon_2 z + D_4 \sinh \varepsilon_2 z \qquad (2)$$

where $$\varepsilon_1, \varepsilon_2 = \alpha \pm \sqrt{\alpha^2 - \beta} \qquad (3)$$

$$\alpha = \frac{1}{2}\left\{ \ell^2 \left(\frac{\sigma_x}{\sigma_z} + \frac{\mu_x}{\mu_z}\right) + k^2 \left(\frac{\sigma_y}{\sigma_z} + \frac{\mu_y}{\mu_z}\right) + js\omega(\sigma_y \mu_x + \sigma_x \mu_y) \right\} \qquad (4)$$

$$\beta = \left(\ell^2 \frac{\mu_x}{\mu_z} + k^2 \frac{\mu_y}{\mu_z} + js\omega \frac{\sigma_z \mu_x \mu_y}{\mu_z}\right)\left(\ell^2 \frac{\sigma_x}{\sigma_z} + k^2 \frac{\sigma_y}{\sigma_z} + js\omega \frac{\mu_z \sigma_x \sigma_y}{\sigma_z}\right) \qquad (5)$$

and $D_1 - D_4$ are constants of integration.

A total of twelve constants of integration result. This number may be reduced to four by applying Maxwell's equations, and then to two by assuming the regions are electrically isolated. Finally a transfer matrix can be calculated, relating field quantities at the upper boundary to those at the lower boundary. This enables surface impedances 'looking up' and 'looking down' from the excitation layer to be determined. If the excitation layer is assumed to have zero thickness, then the winding input impedances may be calculated as shown in ref.1, but if a finite thickness of excitation is incorporated, then thick-excitation formulae should be used[6]. This produces a surface input impedance given by

$$\bar{Z}^{k,\ell}_{IN} = \frac{-1}{\eta\varepsilon^2}\left[\frac{\eta(Z_U + Z_D)(\varepsilon S - \tanh \varepsilon S) + \tanh \varepsilon S(2 \tanh(\frac{\varepsilon S}{2}) - \varepsilon S\eta^2(Z_U Z_D + 1))}{\eta(Z_U + Z_D) - (\eta^2 Z_U Z_D + 1) \tanh \varepsilon S}\right] \quad (6)$$

where $\eta = \frac{jk^2}{\omega\varepsilon\mu_z}$

S = thickness of excitation layer

ε = solution of equation 3

Z_U = surface impedance looking up from the excitation

Z_D = surface impedance looking down from the excitation

For a voltage-forced solution the windings are firstly resolved into a complex double Fourier series. If the x-directed conductor distribution of winding 1 is given by

$$n_{x1} = \sum_{-\infty}^{+\infty}\sum_{-\infty}^{+\infty} \bar{N}^{k,\ell}_{x1}\, e^{-j(ky+\ell x)} \quad (7)$$

$\ell \quad k$

then the coupling impedance between this winding and a second can be shown to be given by the expression

$$\bar{Z}_{12} = 4\tau_x\tau_y \sum_{1}^{\infty}\sum_{1}^{\infty} \bar{N}^{k,\ell}_{x2}\, \bar{N}^{*k,\ell}_{x1}\, \bar{Z}^{k,\ell}_{IN} + \bar{N}^{k,\ell}_{x1}\, \bar{N}^{*k,\ell}_{x2}\, \bar{Z}^{-k,\ell}_{IN} \quad (8)$$

$k \quad \ell$

Calculation of the coupling impedances enables the winding currents, and hence the excitation layer current density harmonics, to be calculated. This then enables the fields at the excitation layer boundaries to be determined, and these in turn allow the fields in any region to be calculated, via the transfer matrices.

Of particular interest is the field at the surface of the rotor plate, since this can conveniently be measured for verification purposes, and can also be used in conjunction with the Maxwell stress technique to calculate the forces on the rotor assembly. In terms of the field quantities normally calculated using the transfer matrices (i.e. B_z and H_y) the lift, propulsion and transverse forces may be shown to be given respectively by the expressions

$$F_z = \frac{2\tau_x\tau_y}{\mu_o} \mathrm{Re}\left\{\sum_{1}^{+\infty}\sum_{-\infty}^{+\infty} \{\mu_o^2(1 + \frac{\ell^2}{k^2})\, |H^{k,\ell}_y|^2 - |B^{k,\ell}_z|^2\}\right\} N \quad (9)$$

$\ell \quad -k$

$$F_y = -4\tau_x\tau_y \mathrm{Re}\left\{\sum_{1}^{+\infty}\sum_{-\infty}^{+\infty} \bar{H}^{k,\ell}_y\, \bar{B}^{*k,\ell}_z\right\} N \quad (10)$$

$\ell \quad -k$

$$F_x = -8\tau_y \mathrm{Im}\left\{\sum_{-\infty}^{+\infty}\frac{1}{k}\sum_{1}^{+\infty}\sum_{1}^{+\infty} H^{k,\ell_1}_y\, \bar{B}^{*k,\ell_2}_z \{\frac{\ell_1\ell_2}{\ell_1^2-\ell_2^2}\}(1-(-1)^{(\ell_1+\ell_2)}\tau_x/\pi)\right\} N \quad (11)$$

$k \quad \ell_1 \quad \ell_2$

$\ell_1 \neq \ell_2$

The 'infinite' summations are, of course, intended to imply that as many terms as necessary should be considered. This is best determined in an empirical basis and is discussed in a later section.

It is interesting to note that the transverse forces arise out of an interaction between odd and even harmonics. This arises because of the nature of the transverse modelling. For a given harmonic pair, B_y and B_z are constrained to vary sinusoidally with x, whilst B_x varies cosinusoidally. The transverse (i.e. x-directed) force is therefore calculated by integrating products of the form $\sin \ell_1 x \cos \ell_2 x$ over one transverse pole-pitch. Such integrals are zero unless one of the pole numbers is odd and the other even.

The 'Herringbone' Motor[4,5] and its Mathematical Model

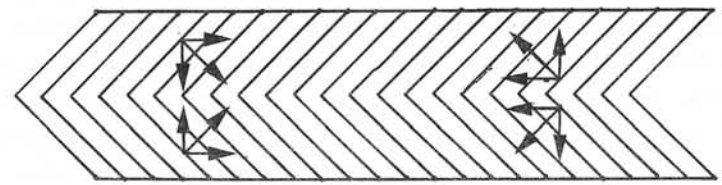

Forwards phase sequence
Inwards-travelling fields

Reverse phase sequence
Outwards-travelling fields

Fig.1 Plan view of Herringbone motor stator, showing doubly-skewed slots and field velocity vectors.

The 'Herringbone' motor was originally designed to enable the self-stabilising properties of doubly-skewed stator slots to be examined. A plan view of the stator is shown in fig.1. When the phase sequence is in the 'forwards' sense the transverse components of the field-velocity vectors produce an 'inwards'-travelling field, as shown. When the phase sequence is reversed an 'outwards'-travelling field is produced. The machine is laminated in the conventional sense, i.e. it is an axial-flux machine. The stator is fitted with a four-pole Gramme-ring winding in sixty slots. The rotor consists of a single sheet of aluminium, backed by a single block of laminated iron. The plane of lamination for the rotor back-iron is the same as that of the stator as indicated in fig.2.

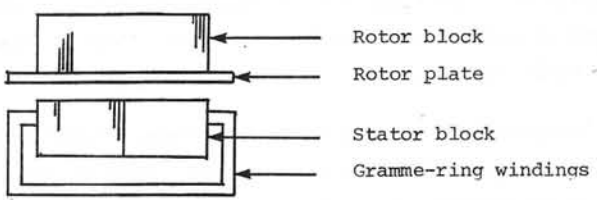

Fig.2 End-view of Herringbone motor

To model the herringbone motor, it was assumed to be one of an infinite two-dimensional array in keeping with the normal layer-theory practice. Longitudinally the machines are arranged in a nose-to-tail fashion at an appropriate separation as shown in fig.3. This allows the windings to be Fourier-analysed in the longitudinal direction, with a period equal to the spacing of the stators. In practice a mark to space ratio of 1:1 was used, since at standstill the flux fringing beyond the stator ends is negligible. In the transverse direction the machines are arranged as shown in fig.4.

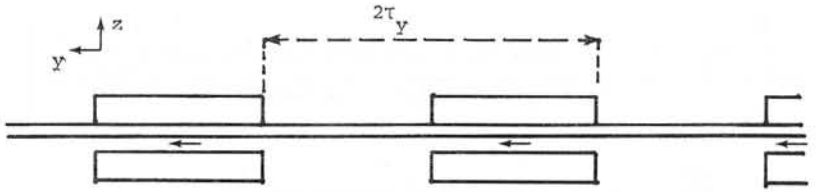

Fig.3 Longitudinal arrangement of stators for Fourier analysis of windings.

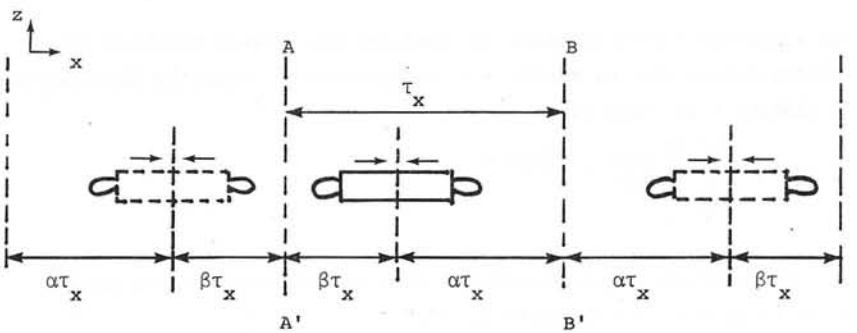

Fig.4 Transverse arrangement of slots for Fourier analysis of windings

Adjacent machines are connected in opposite senses so that the plate current does not cross the lines of symmetry given by AA' and BB' in fig.4. By varying the ratio of $\alpha:\beta$ the effect of off-setting the rotor plate can be simulated. It will, however, be appreciated that this model is only valid when plate widths equivalent to or greater than the stator width are used.

The two-dimensional array is subsequently replaced by a multi-layer model. For the herringbone motor a total of eleven regions was used. These are indicated on fig.5.

Of the eleven regions only two (Nos. 2 and 10) are fully anisotropic. This arises because the stator slot and tooth regions must be assumed non-conducting, and when this is the case $\varepsilon_1 = \varepsilon_2$ (see equa-

tion 2). The same result is obtained for the (isotropic) air and rotor conductor regions.

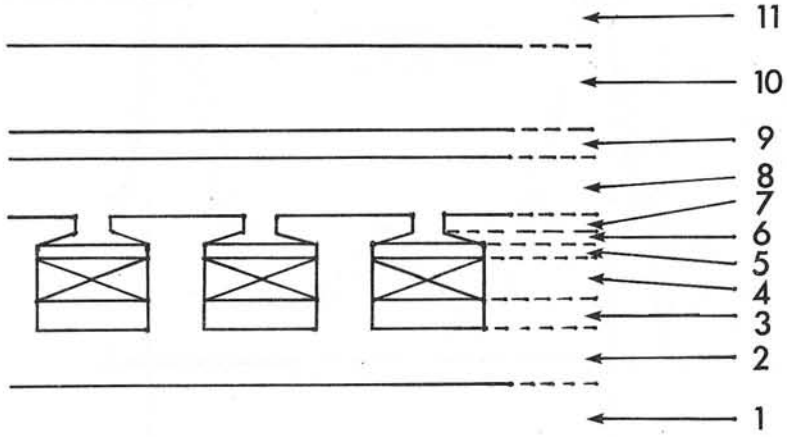

Fig.5 Regional representation of Herringbone motor.

1. Air
2. Stator back-iron
3. Stator slot bottom wedge
4. Stator excitation
5. Stator slot top wedge
6. Stator tooth neck
7. Stator tooth tip
8. Airgap
9. Rotor plate
10. Rotor back-iron
11. Air

Experimental Procedure

The herringbone was tested at standstill with an aluminium plate rotor 25 cm wide and 3.25 mm thick. This represents an overhang of some 2.4 cm either side of the stator, the plate being in the central position. The clearance airgap was set to 6.15 mm and the machine excited in firstly the forwards and then the reverse sense. For each case a search-coil was used to measure the variation in the flux normal to the rotor plate surface with position across the width of the machine. The rotor surface temperature was held at a steady 60°C (±4°C) throughout both tests.

Comparison of Experimental Results with Theory

As pointed out above the herringbone motor was fitted with Gramme-ring windings. These are excessively leaky and, in fact, the machine impedance is dominated by leakage reactance. This leakage accentuates the unbalance inherent in any normally-wound linear motor, and has to be accurately calculated if a voltage-forced solution is required. In order to overcome this difficulty a current-forced solution was obtained. The unbalanced currents used in the experiments were fed into the program as input data, and as output the program predicted the magnitude and phase of the search-coil voltages. Figure 6(a) and 6(b) show the computed and measured search-coil emf magnitudes and phases for the 'forwards' phase sequence, and figures 7(a) and 7(b) do the same for the 'reverse' phase sequence. It will be seen from these figures that the agreement between theory and practice is reasonable. The greatest discrepancy occurs in the plate overhang regions, where the predicted direction of travel (i.e. the slope of the phase variation) is the opposite to that measured. There are two probable causes of this. Firstly, the layer theory model ignores the lateral discontinuities in the iron blocks. In other words the back-iron is assumed to be as wide as the rotor plate. Secondly, the Gramme-ring windings are modelled as if they are conventional (i.e. drum-type) windings. This means that the winding overhang in the model must carry longitudinal currents, whereas in the real machine the stator currents return at the back of the stator iron. The first of these probable causes is inherent to layer-theory in general. The second is a feature of the test machine only.

This phase discrepancy occurs over a narrow width of the machine. It will be seen that over the majority of the plate surface the agreement is very good. In addition, it will be seen that the direction of field travel across the rotor plate surface is, indeed, determined by the angled field. The results shown required a total of 40 transversely-directed and 60 longitudinally-directed harmonics, and represented a medium-sized job, requiring 2½ mins on the Aberdeen University ICL 4/70 machine.

Figs. 6(a) and 6(b)

Variation of search-coil emf magnitude and phase with distance across machine. Forwards phase sequence.

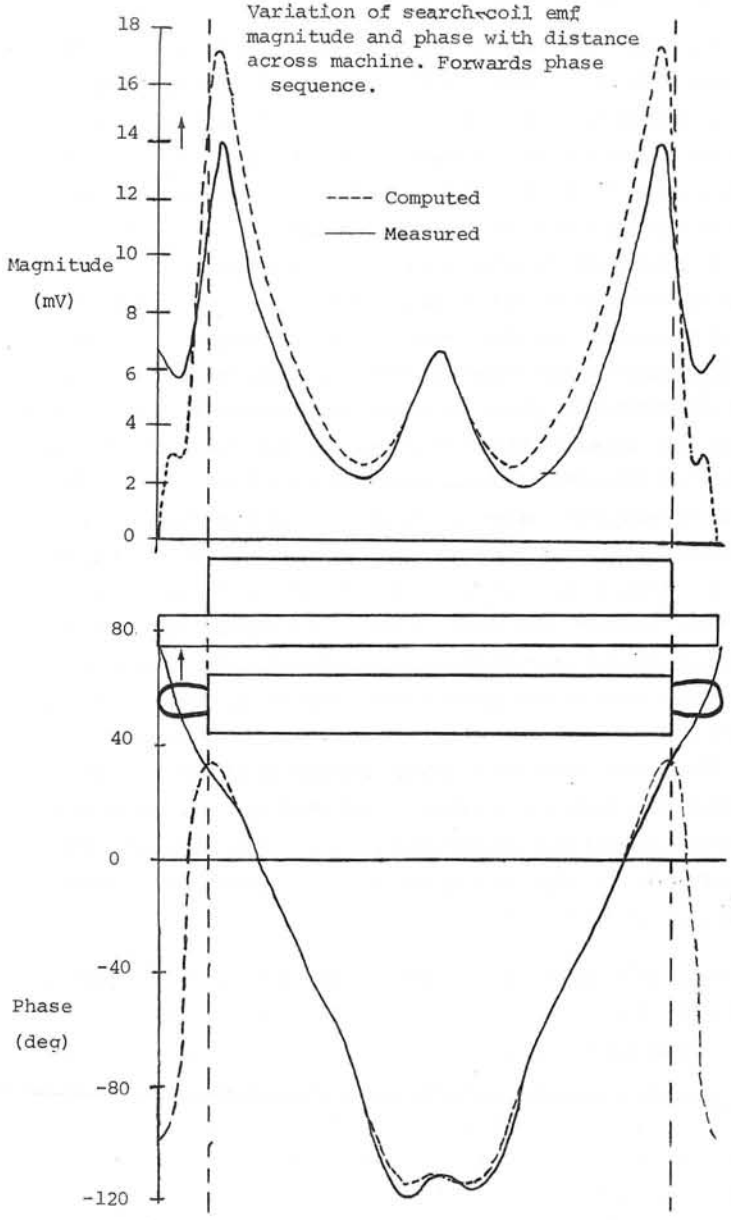

Figs. 7(a) and 7(b)

Variation of search-coil emf magnitude and phase with distance across machine. Reverse phase sequence.

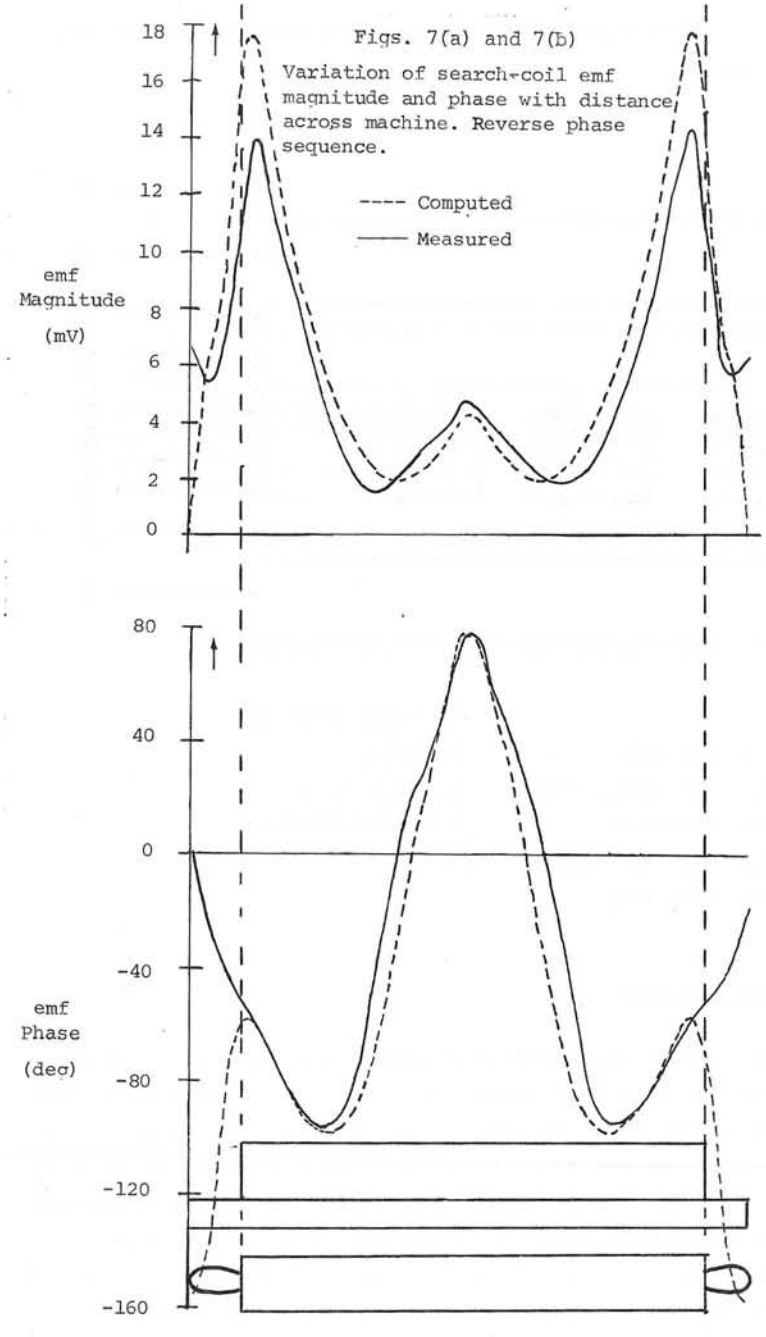

Conclusion

The anisotropic layer theory has been shown to be capable of predicting the airgap field in the herringbone motor to a reasonable accuracy. Further work must now be done to test its value in predicting the performance of a wide variety of machines, in particular those with unusual geometries.

References

1. WILLIAMSON, S.: 'The Anisotropic Layer Theory of Induction Machines and Induction Devices', J. Inst. Maths. Applics., 1976, 17, (1), pp.69-84.

2. LAITHWAITE, E.R., EASTHAM, J.F., BOLTON, H.R. and FELLOWS, T.G.: 'Linear Motors with Transverse Flux', Proc.IEE, 1971, 118, (12), pp.1761-67.

3. EASTHAM, J.F. and ALWASH, J.H.: 'Transverse Flux Tubular Motors', ibid., 1972, 119, (12), pp.1709-18.

4. EASTHAM, J.F. and LAITHWAITE, E.R.: 'Linear-Motor Topology', ibid., 1973, 120, (3), pp.337-343.

5. EASTHAM, J.F. and WILLIAMSON, S.: 'Experiments on the Lateral Stabilisation and Levitation of Linear Induction Motors', Trans.IEEE, 1974, MAG-10, (3), pp.470-473.

6. BALCHIN, M.J. and EASTHAM, J.F.: 'Performance of Linear Induction Motors with Airgap Windings', Proc.IEE, 1975, 122, (12), pp.1382-1290.

Discussions following paper:

(Wyatt, Imp College) First, I congratulate Dr Williamson on a fine piece of work. In the model used, a series of stators is assumed in the transverse direction and I would ask him what the inter-stator distance corresponding to the results shown is. It seems that the accuracy of the method presented must suffer as the plate width approaches the stator width and I would appreciate Dr Williamson's comments on this point.

(Williamson) I would like to thank Mr Wyatt for his kind remarks. The transverse modelling requires the 'inter-stator' distance to be equal to the width of the rotor plate when the plate is central. This constraint is imposed so that there is no current flow between adjacent machines. When the rotor plate is offset the 'inter-stator' distance is varied as shown in fig 4 of my paper, where T_x is the plate width. I should also point out that the discontinuous stator iron is replaced by a continuous slab in the model, and it is this approximation which I believe, produces the phase error at the plate edges. Regarding Mr Wyatt's last point, I would like to comment that because of the inability to model the transverse discontinuity in the iron, I would expect the accuracy of the model to increase rather than decrease as the plate width approaches the stator width.

(Freeman) My congratulations to Dr Williamson for producing an analysis for an anisotropic model. I should like to ask two questions. Firstly is the material in each region continuous or discontinuous? Second, what is the effect of the transverse flux on the iron losses in the machine?

(Williamson) I should like to thank Dr Freeman for his congratulations. The material in each region is continuous in the plane of motion. The results presented in the paper represent a preliminary investigation, in which only the normal component of airgap flux was both measured and calculated. It is hoped that the anisotopic midelling will be able to predict eddy current loss in the backing-iron with a reasonable accuracy, but hysteresis loss is outside the scope of the analysis. No calculation of eddy-current loss in the laminated iron has yet been made, but I would like to thank Dr Freeman for pointing out a useful means of comparing isotropic and anisotropic working.

CALCULATION OF TRANSIENT SKIN-EFFECT IN CONDUCTORS EMBEDDED IN SLOTS

S.P. Verma, Member IEEE S.E. Abo-Shady, Student Member IEEE

Power Systems Research Group
Department of Electrical Engineering
University of Saskatchewan
Saskatoon, Canada

ABSTRACT

Skin-effect has a marked influence on the steady-state performance of electrical machines. In order to study the phenomenon of skin-effect during transients, the general partial differential equation of the vector potential is developed on the basis of two-dimensional analysis. Numerical techniques for solving the field equations obtained from two- and single-dimensional analyses are presented. With the consideration of single-dimensional analysis, a transient analytical solution is derived for the case of a sinusoidal total current applied to a rectangular bar embedded in a slot. The two specific cases of a step total current and a sinusoidal total current applied to a rectangular bar are considered for investigating the skin-effect during transients. The excellent agreement between numerical and analytical results verifies the numerical techniques developed in the paper. The results show the importance of the phenomenon of skin-effect and the need for its incorporation in the transient analysis of electrical machines.

INTRODUCTION

It is well known that the phenomenon of skin-effect has a marked influence on the steady-state performance of electrical machines. The investigations related to this phenomenon for the steady-state conditions are well established in the published literature. It is interesting to note that the behaviour of the phenomenon of skin-effect during transients is quite different from that during the steady-state conditions. This is revealed by the studies conducted on an isolated bar by Tuohy et al.[1] and on a bar embedded in a slot by Mocanu[2] and Probst[3].

In several applications of induction, synchronous and induction-synchronous machines, accurate information about their transient performance with special reference to starting, synchronizing, switching-over and load-changes is required. This necessitates the incorporation of the transient skin-effect in the analysis of the machine under consideration. Important as it is, unfortunately the transient analysis of electrical machines in itself is very complex. In order to study the transient behaviour which takes into account the skin-effect successfully, one requires, firstly, a suitable method of analysis[4] which simultates the machine in a manner suitable for incorporating the skin-effect during transients and, secondly, an appropriate technique to determine the variation of skin-effect with respect to time. This paper is devoted to the investigations of the transient skin-effect in cage windings.

Eddy currents are produced in conductors carrying alternating currents by the virtue of the changing magnetic field. These currents result in a non-uniform distribution of the current density. In the case of a conductor carrying a steady-state alternating current, as well known, the current tends to flow in the outer layers of the conductor. This causes an increase in the effective resistance of the conductor and a decrease in its effective inductance. In general, at any instant of time the amount of skin-effect due to a time-varying current depends on the rate of change of the current at that instant and on the conditions prior to it. It is, therefore, to be expected that the current distribution in a conductor during transients is quite different from the steady-state distribution.

It is worthwhile to mention that although the approaches based on single-dimensional analyses can be successfully applied to the cases of deep bars, such approaches are not suitable for treating end-ring segments or bars having a small height to width ratio. Further, the representation of bars by series and parallel combinations of resistances and inductances requires the development of a suitable technique to solve such a network which in itself is a problem.

In view of the above, it is the main object of this paper to present the general form of the partial differential equation of the vector potential on the basis of two-dimensional analysis and to develop a numerical technique by formulating the difference equations in a form which is suitable for the computation

of transients in electrical machines. This technique can be applied to bars and end-ring segments provided that the boundary conditions are completely defined. Since in the case of deep bars the use of single-dimensional analysis is quite satisfactory and it requires much less computation time, a numerical technique is also presented for the determination of instantaneous distribution of the magnetic field intensity, the current density and the instantaneous voltage drop of a deep bar embedded in a slot. In order to verify the results delivered by the two-dimensional analysis and to determine the degree of its accuracy, the case of a sinusoidal total current applied to a deep bar embedded in a slot is treated and an analytical transient solution is obtained on the basis of single-dimensional analysis. Expressions for the magnetic field intensity, the current density and the voltage drop are presented.

The numerical techniques are applied to study the transient skin-effect of a deep bar embedded in a slot by considering the following two specific cases:

(i) a step total current,

(ii) a sinusoidal total current.

A comparison is then drawn between the numerical results of the two- and single-dimensional analyses. In addition, the analytical results of the single-dimensional analyses are used for further verification.

DEVELOPMENT OF TWO-DIMENSIONAL ANALYSIS

In general, the variation of currents as a function of time in the various bars and end-ring segments of an electrical machine is not known during transients. These currents can, however, be calculated at each instant of time through the numerical solution of the non-linear differential equations of the machine. It is practically impossible to obtain an analytical solution for the purpose of investigating the transient skin-effect in electrical machines. This calls for the development of numerical techniques for studying the skin-effect during transients. The analysis is commenced by formulating the field equations in a manner most suitable for the transient investigations.

General Partial Differential Equation of Vector Potential

Considering two-dimensional variation of the electromagnetic field, the following equations are obtained from the general form of Maxwell's equations:

$$\frac{\partial H_y}{\partial x} - \frac{\partial H_x}{\partial y} = \sigma, \tag{1}$$

$$\frac{\partial \sigma}{\partial y} = - \frac{\mu}{\rho} \cdot \frac{\partial H_x}{\partial t}, \tag{2}$$

and

$$\frac{\partial \sigma}{\partial x} = \frac{\mu}{\rho} \cdot \frac{\partial H_y}{\partial t} . \tag{3}$$

In order to simplify the calculations of the field, one makes use of vector potential A, which is so defined that its line integral around any closed path is equal to the total flux enclosed by the path[16]. As the area of a surface bounded by the path approaches zero, the limiting value of the line integral per unit area, (i.e. curl A), is equal to the flux density B. Hence,

$$\text{curl } A = B = \mu H, \tag{4}$$

where the direction of A is in a plane perpendicular to the direction of B.

With the help of equations (1) to (4), the general partial differential equation of the vector potential A is developed as:

$$\frac{\partial^2 A}{\partial x^2} + \frac{\partial^2 A}{\partial y^2} = \frac{\mu}{\rho} \cdot \frac{\partial A}{\partial t} + f(t) = - \mu\sigma , \tag{5}$$

where f(t) is a function dependent on time and independent of the co-ordinates x and y. The physical meaning of this function will be interpreted later.

The vector potential equation for some particular cases which are of considerable importance in practice can be derived from the general form given by equation (5).

Physical Interpretation of f(t)

As mentioned earlier, f(t) is dependent on time and independent of the co-ordinates x and y. It is a well-known

fact that at any instant of time the voltage drop between two points located at the two ends of a current-carrying conductor is the same irrespective of the location of these two points. As the voltage drop is the only physical quantity which possesses such a property for any mode of operation (e.g., transient or steady-state), there must be a relationship which correlates f(t) with the voltage drop of the current-carrying conductor. This interpretation is confirmed through the mathematical proof given in the following.

Consider a conductor of an arbitrary cross-section and having a unit length, as shown in Fig. 1, which is located in a magnetic field described by the vector potential A. Such a magnetic field may be produced due to a current in the conductor itself and/or due to currents in other conductors. If the vector potential is defined at a point within the conductor, the flux linking with an infinitesimal filament δS situated at that point will be $(A-A_o)$ due to the magnetic field bounded by a flux line whose vector potential is A_o. Further, the voltage drop per unit length of this filament caused by its resistance is "$\rho\sigma$" . Hence, the total drop of the filament under consideration due to the resistance and the magnetic field is given by:

$$v = \rho\sigma + \frac{\partial(A-A_o)}{\partial t}, \qquad (6)$$

which is actually the voltage drop across the conductor as a whole.

Since the line $A = A_o$ is a flux line, the value of A_o is independent of x and y but may be a function of time depending on the mode of operation. Accordingly, equation (5) may be rewritten as:

$$\frac{\partial^2(A-A_o)}{\partial x^2} + \frac{\partial^2(A-A_o)}{\partial y^2} = \frac{\mu}{\rho}\frac{\partial(A-A_o)}{\partial t} + f(t) + \frac{\mu}{\rho}\frac{\partial A_o}{\partial t} = -\mu\sigma. \qquad (7)$$

From equations (6) and (7), the following relationship is obtained:

$$\left[f(t) + \frac{\mu}{\rho}\frac{\partial A_o}{\partial t}\right] = -\frac{v\mu}{\rho}. \qquad (8)$$

The above equation represents the general relationship between f(t) and the voltage drop v. The two terms, $(f(t))$ and $(\frac{\mu}{\rho}\frac{\partial A_o}{\partial t})$, of equation (8) can be combined to form another function directly proportional to the voltage drop across the conductor under consideration. Further, it is much more convenient, if not the only appropriate way, to deal with the quantity $(A-A_o)$ as a vector potential variable. By doing so, the partial differential equation of the vector potential assumes the following form:

$$\frac{\partial^2 A}{\partial x^2} + \frac{\partial^2 A}{\partial y^2} = \frac{\mu}{\rho}\cdot\frac{\partial A}{\partial t} - \frac{v\mu}{\rho} = -\mu\sigma. \qquad (9)$$

Finite Difference Representation

As stated earlier, a numerical technique is required for obtaining the solution of field equations during transients. The finite difference method is adopted for developing the numerical technique.

In order to replace the partial differential equation of the vector potential by a set of finite difference algebraic equations which inter-relate the values of the vector potential at discrete points, any spatial distribution of these points may be chosen. However, it is preferable to make the points lie on the "nodes" of a regular mesh which may consist of squares as is the case presented here. Fig. 2 shows a simple rectangular field region. At a certain time t_n, any node within the boundary is positioned with respect to the neighbouring nodes (including those on the boundary) as shown in Fig. 3 and Fig. 4. As the symmetrical star shown in Fig. 3 is merely a special case of the asymmetrical star, Fig. 4, the difference equation of the latter is presented.

To derive the difference equation of a node (e.g., "i, j, n"), the vector potential function is expanded at the node by using Taylor's series. Expressions for:

$$\left(\frac{\partial^2 A}{\partial x^2}\right)_{i,j,n}, \quad \left(\frac{\partial^2 A}{\partial y^2}\right)_{i,j,n} \quad \text{and} \quad \left(\frac{\partial A}{\partial t}\right)_{i,j,n}$$

are then obtained in terms of the values of the vector potential at this and the neighbouring nodes. The results thus obtained are substituted in equation (9), which gives the following general difference equation:

$$\frac{2(k_1A_{i-1,j,n} + k_3A_{i+1,j,n})}{k_1k_3(k_1+k_3)} + \frac{2(k_2A_{i,j-1,n} + k_4A_{i,j+1,n})}{k_2k_4(k_2+k_4)}$$

$$-\{\frac{\lambda\mu}{\rho} + 2(\frac{1}{k_1k_3} + \frac{1}{k_2k_4})\}A_{i,j,n} + (\Delta x)^2(\frac{\nu\mu}{\rho})_n = -\frac{\lambda\mu}{\rho} A_{i,j,n-1}, \qquad (10)$$

where

$$\lambda = (\Delta x)^2/\Delta t$$

and $(A_{i,j,n-1})$ is the vector potential of the node (i,j,n) at the time interval preceding the one under consideration.

For nodes outside the current-carrying regions, equation (10) becomes:

$$\frac{2(k_1A_{i-1,j,n} + k_3A_{i+1,j,n})}{k_1k_3(k_1+k_3)} + \frac{2(k_2A_{i,j-1,n} + k_4A_{i,j+1,n})}{k_2k_4(k_2+k_4)}$$

$$- 2\,(\frac{1}{k_1k_3} + \frac{1}{k_2k_4})\,A_{i,j,n} = 0\ . \qquad (11)$$

At all boundary points, which may be situated on an iron-air interface or on a magnetic flux line or on an interface between a current-carrying region and a non-current-carrying region, the corresponding difference equation can be suitably developed[16] by modifying equations (10) and (11). Corresponding to the number of nodes "m", a set of m equations similar to equations (10) and (11) can then be formulated. To obtain a complete solution of the vector potential at a given specific instant, one more equation is required for the variable $(\frac{\nu\mu}{\rho})_n$. This particular equation is obtained by equating the line-integral of the magnetic field intensity around a current-carrying conductor to the instantaneous value of the current in the conductor. This integral depends on the vector potential of various nodes. It should be mentioned that in the presence of more than one current-carrying conductor, say ν conductors, a corresponding equation has to be obtained for each conductor due to the fact that each conductor has its own value for $(\frac{\nu\mu}{\rho})_n$. The problem is, therefore, converted to a set of simultaneous algebraic equations having the form:

$$[G]\ [P]_n = [C]_n, \qquad (12)$$

where

$[G]$ is a square matrix of order $(m + \nu)$,

$[P]_n$ is a column of m vector potentials at the various nodes in addition to ν variables of $(\frac{\nu\mu}{\rho})_n$ and

$[C]_n$ is a column of order $(m + \nu)$.

It is evident that the matrix $[G]$ is independent of time. As the solution of the algebraic equations during transients is required at each instant of time, from computation time considerations it is not advisable to solve these equations by employing iterative methods. Instead, the inverse of $[G]$ should be determined and stored in the computer. By calling $[G]^{-1}$ from the storage, the vector potential at the various nodes and the variable $(\frac{\nu\mu}{\rho})_n$ can then be evaluated at a specific instant from the following simple algebraic equation:

$$[P]_n = [G]^{-1}[C]_n. \qquad (13)$$

Knowing the vector potential at every node of the region under consideration, any other variables (e.g., current density, magnetic field intensity, flux density) can be easily determined at these nodes with the help of simple algebraic equations.

SINGLE-DIMENSIONAL ANALYSIS

In studying the skin-effect of deep bars in electrical machines, the problem can be simplified to a single-dimensional one without committing great errors. This is achieved by assuming the flux lines in the slots to be parallel to the periphery of the rotor. With this assumption, the partial differential equation of the magnetic field intensity in a rectangular bar as shown in Fig. 5 assumes the following form:

$$\frac{\partial^2 H_x}{\partial y^2} = \frac{\mu}{\rho\alpha}\frac{\partial H_x}{\partial t}\ , \qquad (14)$$

where

$$\alpha = \frac{b}{a}.$$

It should be pointed out that the boundary conditions of the magnetic field intensity are much easier to define than those of the current density. It is, therefore, preferable to deal with the magnetic field intensity H_x instead of the current

density σ. Equation (14) is a parabolic differential equation. In order to solve such an equation, both an initial condition and subsequent time-dependent boundary conditions are required. In the case of a rectangular bar, Fig. 5, the boundary conditions are:

$$H_x = 0 \quad \text{at} \quad y = 0 \tag{15}$$

and

$$H_x = \frac{i}{b} \quad \text{at} \quad y = h \tag{16}$$

where i is the total current carried by the bar. Having recognized the initial and the boundary conditions, equation (14) can be solved either numerically or analytically.

Analytical Solution

A transient analytical solution can be obtained for equation (14) only if the total current is defined by an explicit function with respect to time. Although this condition is not satisfied in electrical machines during transients, the analytical solution of the case of a sinusoidal total current applied to a rectangular bar embedded in a slot is derived, firstly, to use the solution for confirming the validity of the numerical techniques presented in this paper and, secondly, because such a solution is not available in the published literature.

Equation (14) can be rewritten as:

$$\frac{\partial^2 H_x}{\partial y^2} = \frac{1}{k^2} \frac{\partial H_x}{\partial t} , \tag{17}$$

where $k^2 = \frac{\alpha\rho}{\mu}$.

Considering the boundary conditions given by equations (15) and (16), the solution for a sinusoidal applied total current is obtained as:

$$H_x(t) = \frac{\hat{i}}{b} \left[\sum_{\eta=1}^{\infty} \left\{\frac{2\eta\pi k^2\omega(-1)^{\eta+1}}{h^2(\omega^2+(\eta\pi k/h)^4)} e^{-(\eta\pi k/h)^2 t} \cdot \sin(\eta\pi y/h)\right\}\right.$$

$$\left. + \sqrt{\frac{(\sinh(y/AA)\cdot\cos(y/AA))^2+(\cosh(y/AA)\cdot\sin(y/AA))^2}{(\sinh(h/AA)\cdot\cos(h/AA))^2+(\cosh(h/AA)\cdot\sin(h/AA))^2}} \cdot \sin(\omega t+\alpha_1)\right] , \tag{18}$$

where $AA = k\sqrt{2/\omega}$

and

$$\alpha_1 = \tan^{-1}(\text{cotanh}(y/AA).\tan(y/AA)) - \tan^{-1}(\text{cotanh}(h/AA).\tan(h/AA)).$$

Differentiating equation (18) partially with respect to y and multiplying the results thus obtained by $(-\alpha)$, the transient distribution of the current density is obtained as:

$$\sigma(t) = \frac{\hat{i}}{a} \left[\sum_{\eta=1}^{\infty} \left\{\frac{2\eta^2\pi^2k^2\omega(-1)^{\eta+1}}{h^3(\omega^2+(\eta\pi k/h)^4)} e^{-(\eta\pi k/h)^2 t} \cdot \cos(\eta\pi y/h)\right\} + \right.$$

$$\left. + \sqrt{\frac{(\cosh(y/AA)\cdot\cos(y/AA))^2+(\sinh(y/AA)\cdot\sin(y/AA))^2}{(\sinh(h/AA)\cdot\cos(h/AA))^2+(\cosh(h/AA)\cdot\sin(h/AA))^2}} \cdot \frac{\sqrt{2}}{AA} \sin(\omega t+\alpha_2)\right] , \tag{19}$$

where $\alpha_2 = \pi/4 + \tan^{-1}(\tanh(y/AA).\tan(y/AA)) - \tan^{-1}(\text{cotanh}(h/AA).\tan(h/AA))$.

The voltage drop per unit length can be obtained by replacing the variable y by h in equation (19) and multiplying the results thus obtained by ρ.

COMPUTED RESULTS

The various results presented here were calculated for a rectangular bar embedded in a slot by considering the two specific cases of a step applied total current and a sinusoidal applied total current. In the latter case, the frequency is assumed to be 50 Hz.

The dimensions of the bar under consideration are:

$$a = b = 10 \text{ mm}, \quad h = 50 \text{ mm},$$

and the length of the bar is assumed to be unity, i.e. 1 meter.

For the generalization of the results, the different variables are normalized as follows:

$$t_{p.u.} = \frac{t\rho}{\mu h^2} , \qquad H_{p.u.} = \frac{Hb}{\hat{i}} ,$$

$$\sigma_{p.u.} = \frac{\sigma a h}{\hat{i}} \quad \text{and} \quad v_{p.u.} = \frac{v a h}{\rho \hat{i}} .$$

A computer programme was developed for the numerical calculation of the instantaneous voltage drop across the bar on the basis of the two-dimensional analysis. Also, a computer programme was developed by considering the single-dimensional analysis for the analytical and numerical determination of the instantaneous voltage drop across the bar and the instantaneous distribution of the magnetic field intensity & the current density along the height of the bar.

Case 1 - Step Applied Total Current

Fig. 6 shows the variation of the instantaneous normalized voltage drop versus the normalized time for a step applied total current. It is interesting to note that the voltage drop reaches a value of more than 15 times the steady-state value. Although the application of a step total current is not actually encountered in electrical machines, nevertheless this important result shows the significance of the transient skin-effect.

Case 2 - Sinusoidal Applied Total Current

The variation of the instantaneous normalized voltage drop versus the normalized time is shown in Fig. 7 for a sinusoidal applied total current. It may be observed that the variation of the voltage drop during the first cycle is quite different from the steady-state variation.

The distribution of the normalized magnetic field intensity along the height of the bar at different values of $t_{p.u.}$ was obtained by using the single dimensional analysis and it is shown in Fig. 8(a) and Fig. 8(b). The results shown are for the first cycle of the applied current. It is observed that initially the magnetic field is concentrated in the upper layers of the bar and as time lapses, the field spreads down to the lower layers.

The variation of the normalized current density along the height of the bar is shown in Fig. 9(a) and Fig. 9(b) at different values of $t_{p.u.}$. As in the case of the magnetic field intensity, initially the current is concentrated in the upper layers of the bars and then it spreads downwards as time increases.

It should be pointed out that the difference between the numerical and analytical results shown in Figs. 6 to 9 is practically negligible, which supports the accuracy of the numerical techniques presented in this paper.

CONCLUSIONS

The general partial differential equation of the vector potential has been developed on the basis of two-dimensional analysis. The corresponding vector potential equations have been derived from the general equation. The numerical solution of such equations has been described in a manner which is suitable for transient conditions.

In the case of deep bars embedded in slots, the phenomenon of skin-effect can be investigated with sufficient accuracy by using the single-dimensional analysis. For this purpose, the procedure for solving the field equations numerically has been presented. In addition, the transient analytical solutions of the magnetic field intensity, the current density and the voltage drop have been derived for the case of a sinusoidal total current applied to a rectangular bar in a slot.

The transient skin-effect in a deep bar embedded in a slot has been investigated by considering the two specific cases of a step and a sinusoidal applied total current. The excellent agreement between the analytical results and the results obtained by using the numerical techniques developed on the basis of two and single dimensional analyses verifies the validity of the numerical techniques.

NOMENCLATURE

A	= Vector potential
B	= Flux density
a	= Width of the bar
b	= Slot opening
H	= Magnetic field intensity
h	= Height of the bar
i	= Instantaneous total current
$k_1, k_2, k_3 \& k_4$	= Constants less than or equal to unity
m	= Number of nodes
t	= Time, sec.
x, y	= x and y Cartesian co-ordinates
v	= Instantaneous voltage drop per unit length
ω	= Frequency of the applied current, rad./sec.
σ	= Current density
ρ	= Resistivity
μ	= Permeability

ν = Number of current-carrying conductors
Δx = Width of a square mesh
Δt = Time increment

Subscripts:

i = The variable at the i^{th} x co-ordinate
j = The variable at the j^{th} y co-ordinate
n = The variable at the n^{th} interval of time
p.u. = The normalized value of the variable
x = The variable component in the x direction
y = The variable compenent in the y direction

ACKNOWLEDGEMENT

The authors are thankful to the National Research Council of Canada for the financial support of this project. They also wish to thank the Department of Electrical Engineering, University of Saskatchewan, Saskatoon, for the facilities in connection with this work.

REFERENCES

1. Tuohy, E.J., Lee, T.H. and Fullerton, H.P., "Transient resistance of conductors", IEEE Trans., Vol. PAS-87, No. 2, Feb. 1968, pp. 455-462.
2. Mocanu, C.I., "Transient skin-effect in a rectangular conductor in a slot", Archiv für Elektrotechnik, Bd. 55, 1973, pp. 164-170.
3. Probst, R., "Transient behaviour of asynchronous motors in the case of system switchover, taking into account the skin effect in the rotor bars", ETZ-A, Bd. 94, H.9, 1973, pp. 515-520.
4. Abo-Shady, S.E. and Verma, S.P., "A novel approach for the analysis of rotor cage windings of salient-pole machines", Paper no. C 75 129-2, IEEE PES Meeting, New York, N.Y., January 1975.
5. Štafl, M., "Electrodynamics of Electrical Machines", Iliffe Books Ltd., London, 1967.
6. Dwight, H.B., "Electrical Elements of Power Transmission Lines", The Macmillan Company, New York, 1954.
7. Babb, D.S. and Williams, J.E., "Circuit analysis method for determination of A.C. impedances of machine conductors", AIEE Trans., Vol. 70, Part I, 1951, pp. 661-666.
8. Babb, D.S. and Williams, J.E., "Network analysis of A.C. machine conductors", AIEE Trans., Vol. 70, 1951, pp. 2001-2005.
9. Liwschitz-Garik, M., "Skin-effect bars of squirrel-cage rotors", AIEE Trans., Vol. 73, Part III-A, April 1954, pp. 255-258.
10. Liwschitz-Garik, M., "Computation of skin-effect in bars of squirrel-cage rotors", AIEE Trans., Vol. 74, Part III, August 1955, pp. 768-771.
11. Dwight, H.B., "Effective resistance of isolated nonmagnetic rectangular conductors", AIEE Trans., Vol. 66, 1947, pp. 549-552.
12. Silvester, P., "Modal network theory of skin effect in flat conductors", Proc. of IEEE, Vol. 54, No. 9, Spt. 1966, pp.1147-1151.
13. Silvester, P., "A.C. resistance and reactance of isolated rectangular conductors", IEEE Trans., Vol. PAS-86, No. 6, 1967, pp. 770-774.
14. Silvester, P., "The accurate calculation of skin-effect in conductors of complicated shape", IEEE Trans., Vol. PAS-87, No. 3, March 1968, pp. 735-742.
15. Silvester, P., "Dynamic resistance and inductance of slot-embedded conductors", IEEE Trans., Vol. PAS-87, No. 1, Jan. 1968, pp. 250-256.
16. Binns, K.J. and Lawrenson, P.J., "Analysis and Computation of Electric and Magnetic Field Problems", The Macmillan Company, New York, 1963.
17. Lammeraner, J. and Štafl, M., "Eddy Currents", Iliffe Books Ltd., London, 1966.

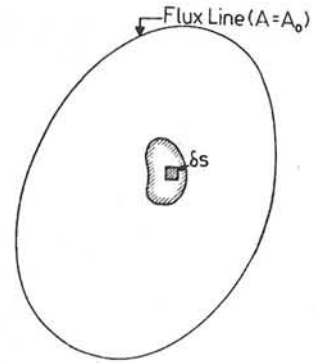

Fig.1. Conductor in a magnetic field

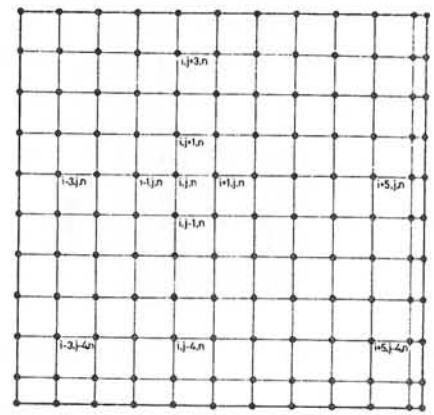

Fig.2. Simple rectangular field region at t_n

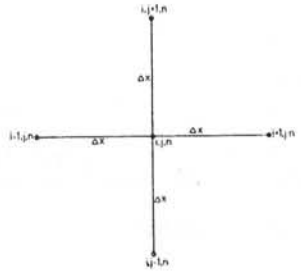

Fig.3. Symmetrical star

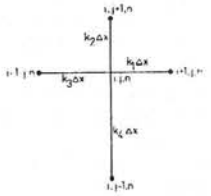

Fig.4. Asymmetrical star

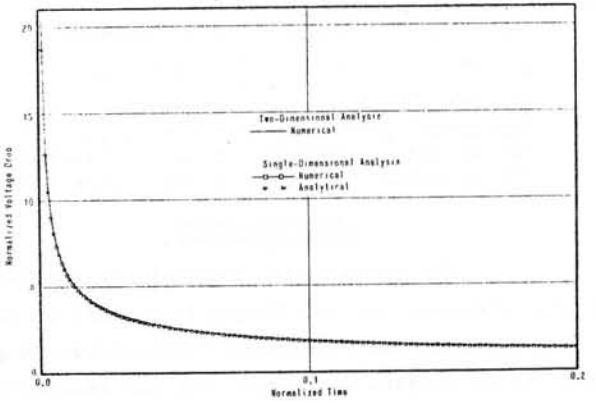

Fig.6. Instantaneous value of the normalized voltage drop due to a step total current

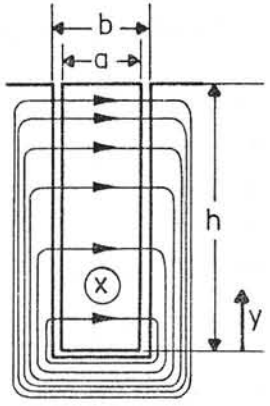

Fig.5. Flux distribution of a deep bar embedded in a slot

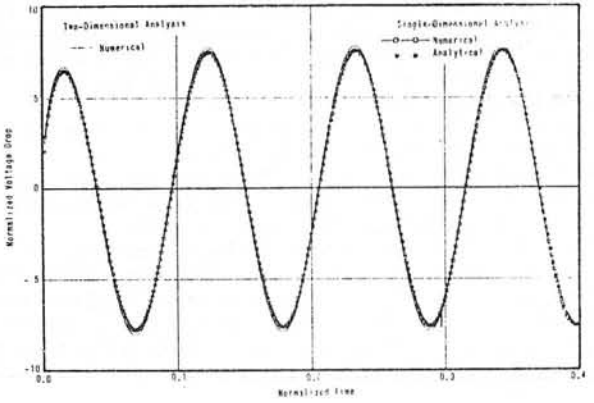

Fig.7. Instantaneous value of the normalized voltage drop due to a sinusoidal total current of frequency 50 Hz

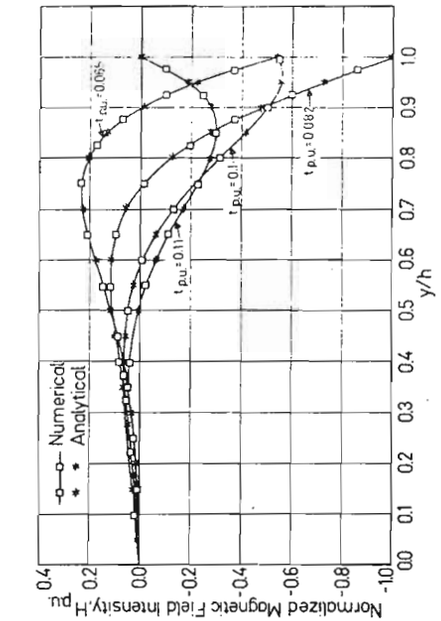

(b)

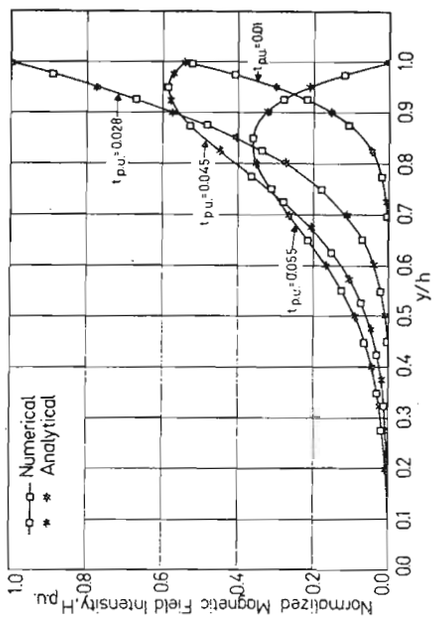

(a)

Fig.8. Distribution of the magnetic field intensity at different values of time due to a sinusoidal total current of frequency 50 Hz

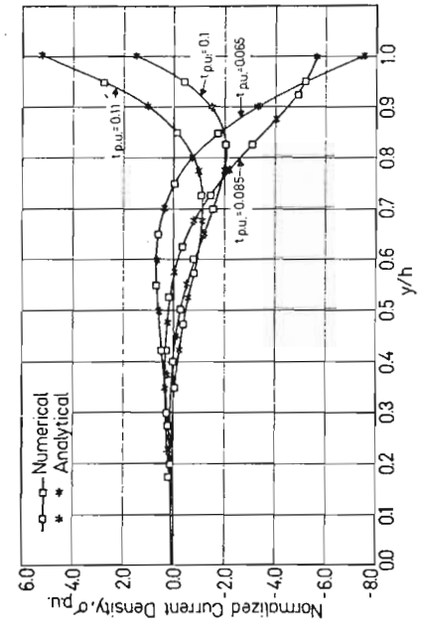

(b)

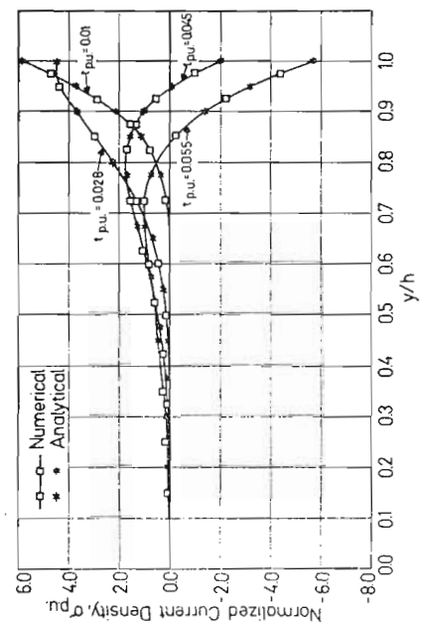

(a)

Fig.9. Distribution of the current density at different values of time due to a sinusoidal total current of frequency 50 Hz

Discussions following paper:

(Reichert) What boundary conditions were assumed in the airgap over the slot? There are two possibilities, either field parallel in the airgap or perpendicular on the iron.

(Verma, Univ of Saskatchewan) In the case of a deep bar embedded in a slot as presented in the paper, the field is considered to be parallel to the periphery of the rotor. The main purpose here was to verify the validity of the numerical techniques developed in the paper.

The method can, however, be applied to the cases where the airgap field is radial on iron by considering the boundary conditions properly.

MAGNETIC FIELD DIFFUSION IN FAST DISCHARGING HOMOPOLAR MACHINES: A FINITE ELEMENT APPROACH

E. B. Becker, R. D. Pillsbury, M. D. Driga
Energy Storage Group and Texas Institute for Computational Mechanics
The University of Texas Austin, Texas

The Energy Storage Group at The University of Texas have engaged in the preliminary design of several homopolars for fusion reactor applications, have designed and built two experimental homopolar machines and are currently designing and will build a very fast discharging experimental homopolar machine. This machine, shown in Figure 1, consists of two counter-rotating rotors which turn in a field with a maximum strength of approximately 8 Tesla produced by the circumferential field coil. The 6" diameter rotors, at their initial velocity of 28000 rpm, produce an open circuit voltage of 100 volts. The shaping of the rotors is to reduce the stored energy while maintaining the voltage, thereby reducing, as far as possible, the discharge time. It is expected that the .35 MJ of stored energy will be discharged in approximately 1.25 msec. with a peak current of some 2.8×10^6 amps. The forces and torques produced in the rotors and brushes by the large currents and fields (both applied and induced) are a limiting factor in the mechanical design of the machine; thus the accurate prediction of the force distribution is required. Since the penetration time for a conductor of dimensions comparable to the rotors is roughly the same as the discharge time of 1.25 msec., the determination of the current distribution in the system is truly a transient problem, the driving function of which is the motion of the rotating conductors in the (relatively) steady magnetic field.

Formulation of the Boundary Value Problem

With a few exceptions, notably Silvester (1), computational approaches fo field penetration problems have been limited to either the a.c. steady state case, or, as in the work of Miya (2), to situations in which the field is driven by a current whose spatial as well as temporal distribution is assumed to be known. In these situations the penetration is conveniently expressed in terms of the magnetic field H which satisfies an homogeneous diffusion equation driven by boundary values of H which can be inferred from the assumed conditions.

In the present application, as in many instances involving, say, electrical machines, commutating gear or fusion experiments, there is a conversion of energy that is stored in one form and converted into another, in the process of which the magnetic fields and currents are unknown and cannot reasonably be assumed a priori.

In order to employ the driving function $v \times B$ directly we introduce the electric potential Ψ and the magnetic vector potential A as primary dependent variables. Standard definitions of the potentials (1), Ohm's law for moving media (2), and Maxwell's equations (3) (neglecting displacement current) are the basis of our formulation.

$$-\nabla\Psi = E + \frac{\partial A}{\partial t}$$
$$B = \nabla \times A \qquad (1)$$

$$J = \sigma(E + v \times B_o) \qquad (2)$$

$$\nabla \times H = J$$
$$\nabla \cdot B = 0$$
$$\nabla \times E = -\frac{\partial B}{\partial t} \qquad (3)$$
$$\mu H = B$$

To these equations we adjoin the constraints that J and A be divergence free - the first on physical grounds and the second on mathematical ones. Combining these conditions we see that the field equations are equivalent to

$$\sigma\dot{A} + \nabla\times\frac{1}{\mu}\nabla\times A - \sigma(v\times\nabla\times A_0 + \nabla\Psi) = 0 \qquad (4)$$

$$\nabla\cdot\sigma\nabla\Psi - \nabla\cdot\sigma(v\times\nabla\times A_0 - \dot{A}) = 0$$

SUBJECT TO

$$\nabla\cdot A = 0 \qquad (5)$$

Because both the rotor motion v and the potential of the applied magnetic field A_0 are axisymmetric and have only Θ components the problem separates into two weakly coupled ones, namely, (6) which governs the distribution of the steady applied field and (7) in which the vector A has only r and z components.

$$\nabla\times\frac{1}{\mu}\nabla\times A_0 = J \qquad (6)$$

$$\sigma\dot{A} + \nabla\times\frac{1}{\mu}\nabla\times A + \sigma\nabla\Psi = \sigma\, v\times\nabla\times A_0$$

$$\nabla\cdot\sigma\dot{A} + \nabla\cdot\sigma\nabla\Psi = \nabla\cdot\sigma\, v\times\nabla\times A_0 \qquad (7)$$

$$\nabla\cdot A = 0$$

The finite element solution of (6), although necessary to our problem, is a standard one and need not be discussed further here.

In addition to the equations (7) we have as side conditions the vanishing of the potentials at large distance from the conductors and the usual continuity or jump conditions on current and field. These take the form (8) and (9).

$$A_r = A_z = \Psi = 0 \qquad \vec{r}\to\infty \qquad (8)$$

$$[\![\, \tfrac{1}{\mu}\nabla\times A \,]\!] = 0$$

$$[\![\, \sigma(v\times\nabla\times A_0 - \nabla\Psi - \dot{A}\,]\!] = 0 \qquad (9)$$

In (8) the brackets denote the jump in the enclosed quantity across an interface between different materials or between moving and stationary materials. In the finite element model of the region shown in Figure 1, the symmetry about r = 0 and anti-symmetry about z = 0 give rise to the following additional boundary conditions

$$A_r = 0 \quad \text{ON } r = 0$$

$$A_\theta = \Psi = 0 \quad \text{ON } z = 0 \qquad (10)$$

Finite Element Formulation

We seek solutions to (7) and (9) subject to the conditions (8) and (10) in the weak or Galerkin sense. To this end we introduce a Lagrange multiplier λ corresponding to the constraint (7c) and the test functions u, η, and τ corresponding to A, Ψ and λ. The weak statement of the problem is

$$\sum_i \Big\{ \iint_{\Omega_i} [\sigma\dot{A} + \nabla\times\tfrac{1}{\mu}\nabla\times A + \sigma\nabla\Psi - \sigma\, v\times\nabla\times A_0]\cdot u\, da - \int_{\partial\Omega_i} [\![\tfrac{1}{\mu}\nabla\times A_0]\!]\cdot u\, ds \Big\} = 0 \quad \text{FOR ALL } u \qquad (11)$$

AND

$$\sum_i \Big\{ \iint_{\Omega_i} [\nabla\cdot\sigma\dot{A} + \nabla\cdot\sigma\nabla\Psi - \nabla\cdot\sigma\, v\times\nabla\times A_0]\,\eta\, da - \int_{\partial\Omega_i} [\![\sigma(v\times\nabla\times A_0 - \nabla\Psi - \dot{A}\,]\!]\cdot n\,\eta\, ds \Big\} = 0 \qquad (12)$$

FOR ALL η

In (11) and (12) the regions Ω_i are regions within which all fields are continuous i.e. all the jumps are across the boundaries $\partial\Omega_i$ of these regions. Applying the divergence theorem to each region Ω_i and introducing the constraint (7c) with its multiplier and test function leads to the final weak form

$$\sum \Big\{ \iint [\sigma u\dot{A} + \tfrac{1}{\mu}(\nabla\times A)\cdot(\nabla\times A) + \sigma u\cdot\nabla\Psi + \lambda\nabla\cdot u + \tau\nabla\cdot A - \sigma\, v\times\nabla\times A_0\cdot u]\, da \Big\} = 0$$

$$\Sigma\left\{\iint\left[-\sigma\nabla\eta\cdot\nabla\psi-\dot{A}\cdot\nabla\eta+\sigma\nu_{x}\nabla_{x}A_{c}\cdot\nabla\eta\right]da\right\}=0 \qquad (13)$$

FOR ALL u, η, AND τ.

for arbitrary u, η, and τ vanishing at ∞.

It is significant that the jump terms have equilibrated the boundary integrals from the integration by parts i.e. the jump conditions are natural conditions that follow as a consequence of (13).

The discrete form of (13) is obtained by introducing the finite element approximation of the fields A, u, ψ, η, λ and τ. The elements are quadrilaterals and the shape functions are quadratic for A, u, ψ, and η and linear for λ and τ. Thus each corner node of the mesh has a total of four unknowns, i.e. A_r, A_z, ψ and λ, while the midside nodes have only A_r, A_z and ψ. If the set of nodal point values is denoted q then the discrete form of (13) can be written as

$$\underset{\sim}{C}\,\dot{q}+\underset{\sim}{K}\,q=f \qquad (14)$$

In (14) $\underset{\sim}{C}$ and $\underset{\sim}{K}$ are, for an element, 28×28 matrices whose elements are the integrals of products of shape functions. It is apparent from (13) that neither $\underset{\sim}{C}$ nor $\underset{\sim}{K}$ is symmetric. The forcing function f in (14) contains terms proportional to $\nu_{x}\nabla_{x}A_{c}$. The motion of the rotor is treated as given in this analysis and the value of the applied field A_c is known from an initial finite element solution for the single component $A_{c\theta}$.

Although, in some designs, there is iron shielding around the field coil making the equations for $A_{c\theta}$ non linear, the complete compensation of the machine as shown in Figure 1 confines the magnetic field governed by (14) to the region within the return conductor. There is no iron in the in the machine itself - the rotors being aluminum to reduce the capacitance of the machine - and so (14) is linear.

The initial value problem for q is solved using a combination of algorithms. Using the approximation

$$\dot{q}\equiv\left(q^{n+1}-q^{n}\right)/\Delta t$$

leads either to

$$\left(\frac{2}{\Delta t}\underset{\sim}{C}+\underset{\sim}{K}\right)q^{n+1/2}=\frac{2}{\Delta t}\underset{\sim}{C}\,q^{n}+f^{n+1/2} \qquad (15)$$

$$\left(\frac{1}{\Delta t}\underset{\sim}{C}+\underset{\sim}{K}\right)q^{n+1}=\frac{1}{\Delta t}\underset{\sim}{C}\,q^{n}+f^{n+1} \qquad (16)$$

In (15) $q^{n+1/2}\equiv\frac{1}{2}\left(q^{n+1}+q^{n}\right)$ is taken as the value of at $(n+\frac{1}{2})\Delta t$. Both (15) and (16) are implicit and clearly each involves the same amount of computation. We find that, once started adequately, longer time steps can be used with (15) but that the use of (15) for the first few time steps leads to unacceptably noisy solutions. Since, with either scheme, a change in time step means reassembly and decomposition, there is no computational penalty paid in changing scheme when the initial small time step is increased.

It is of great significance that, although neither $\underset{\sim}{C}$ nor $\underset{\sim}{K}$ is symmetric, $(\alpha\underset{\sim}{C}+\underset{\sim}{K})$ can be made symmetric simply by dividing the ψ equations thru by α. We have employed both symmetric band solvers and a frontal solver to reduce (15) and (16).

Results

The computational sequence begins with the solution of (6) for the values of the applied field $\bar{B}_o = \nabla \times \bar{A}_o$. The values of $\bar{B}_o$ are calculated at the integration points of each element and saved for use in calculating the forcing function in the transient problem. Figure 2 shows a flux plot (contours of constant values of $r\bar{B}_{o_\theta}$) for a current density of 1.18×10^8 amps/m^2 in the field coil. Incidentally this coil, which is LN_2 cooled copper, is energized by the discharge of a 5 MJ homopolar machine. This pulse is of the order of a second, quite long compared to the transient phenomena under consideration.

The computation proceeds using (15) and/or (16). Figures 3, 4, and 5 show contours of constant values of the magnetic field $\bar{B}_\theta$ induced by the current at an early time, $t = 20 \times 10^{-6}$sec. an intermediate time, $t = 200 \times 10^{-6}$sec., and a time, $t = 1000 \times 10^{-6}$sec. The diffusion of the current into the rotor the brushes and the return conductor is apparent. At selected time steps the body force density $\bar{J} \times \bar{B}$ is calculated and used as input to a finite element stress analysis. Both azimuthal and inplane forces give rise to significant stresses. In addition to the stress calculation it is possible to accumulate the time integral of ohmic heating in each element obtaining a detailed map of the resulting temperature distribution.

For reference, Figure 6 shows the long time distribution of $\bar{B}_\theta$ together with the finite element mesh used to model the problem. This state is not actually reached in teh course of discharging the machine since the rotor speed decreases to zero before the steady state could be reached.

Comments

The formulation described above, in conjunction with finite element techniques, makes possible the solution of quite a general class of problems involving transient magnetic phenomena. Arbitrary geometries, material interfaces etc. can be treated routinely. This formulation has evolved only after a good many false starts. The formulation is cumbersome and the computations expensive, but can furnish approximate solutions to problems that are otherwise unapproachable.

References

[1] Silvester, P., "Modal Network Theory of Skin Effect in Flat Conductors," Proceedings of the I.E.E.E., Vol. 54, No. 9, 1960.

[2] Mita, K., Ando, Y., Ohta, M., and Suzuki, Y., "Application of F.E.M. to Electro-Magneto-Mechanical Dynamics of Superconducting Magnet Coil and Vacuum Vessel," Symposium on Engineering Problems of Fusion Research, San Diego, California.

[3] Stratton, J. A., Electromagnetic Theory, McGraw-Hill, 1941.

[4] Rowberg, R. E., Becker, E. B., Rylander, H. G., and Woodson, H. H., "Characteristics of a Homopolar Machine as a Power Supply for Large Pulsed Magnetic Fields for Fusion Experiments," 1973 S.W.I.E.E. Conference Record of Technical Papers, p. 453, April 1973.

[5] Driga, M. D., Nasar, S. A., Rylander, H. G., Weldon, W. F., and Woodson, H. H., "Fundamental Limitations and Topological Considerations for Fast Discharge Homopolar Machines," I.E.E.E. Trans. on Plasma Science, Vol. PS-3, No. 4, December 1975.

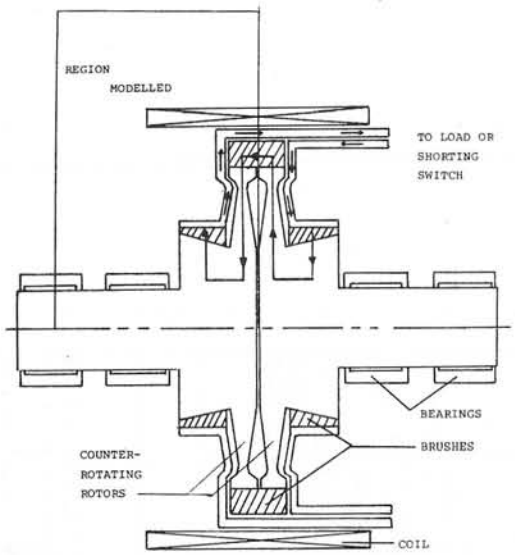

FIGURE 1. MACHINE CONFIGURATION

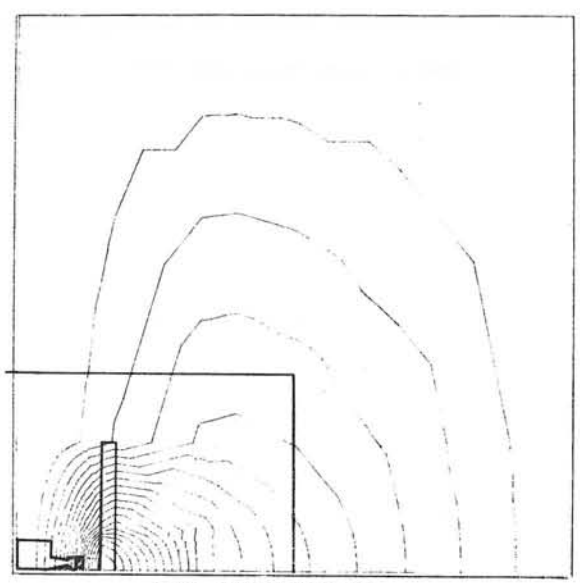

FIGURE 2. APPLIED MAGNETIC POTENTIAL A_0

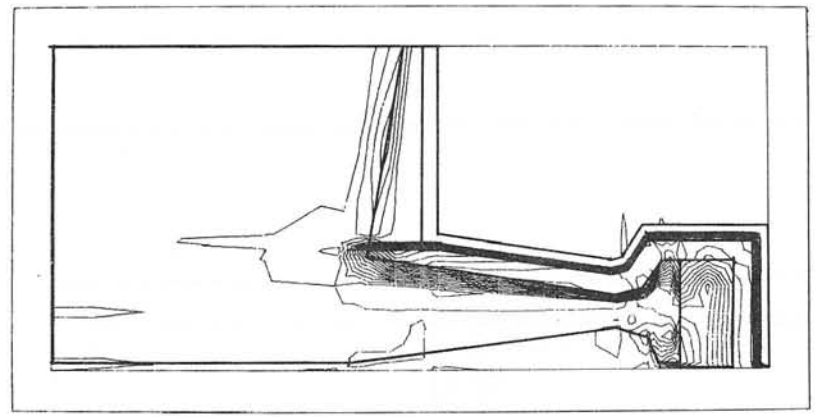

FIGURE 3. INDUCED FIELD B_θ AT t = 20 μ sec.

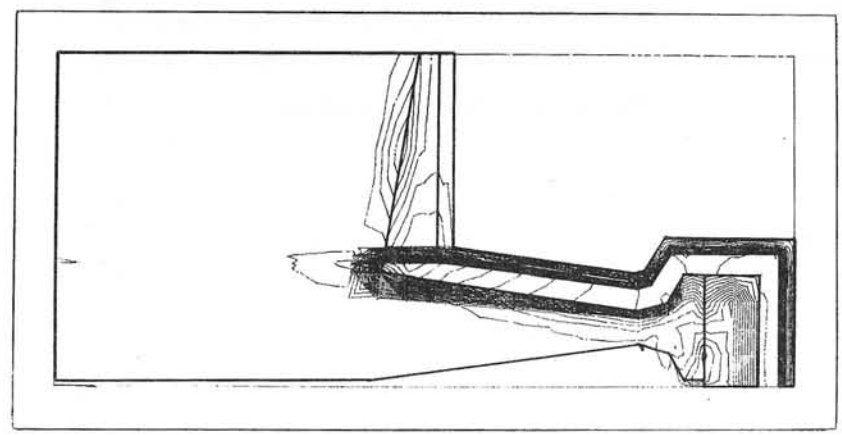

FIGURE 4. INDUCED FIELD B_θ AT t = 200 μ sec.

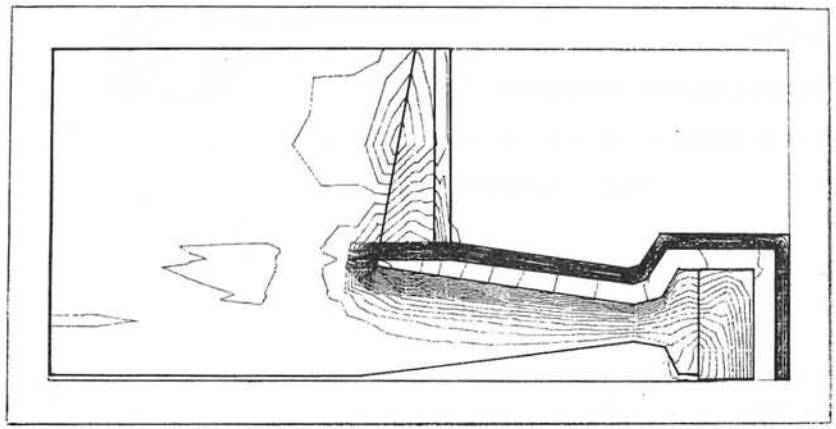

FIGURE 5. INDUCED FIELD B_θ AT t = 1000 μ sec.

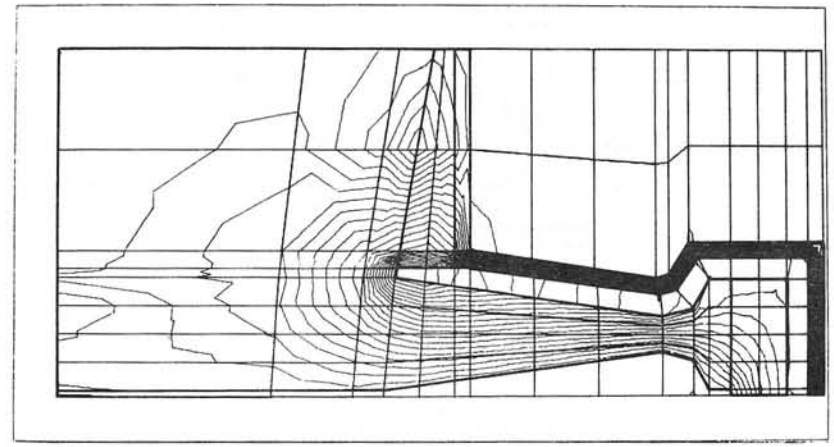

FIGURE 6. INDUCED FIELD B_θ STEADY STATE

FIELD PENETRATION INTO A VARIABLE-μ MATERIAL

I. Gumowski
CERN, Geneva, Switzerland

Abstract

A non-linear partial differential equation is formulated which describes the distribution of H inside a material of non-constant relative permeability μ. The assumption $\mu = \mu(H)$ leads to the existence of solutions differing qualitatively from those obtained with the assumption $\mu = \text{const}$. One of these solutions suggests that remanence is not an independent phenomenon, but merely a consequence of $\mu = \mu(H)$. Conditions are established for the field penetration to be of the usual diffusion type. A recursive method of calculating H is proposed.

1. INTRODUCTION AND STATEMENT OF THE PROBLEM

In field calculations the internal properties of magnetic materials are rarely specified microscopically, in terms of molecular and crystalline structure. The specifications are usually macroscopic ones, in terms of remanence, hysteresis, static-, incremental-, a.c.- and effective-relative permeability. Since an explicit relation between the microscopic and macroscopic descriptions is not yet available, the Ising model notwithstanding, the macroscopic description is obtained phenomenologically, in the form of a set of flux-density versus field curves (B versus $\mu_0 H$, μ_0 = permeability of vacuum, MKSA units used in this paper). The corresponding mathematical problem is extremely complex, because these curves are not single-valued. If it is assumed that the knowledge of the geometric configuration and of the relative permeability μ is sufficient for a complete description of H, then μ is a function of instantaneous as well as past values of H and $\partial H/\partial t$.

The problem of constructing macroscopic models of field penetration of minimal mathematical complexity constitutes in essence a problem of successive approximation, each approximation step describing a physically richer situation. The coarsest possible approximation is based on the assumption $\mu = \mu_e = \text{const}$, describing some "mean" or "effective" static state of the material. The next step, discussed in this paper, is based on the assumption that μ depends also on the instantaneous value of H. The assumption $\mu = \mu(H)$ involves some dynamic effects excluded by the simplification $\mu = \text{const}$. For example, the diffusion of H changes into a wave propagation with finite velocity (unrelated to displacement currents), and remanence appears as a limiting case.

The paper emphasizes qualitative aspects, i.e. conditions of physically distinct behaviour of H. When the propagation of H corresponds to the usual diffusion process, a computation method based on successive corrections is proposed. In order to reduce the notational bulk and render the procedure physically transparent a very simple geometric configuration is used. The resulting mathematical model is one-dimensional. A generalization to more dimensions is straightforward.

2. FORMULATION OF THE MATHEMATICAL MODEL

Let the magnetic material have the form of a rather thick C in the x-z plane and be quite long along y. The origin of the rectangular coordinates is placed so that the x-axis bisects horizontally the rectangular air gap of the C, $x = 0$ and $x = \bar{x}$ representing the inner and outer edges of the latter. Let $h = \text{const}$ be the height of the air gap and ℓ the length of a flux line inside the magnetic material. If $\mu = \text{const}$ and $\ell = \text{const}$, the time scale can be so chosen that the product $\sigma\mu_0$, σ = electrical conductivity, is absorbed into t, and the field $H(x,t)$ inside the air gap is described by

$$\frac{\partial}{\partial x}\left(k\,\frac{\partial H}{\partial x}\right) = \frac{\partial H}{\partial t}\,, \qquad t > t_0\,,\ 0 < x < \bar{x}\,, \tag{1}$$

where $k = h/\ell + 1/\mu$ and $t_0 = \text{const}$. A unique solution of eq. (1) is defined, for example, by the boundary conditions

$$H(0,t) = G_1(t)\,, \qquad H(x,t_0) = G_2(x)\,, \tag{2}$$

G_1, G_2 being two given (sufficiently smooth) functions.

When $\mu = \mu(H)$ and $\ell = \ell(H)$, the form of eq. (1) changes only slightly (cf. Appendix):

$$\frac{\partial}{\partial x}\left[F(H)\,\frac{\partial H}{\partial x}\right] = \frac{\partial H}{\partial t}\,, \qquad t > t_0\,,\ 0 < x < \bar{x}\,, \tag{3}$$

$$F(H) = \frac{h}{\ell} + \frac{1}{\mu} + \frac{1}{\ell}\,H\,\frac{\partial}{\partial H}\,\frac{\ell}{\mu}\Big)\,. \tag{3a}$$

The specific problem consists at this stage in ascertaining properties of $\mu(H)$, and eventually of $\ell(H)$, which define qualitatively different solutions of eqs. (1), (2) and (3), (2), respectively. From the theory of nonlinear parabolic equations it is known that eq. (3) is singular when

$$F(H) = 0 \qquad (4)$$

for some real $H = H_c$. Near the critical field H_c there exist no solutions of eq. (3) in the usual sense, i.e. there is no function $H(x,t)$ possessing a continuous second derivative with respect to x and verifying eq. (3) identically. Normal numerical methods are known to yield meaningless results under these circumstances. Physically significant solutions exist in a mathematically generalized sense, subject to the condition that $F(\partial H/\partial x)$ is a continuously differentiable function with respect to x. The function $\partial H/\partial x$ need not be continuous[1]. Appropriate numerical methods have already been worked out[2]. Moreover, some analytical solutions are known when F has a special form. Such solutions are mainly a source of physical insight. Equations of type (3) arise also in other fields, for example, in plasma physics[3], heat conduction[4], and filtration of fluids by porous media[5,6].

The question arises whether eq. (4) is ever satisfied in the case of a magnetic material. As a preliminary step it is necessary to fit $\mu(H)$ and $\ell(H)$ by some analytically simple functions, because otherwise the physical content of eq. (4) is obscured by the mathematical manipulations in eq. (3a). It is obvious that the μ involved in eq. (3a) is intermediate between the conventional a.c.- and static-μ's. $\mu(H)$ is thus a single-valued function possessing one maximum, say μ_m at H_m, which implies $\partial\mu/\partial H > 0$ for $H < H_m$ and $\partial\mu/\partial H < 0$ for $H > H_m$. Physical concepts, like leakage flux and edge effects near an air gap, suggest that $\partial\ell/\partial H \geq 0$. An elementary analysis of $F(H)$ shows then that $F > 0$ when $\partial\mu/\partial H \leq 0$, and a real H_c can only exist when $\partial\mu/\partial H > 0$. Whether H_c actually exists depends on the specific values of $\max(h/\ell)$, $\min \mu$ and $\partial\mu/\partial H$. A good fit to experimental data is provided by

$$\mu(H) = \mu_i + H^n (\mu_m - \mu_i)/(H_0^n + H^n) , \qquad 0 \leq H < H_m , \qquad (5)$$

where $\mu_i = \mu(0)$, and H_0, n are determined numerically. The parameters H_0 and n characterize the scale of H and the rate of increase of μ, respectively. For a typical silicone steel $\mu_i = 1.2$, $\mu_m = 8.5$, $H_m = 100$, $H_0 = 17$, $n = 3.5$, whereas for a low-μ ferrite (type U60) $\mu_i = 3$, $\mu_m = 33$, $H_m = 1000$, $H_0 = 376$, $n = 2.3$.

Consider first the simplest possible case $\ell = \text{const}$. Combining eqs. (3a) and (5) yields a ratio of two quadratic polynomials in H^n. The vanishing of the numerator being equivalent to eq. (4), the critical field H_c can be expressed explicitly as a function of h/ℓ and the parameters of eq. (5). Two simple roots of eq. (4) exist when $h/\ell \ll 1$, $n > 1$ and μ_i is not too large. In the case of the above examples: $H_{c1} = 9.3$, $H_{c2} = 14$ when $h/\ell = 0.1$; $H_{c1} = 8.2$, $H_{c2} = 20$ when $h/\ell \approx 0$ for silicone steel, and $H_{c1} = 140$, $H_{c2} = 360$, $h/\ell \approx 0$ for the ferrite. The non-existence of real H_c as h/ℓ increases describes simply the diminishing role of the magnetic material compared to that of the air gap. For small n the dynamic effect of $\partial\mu/\partial H$ is weaker than the static effect of the constant part of μ. When $\ell = \text{const}$ is replaced by $\ell = \ell(H)$, eq. (4) becomes too complicated to allow an explicit solution. Numerical tests with particular forms of $\ell(H)$ have shown that flux-line lengthening has a rather weak effect on the roots of eq. (4); they tend, however, to be slightly more separated.

The existence of critical fields H_c permits a rough qualitative assessment of the solutions of eq. (3). Assume, in fact, that the boundary conditions (2) place $H(x,t)$ into the interval $H_{c1} < H < H_{c2}$. In this interval $F(H) < 0$. Replacing t by -t reduces eqs. (3), (2) to a "normal" diffusion problem, with $F(H) > 0$, except that the new time runs backwards. In the original t there exists therefore a process of "inverse" diffusion, with a possible steepening of the spatial profile of H.

3. SOME INVERSE DIFFUSION EFFECTS

Consider eq. (3) in the field range defined by $F(H) \leq 0$. Replace $H - H_{c1}$ by H in order to render H_{c1} a static reference solution, and t by -t in order to make all terms nominally positive. When only the largest term is kept in the transformed F, eq. (3) simplifies into

$$a \frac{\partial}{\partial x}\left(H \frac{\partial H}{\partial x}\right) = \frac{\partial H}{\partial t} , \qquad 0 \leq H < H_{c2} - H_{c1} , \qquad (6)$$

where $a = F'(H_{c1})$. The usefulness of eq. (6) consists in the fact that some of its solutions can be found in explicit form. These solutions can be verified by direct substitution. For conciseness, the statement "$H(x,t) \equiv 0$ outside the specified range of x" is omitted below. All symbols not mentioned explicitly are positive constants whose values are given by the boundary conditions (2) after insertion of the relevant $H(x,t)$.

In contrast to normal diffusion, eq. (6) admits a non-constant stationary state

$$H(x,t) = H_i\ (x_0 - x)^{\frac{1}{2}}\ , \qquad 0 \le x \le x_0\ , \tag{7}$$

where H_i and x_0 represent the boundary field intensity and the field penetration depth, respectively. From a physical point of view, solutions of type (7) represent a spatially non-uniform remanence. Hence, remanence does not appear to be an independent phenomenon, distinct from the non-linearity introduced by $\mu(H)$.

Various wave-type solutions are also possible. The simplest case is

$$H(x,t) = \frac{c}{a}\ (ct + x_0 - x)\ , \qquad 0 \le x \le x_0 + ct\ , \tag{8}$$

where the propagation velocity c is defined indirectly by the boundary field intensity H_i. A wave with a steepening profile and a non-propagating front is described by

$$H(x,t) = (x_0 - x)^2/[6a(c - t)]\ , \qquad 0 \le x \le x_0\ . \tag{9}$$

Variable velocity waves are represented by the family of functions

$$H(x,t) = H_i\ (c + t)^m\ f(u)\ , \quad u = \frac{x}{A}\left[a\,H_i\ (c + t)^{m+1}\right]^{-\frac{1}{2}}\ , \qquad 0 \le u \le 1\ , \tag{10}$$

where $f = v(u)$ is a particular solution of the ordinary differential equation

$$vv'' + v'^2 + \frac{1}{2}(1 + m)\,A^2uv' - mA^2v = 0\ . \tag{11}$$

When $(1+m)A^2 = B$, one solution of eq. (11) is

$$v(u) = \frac{w}{B}\sum_{i=0}^{\infty} b_i w^i\ , \qquad B = \sum_{i=0}^{\infty} b_i\ , \tag{12}$$

where $w = 1 - u$, $b_0 = 1$, $b_1 = 1/4$, $b_2 = -1/24$, ...

Non-constant stationary states, and wave propagation with a finite velocity exist also in two- and three-dimensional inverse diffusion problems. There is no inherent need for symmetry as far as the different spatial directions are concerned. The resulting macroscopic anisotropy is also a mere consequence of $\mu(H)$.

4. A RECURSIVE SOLUTION METHOD FOR THE NON-SINGULAR CASE

When the field penetration problem is described by eq. (3) and $F(H) > 0$, the analytical fitting (5) is inappropriate. A convenient replacement, emphasizing the range $\partial\mu/\partial H < 0$, is

$$\mu(H) = \mu_i + mH_0H^n/(H_0^{n+1} + H^{n+1})\ , \qquad H > H_{c_2}\ (H \ge 0 \text{ if } \mathrm{Im}\ H_c \ne 0)\ , \tag{13}$$

where, as before, the constants are empirically determined. For silicone steel, for example, $\mu_i = 1.2$, $H_0 = 82$, $m = 13$, $n = 2.8$, and for a low-μ ferrite (type K12, $\mu_m = 34$, $H_m = 2700$), $\mu_i = 18$, $H_0 = 2090$, $m = 27$, $n = 2.4$. Let ℓ_e, μ_e be the effective values used in the linearization (1), where $k = h/\ell_e + 1/\mu_e$. The difference $g = F(H) - k$ represents therefore the effect of the non-constancy of ℓ and μ. Since the effective values are well chosen by definition, g is a small correction of k. Formally this property is described by

$$F(H) = k + \varepsilon g(H)\ , \qquad 0 < \varepsilon \le 1\ , \tag{14}$$

where ε is the coefficient of the dominant non-constant term of $F(H)$, or simply an auxiliary ordering parameter (set to unity in the final result). If a solution of eqs. (3), (2) and (14) is written in the form

$$H(x,t) = \sum_{i=0}^{\infty} H_i(x,t)\ \varepsilon^i\ , \quad H_i(0,t) = H_i(x,t_0) \equiv 0\ , \qquad i > 0\ , \tag{15}$$

then the non-linear problem reduces to a sequence of linear ones

$$\left.\begin{aligned} k\frac{\partial^2 H_0}{\partial x^2} - \frac{\partial H_0}{\partial t} &= 0 \\ k\frac{\partial^2 H_1}{\partial x^2} - \frac{\partial H_1}{\partial t} &= -\frac{\partial}{\partial x}\left[g(H_0)\ \frac{\partial H_0}{\partial x}\right] \\ k\frac{\partial^2 H_2}{\partial x^2} - \frac{\partial H_2}{\partial t} &= -\frac{\partial}{\partial x}\left[g(H_0)\ \frac{\partial H_1}{\partial x} + g'(H_0)\ H_1\ \frac{\partial H_0}{\partial x}\right] \\ &\cdots\cdots \end{aligned}\right\} \tag{16}$$

the first to be solved with the boundary conditions (2), and the other with homogeneous ones given in eq. (15). The boundary-value problems (16)

can be solved by standard analytical or numerical methods. When k represents a good linearization, the corrections $H_i(x,t)$ diminish rapidly as i increases. It is noteworthy that no direct analytical methods of solving eqs. (3), (2) and (14) are known. Numerical methods require the solving of sets of non-linear algebraic equations, which is a considerable complication compared to the computations involved in solving eq. (16).

CONCLUSION

When the assumption μ = const is replaced by $\mu = \mu(H)$ the field penetration into a magnetic material constitutes a non-linear diffusion process. In the range $\partial\mu/\partial H > 0$ an inverse diffusion is possible. Two distinct inverse diffusion effects are illustrated. The full set of such effects, and their stability with respect to small structural perturbation of the differential equation, are still unknown. The most relevant structural perturbation appears to be a dependence of μ on $\partial H/\partial t$, which can be made to simulate the presence of hysteresis.

APPENDIX

Consider the geometric configuration described in Section 2. For conciseness, let $H_z = H$, $\ell = \ell(x,y)$, $\ell(\Delta x) = \ell(x + \Delta x, y)$, and similarly for other variables. Integrate H around two flux lines separated by Δx in the x-z plane of the air gap:

$$\oint \vec{H} \cdot d\vec{s} = \left(h + \frac{\ell}{\mu}\right) H - \left[h + \ell(\Delta x)/\mu(\Delta z)\right] H(\Delta x)$$

$$= -\left[H \frac{\partial}{\partial x}\left(\frac{\ell}{\mu}\right) + \left(h + \frac{\ell}{\mu}\right)\frac{\partial H}{\partial x}\right]\Delta x + \ldots = J_y \ell \Delta x ,$$

where J is the current density. Neglecting $\partial\ell/\partial y$, $\partial\mu/\partial y$ and keeping only terms of first order in Δx yields

$$-J_y = +\frac{H}{\ell}\frac{\partial}{\partial x}\left(\frac{\ell}{\mu}\right) + \left(\frac{h}{\ell} + \frac{1}{\mu}\right)\frac{\partial H}{\partial x}, \quad J_x = \left(\frac{h}{\ell} + \frac{1}{\mu}\right)\frac{\partial H}{\partial y}, \quad J_z = 0 .$$

Inside the air gap $(1/\sigma)$ curl $\vec{j} = -\mu_0(\partial\vec{H}/\partial t)$, which implies

$$\left(\frac{h}{\ell} + \frac{1}{\ell}\right)\frac{\partial^2 H}{\partial y^2} + \frac{\partial}{\partial x}\left[\left(\frac{h}{\ell} + \frac{1}{\mu}\right)\frac{\partial H}{\partial x} + \frac{H}{\ell}\frac{\partial}{\partial x}\left(\frac{\ell}{\mu}\right)\right] = \sigma\mu_0 \frac{\partial H}{\partial t} .$$

Equation (3) is obtained by neglecting the dependence on y, and replacing $\mu(x,y)$, $\ell(x,y)$ by $\mu(H)$, $\ell(H)$, respectively.

REFERENCES

1) O.A. Oleink, A.S. Kalashnikov and Chou-Jui-Lin, Izv. Akad. Nauk. Ser. Mat. 22, 667-704 (1958).

2) A.A. Samarskii, Zh. vych. mat. 3, No. 2, 266-298 (1963).

3) N.V. Zmitrenko and S.P. Kurdiumov, Dokl. Akad. Nauk. 218, 1306-09 (1974).

4) L.K. Martinson and K.B. Pavlov, Zh. vych. Mat. mat. Fiz. 12, No. 4, 1048-53 (1972).

5) G.I. Barenblatt, Prikl. mat. 16, No. 1, 67-78 (1952).

6) D.G. Aronson, SIAM J. Appl. Math. 17, No. 2, 461-467 (1969).

Use of Bubnow - Galerkin Method for Calculation of Transient Skin Effect in Foil Wound Chokes

P. Rolicz*

Abstract

It is shown that the Bubnow - Galerkin method can be applied for the analysis of non - steady states in conductors. The Joule power dissipated in a foil wound choke with an air gap is calculated in this paper. The particular case, when the excitation current is sinusoidal, is also considered.

1 Introduction

The steady state in foil wound chokes and transformers has been investigated by using numerical [4] experimental [6] and analytical [1,5] methods. The transient skin effect in the winding lying in the window of a foil wound choke with an air gap is examined in this paper by using the Bubnow - Galerkin method.

2 Use of Bubnow - Galerkin method for parabolic equation

The theory of the application of the Bubnow - Galerkin method for the parabolic equation has been considered by Sobolevskii[7]. Let H be a real Hilbert space with a countable base, and C a linear positive and self - adjoint operator in H. The operator equation

$$CE + \frac{\partial E}{\partial t} = 0 , \qquad 0 \leq t \leq T \tag{1}$$

is given with the initial condition $E = E_o$ at $t = 0$. We chose the sequence $\{\varphi_i\}$, φ_i belongs to the domain of the operator C, complete in the energetic space H_C of the operator C such that the elements $\varphi_1, \varphi_2, \cdots, \varphi_n$ are linear independent for arbitrary n. In order to find the approximate solution of equation (1) we take

$$E^{(n)} = \sum_{i=1}^{n} E_i \varphi_i \tag{2}$$

and we solve this equation with the initial condition $E_o^{(n)} = P_n E_o$ at $t=0$, where P_n denotes the orthogonal projection onto the n - dimensional subspace spanned upon the elements $\varphi_1, \varphi_2, \cdots, \varphi_n$. This leads to the following system of equations

$$\sum_{i=1}^{n} \left[E_i (C\varphi_i | \varphi_m) + \frac{dE_i}{dt} (\varphi_i | \varphi_m) \right] = 0, \quad m=1,2,\ldots,n \tag{3}$$

where $(x|y)$ denotes the scalar product in the space H. The following theorem holds[7] (Theorem 1 c at $\alpha = 1/2$).

Theorem1. If E, $E^{(n)}$ denote the exact solution of the equation (1) and the approximate solution of one obtained by the Bubnow - Galerkin method, then

$$\lim_{n \to \infty} \sup_{0 \leq t \leq T} \sqrt{t}\, \| E^{(n)} - E \| = 0 ,$$

where $\|x\|$ denotes the norm of x in the space H_C.

Hence and from positive definition of the operator C results the convergency in the initial space H.

Let L_2 denotes the real Hilbert space of quadratically integrable functions in a closed and bounded set Ω . The scalar product of the elements $f, g \in L_2(\Omega)$ is defined as follows

$$(f \mid g) = \int_{\Omega} f\, g\, d\Omega . \tag{4}$$

The operator $-\nabla^2$ is positive definite and self - adjoint[3] in $L_2(\Omega)$ for homogeneous boundary problems: Dirichlet, Neumann and mixed.

The Joule power (formula (10)) dissipated in windings lying in the window of a choke is proportional to square of the norm of E in the space $L_2(\Omega)$. Thus, by Theorem 1, the Bubnow - Galerkin method can be used for the calculation of the Joule power.

*The author is with Dept.of Electrical Engineering, Polytechnic of Białystok, Poland

3 Joule power dissipated in winding of choke

3.1 Non - steady state

The choke section is shown in fig.1. We assume that the permeability of ferromagnetic substance is infinitely great, the field in the gap is homogeneous and that foils are such thin that the current density is independent of x in each of them.

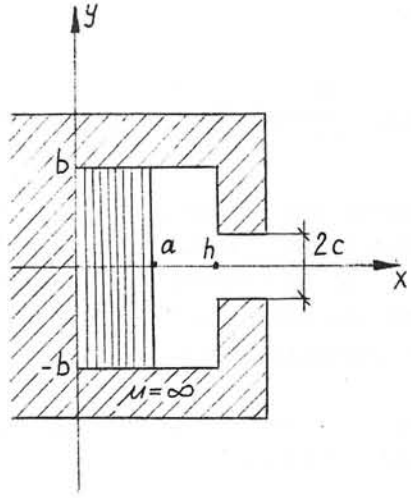

Fig.1 Choke section

The z component E of the electric field fulfils the following equation

$$\nabla^2 E = \begin{cases} \mu_o \gamma w \dfrac{\partial E}{\partial t} & \text{for } 0 \leq x \leq a \\ 0 & \text{for } a < x \leq h \end{cases} \quad , \tag{5}$$

where μ_o, γ, w denote the permeability, the conductance and the filling factor, respectively. By the received assumptions, the Green´s formula and (1) - (5) , the Bubnow - Galerkin system of equations has the form

$$\int_0^h dx \int_{-b}^{b} \operatorname{grad}\varphi_i \operatorname{grad} E \, dy + \mu_o \gamma w \frac{d}{dt} \int_0^h dx \int_{-b}^{b} \varphi_i E dy = \frac{\mu_o}{2c} \frac{dI_\Sigma}{dt} \int_{-c}^{c} \varphi_i \Big|_{x=h} dy \ , \tag{6}$$

where $I_\Sigma = n\,I$, I - a current flowing in a foil, n-number of foils. We assume that I has the form

$$I = I_o \sin(\omega t + \alpha_o) + \sum_{i=1}^{N} I_i e^{-\alpha_i t}, \quad I=0 \text{ at } t \leq 0 \ . \tag{7}$$

The Stone-Weierstrass Theorem[2] can be used for the determination of the sequence $\{\varphi_i\}$. By one, any even (with respect to the y - axis) continuous function on $\Omega = \{(x,y) : 0 \leq x \leq h, \ |y| \leq b\}$ may be uniformly approximated by linear combinations of functions of the sequence

$$\left\{ \cos h \left(m\, 0{,}65\pi \frac{x}{h} \right) \cdot \cos\left(l\pi \frac{y}{b} \right) \right\} \quad m,l = 0,1,2\ldots$$

We admit that E has the following form

$$E = E_1 + E_2 \cos h\left(0{,}65 \frac{\pi x}{h}\right) \cdot \cos \pi \frac{x}{b} \ . \tag{8}$$

From (6) - (8) it follows that

$$E_1 = \frac{I_\Sigma}{2ab\gamma w} \tag{9a}$$

$$E_2 = n\varsigma \left[I_o \frac{\omega \cos(\omega t + \alpha_o - \psi) + \delta \sin(\alpha_o - \psi)\, e^{-\delta t}}{\sqrt{\delta^2 + \omega^2}} + \right.$$

$$\left. + \sum_{i=1}^{N} I_i \frac{\delta e^{-\delta t} - \alpha_i e^{-\alpha_i t}}{\delta - \alpha_i} \right] , \tag{9b}$$

where

$$\varsigma = 7{,}8 \mu_o \rho \frac{\sin \pi \frac{c}{a}}{\pi \frac{c}{a}} \ , \quad \delta = \left(25{,}7 \frac{b}{h} + 80{,}7 \frac{h}{b}\right)\rho \ ,$$

$$\varrho = \left\{ \mu_0 \gamma w a b \frac{h}{4{,}08a} \left[\sin h\left(\frac{4{,}08a}{h}\right) + 1 \right] \right\}^{-1}, \quad \psi = \tan^{-1}\frac{\omega}{\delta} \quad .$$

The Joule power dissipated in the foils lying in the window of the choke is equal to

$$P = w\gamma \int_0^a dx \int_{-b}^{b} E^2 \, dy = \frac{I^2}{2abw\gamma} + \frac{1}{2\mu_0 \varrho} E_2^2 \cdot \left[\frac{W}{m}\right] \qquad (10)$$

3.2 Steady state

The steady state in the choke is considered later on. From (9b) it follows that

$$E_2 = n \varsigma I_0 \frac{\omega \cos(\omega t + \alpha_0 - \psi)}{\sqrt{\delta^2 + \omega^2}} \quad . \qquad (11)$$

The mean value of P is equal to

$$\hat{P} = \frac{1}{T} \int_0^T P \, dt = \frac{n^2 I_0^2}{4w\gamma ab} \left[1 + \frac{\varsigma^2 \omega^2 \gamma w a b}{\mu_0 \varrho (\delta^2 + \omega^2)} \right] \cdot \left[\frac{W}{m}\right] \qquad (12)$$

The current density J may be written

$$J = \gamma E = \mathrm{Im}\left[\sqrt{2}\, \underline{J}\, e^{j(\omega t + \alpha_0)}\right] \quad , \qquad (13)$$

where Im denotes imaginary part and

$$\underline{J} = J_0 \left[1 + \frac{2j\varsigma\omega\gamma w a b}{\delta + j\omega} \cos h\left(2{,}04 \frac{x}{h}\right) \cos\frac{\pi y}{b} \right] = |\underline{J}|\, e^{j\varphi} \quad , \qquad (14)$$

$$J_0 = \frac{n I_0}{2\sqrt{2}\, a b w \gamma} \quad .$$

In[1], using the serial reactions of eddy currents method, the following formula has been worked out

$$\underline{J} = \underline{J}_1 \left[1 + j\alpha \sum_{n=1}^{\infty} \left(\cos n\pi \frac{y}{b} - \cos n\pi \right) F_n(x) \right] , \qquad (15)$$

where

$$\underline{J}_1 = J_0 \frac{1 + j\alpha \sum_{n=1}^{\infty} \left(\cos n\pi \frac{y}{b} - \cos n\pi \right) F_n(x)}{1 - j\alpha \sum_{n=1}^{\infty} F_n(x) \cos \pi n} \quad ,$$

$$F_n(x) = \frac{\sin \pi \frac{c}{b}}{n^2 \sin h\left(n\pi \frac{h}{b}\right)} \cos h\left(n\pi \frac{x}{b}\right) \quad ,$$

$$\alpha = \frac{2\omega\mu_0\gamma\, w a b^2}{\pi^2 c} \quad .$$

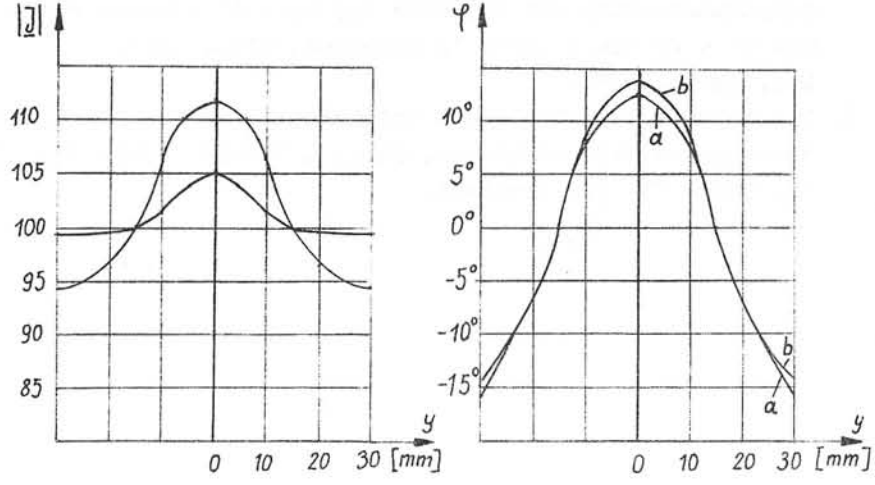

Fig.2 Diagrams of the function $|\underline{J}|$ and φ for x = 0 a) according to (15), b) according to (14).

In order to compare the results, the calculations were made for $c = 1$ mm, $a = 4c$, $b = 30c$, $h = 20c$, $w = 1$, $J_o = 100$, $\omega\mu_o\gamma = 12600\ m^{-2}$ - Al at $f = 50$ Hz. On the ground of them fig.2 is made. The differences between $|\underline{J}|$ and φ given by (14) and the exact values of these parameters given by (15) are not greater than 7 %.

References

1. W. Lipiński, "Analysis of Current Density Distribution in Foil Windings of Chokes", Archiwum Elektrotechniki, 1974, 23, (3), pp. 667 - 675 (in Polish)
2. K. Maurin, " Methods of Hilbert Spaces" (PWN, 1967)
3. S.G. Mikhlin, "The Problem of the Minimum of a Quadratic Functional" (Holden - Day, 1966)
4. N. Mullineux, J. Reed, I. Whyte, "Current Distribution in Sheet and Foil Wound Transformers", Proceedings IEE, 1969, 116, (1), pp. 127 - 130
5. P. Rolicz, "Calculation of Impedance of Conductors by Direct Methods of Functional Analysis", Doctoral Thesis, Polytechnic of Szczecin, 1973 (in Polish)
6. I. Sieradzki, "Stromverteilung im Leiterquerschnitt bei Wechselstromspulen mit Al - Folienwicklung und Optimierungsmassnachmen für Drosseln von Hg - Etlandungslampen mit Al - Folienspulen", XI Internat. Wiss. Koll. T.H. Ilmenau, 1966
7. P.E. Sobolevskii, "Bubnow - Galerkin Method for Parabolic Equation in Hilbert Space", Dokl. A.N.SSSR, 1968, 178, (3), pp. 548 - 551 (in Russian).